

1. REPORT NO. NASA TM-78270		2. GOVERNMENT ACCESSION NO.		3. RECIPIENT'S CATALOG NO.	
4. TITLE AND SUBTITLE A Study of the Effect on a Typical Orbiter Payload Thermal Environment Resulting from Specular Reflections from the Forward Orbiter Radiators				5. REPORT DATE March 1980	
				6. PERFORMING ORGANIZATION CODE	
7. AUTHOR(S) R. Humphries, L. Turner, and J. W. Littles				8. PERFORMING ORGANIZATION REPORT #	
9. PERFORMING ORGANIZATION NAME AND ADDRESS George C. Marshall Space Flight Center Marshall Space Flight Center, Alabama 35812				10. WORK UNIT NO.	
				11. CONTRACT OR GRANT NO.	
12. SPONSORING AGENCY NAME AND ADDRESS National Aeronautics and Space Administration Washington, D.C. 20546				13. TYPE OF REPORT & PERIOD COVERED Technical Memorandum	
				14. SPONSORING AGENCY CODE	
15. SUPPLEMENTARY NOTES Prepared by Structures and Propulsion Laboratory, Science and Engineering					
16. ABSTRACT Most analyses performed to determine the Shuttle Payload Bay on-orbit thermal environment have considered all Orbiter, as well as payload surfaces, to be diffuse. The Orbiter radiator external coating is highly specular silverized teflon. This study considers solar energy specularly reflected from these radiators on a typical payload which, when deployed, extends above the payload bay envelope. Comparisons are made between the flux levels assuming both diffuse and specular radiators.					
17. KEY WORDS Specular, Orbiter, Radiator, Thermal, Radiation, Analysis, Diffuse			18. DISTRIBUTION STATEMENT Unclassified-Unlimited		
19. SECURITY CLASSIF. (of this report) Unclassified		20. SECURITY CLASSIF. (of this page) Unclassified		21. NO. OF PAGES 107	22. PRICE NTIS

TABLE OF CONTENTS

	Page
I. INTRODUCTION	1
II. SPECULAR/DIFFUSE RADIATION THEORY	1
III. PREVIOUS STUDIES	3
VI. PROBLEM DESCRIPTION	5
A. IPS/IPS Payload	5
B. Approach	6
C. Forward Orbiter Radiator Contour	8
V. ANALYTICAL TECHNIQUE	9
VI. DISCUSSION OF RESULTS	13
A. Ray Tracings	13
B. Solar Flux Determination from TRASYS II Output Data	14
C. Payload Inclination Angle	14
D. Lateral Location of Payload Surfaces	15
E. Degree of Radiator Specularity	16
VII. FUTURE STUDY PLANS	16
VIII. CONCLUSIONS	17
REFERENCES	19

LIST OF ILLUSTRATIONS

Figure	Title	Page
1.	Two dimensional radiation reflection from diffuse and specular surfaces	22
2.	Orbiter geometry and nomenclature used in Northrup study	23
3.	Closeup view of Orbiter radiator panel	24
4.	Scale model of Orbiter with SL-2 payload configuration	25
5.	SL-2 payload irradiated by forward Orbiter radiators in stowed configuration	26
6.	SL-2 payload irradiated by forward Orbiter radiators in deployed configuration	27
7.	Overall payload configuration, SL-2	28
8.	Cruciform/experiment configuration	29
9.	Deployed forward Orbiter radiators	31
10.	Solar reflectance versus wavelength for silver-Teflon sample	32
11.	Parameters investigated in specular radiation study	33
12.	Orbiter port radiator panels	34
13.	Forward Orbiter radiator contour (mid forward panel) as defined by Rockwell supplied equations	35
14.	Forward Orbiter radiator surface angle (mid forward panel)	36
15.	"Smoothed" contour of forward Orbiter radiator (mid forward panel)	37
16.	Energy reflected from radiator for configuration studied that created narrowest cavity	38
17.	Three-dimensional TRASYS II based model	39
18.	Geometry used in three-dimensional TRASYS II based model	40

LIST OF ILLUSTRATIONS (CONTINUED)

Figure	Title	Page
19.	"Two-dimensional" TRASYS II based model.....	41
20.	Reflected ray overlap characteristic of TRASYS II based models	42
21.	Two-dimensional specular heat flux program geometry	43
22.	Heat flux calculation in the two dimensional specular heat flux program	44
23.	Manual tracings of reflected solar rays from the Orbiter radiator; fixed IPS	45
24.	Manual tracings of reflected solar rays from the Orbiter radiator; sun-tracking IPS	51
25.	Tracings of reflected solar rays from the Orbiter radiator as generated using the two dimensional specular heat flux program	57
26.	Areas of highest solar ray concentration (focal region) above the deployed forward Orbiter radiator	66
27.	Projection of specular energy reflections from radiators to vertical plane at Orbiter centerline.....	67
28.	Projection of specular energy reflections from radiators to plane parallel to sun's rays	68
29.	Payload heat rates computed with "two-dimensional" TRASYS II based model for a 0° payload inclination angle	69
30.	Grouping of nodes to smooth heat rates calculated with "two-dimensional" TRASYS II based model	70
31.	Cumulative solar energy absorbed on IPS payload from "two-dimensional" TRASYS II based model data	71
32.	Payload heat flux computed with "two-dimensional" TRASYS II based model for a 0° payload inclination angle	72

LIST OF ILLUSTRATIONS (CONTINUED)

Figure	Title	Page
33.	Payload heat rates computed with "two-dimensional" TRASYYS II based model for a -15° payload inclination angle	73
34.	Payload heat rates computed with "two-dimensional" TRASYYS II based model for a -10° payload inclination angle	74
35.	Payload heat rates computed with "two-dimensional" TRASYYS II based model for a -5° payload inclination angle	75
36.	Payload heat rates computed with "two-dimensional" TRASYYS II based model for a 5° payload inclination angle	76
37.	Payload heat rates computed with "two-dimensional" TRASYYS II based model for a 10° payload inclination angle	77
38.	Payload heat rates computed with "two-dimensional" TRASYYS II based model for a 20° payload inclination angle	78
39.	Payload heat rates computed with "two-dimensional" TRASYYS II based model for a 30° payload inclination angle	79
40.	Payload heat rates computed with "two-dimensional" TRASYYS II based model for a 40° payload inclination angle	80
41.	Payload heat flux computed with the "two-dimensional" TRASYYS II based model for a -15° payload inclination angle	81
42.	Payload heat flux computed with the "two-dimensional" TRASYYS II based model for a -10° payload inclination angle	82
43.	Payload heat flux computed with the "two-dimensional" TRASYYS II based model for a -5° payload inclination angle	83

LIST OF ILLUSTRATIONS (CONTINUED)

Figure	Title	Page
44.	Payload heat flux computed with the "two-dimensional" TRASYYS II based model for a 5° payload inclination angle	84
45.	Payload heat flux computed with the "two-dimensional" TRASYYS II based model for a 10° payload inclination angle	85
46.	Payload heat flux computed with the "two-dimensional" TRASYYS II based model for a 20° payload inclination angle	86
47.	Payload heat flux computed with the "two-dimensional" TRASYYS II based model for a 30° payload inclination angle	87
48.	Payload heat flux computed with the "two-dimensional" TRASYYS II based model for a 40° payload inclination angle	88
49.	IPS payload heat flux computed with the two-dimensional specular heat flux program for payload inclination angles from -15° to 0°	89
50.	IPS payload heat flux computed with the two-dimensional specular heat flux program for payload inclination angles from 10° to 40°	90
51.	Comparison of "two-dimensional" TRASYYS II based model and two-dimensional specular heat flux program for heat flux on the IPS payload at a 0° payload inclination angle	91
52.	Characteristics of energy absorbed on the IPS payload for various payload inclination angles	92
53.	Unsymmetrical irradiation of IPS payload	94
54.	Cases defined to determine the effect of the IPS payload surface lateral location on the absorbed solar flux levels	95
55.	Effect of the IPS payload surface lateral location on the absorbed solar heat flux levels of the IPS payload	96

LIST OF ILLUSTRATIONS (CONCLUDED)

Figure	Title	Page
56.	Effect of the degree of the radiator specularity on the absorbed solar flux levels of the IPS payload	97
57.	Effect of radiator specularity on the maximum solar heat flux absorbed by the IPS payload	98

LIST OF TABLES

Table	Title	Page
1	Specular Reflectance Data for Silver-Teflon (Teflon Side)	20
2	Characteristics of Solar Energy Reflected from the Forward Radiators for Various Payload Inclination Angles	21

TECHNICAL MEMORANDUM

A STUDY OF THE EFFECT ON A TYPICAL ORBITER PAYLOAD THERMAL ENVIRONMENT RESULTING FROM SPECULAR REFLECTIONS FROM THE FORWARD ORBITER RADIATORS

I. INTRODUCTION

Most analyses performed to determine the Shuttle Payload Bay on-orbit thermal environment have considered all Orbiter, as well as payload surfaces, to be diffuse. The Orbiter radiator external coating is silver coated Teflon which is a mirror-like (i.e., specular) material. The forward radiator panels are normally deployed away from the doors to provide additional heat rejection. In this configuration, payload elements extending above the Orbiter sill in the vicinity of the forward radiator panels have a greater thermal interaction with the radiators than is present with the radiators undeployed on the doors. Complicating this is the fact that the radiator is concave in shape. This causes a focusing of specularly reflected rays to occur which concentrates energy in the radiator's viewing area. As a result, accurate determination of the thermal environment for Shuttle equipment located in this vicinity must consider both diffuse and specular surface assumptions.

Previous thermal environments for the Orbiter, which have been analyzed by MSFC thermal elements, have been generated using a thermal radiation computer program known as TRASYS I. This program has only a diffuse analysis capability. However, TRASYS II, an update to TRASYS I, which has the capability to analyze combined diffuse/specular surfaces, has recently been made available. Since TRASYS II is a relatively untested tool in specular analyses, it required verification before use in large scale studies. To this end, a FORTRAN based specular heat flux model was developed. This program, along with TRASYS II based models, were used to generate thermal environments resulting from specular reflections from the forward radiator onto a hypothetical plane. These environments were generated for varying sun inclination angles, but were limited to sun vectors into the bay which lie in the port/starboard plane (i.e., yz plane of the Orbiter). Only pure vehicle roll angle effects (with respect to a +z solar inertial attitude) were addressed. Vehicle pitch angles, since they create less severe effects, are not examined.

II. SPECULAR/DIFFUSE RADIATION THEORY

There are two different types of surface models used when analyzing the radiant energy transfer from/to a surface. The most commonly assumed model is known as a diffuse model. The term "diffuse" denotes

directional uniformity. In particular, the intensity of the radiation leaving a diffusely emitting and diffusely reflecting surface is uniform in all angular directions (Fig. 1). In the case of a diffusely reflecting surface, this intensity of reflected radiation is uniformly distributed irrespective of the nature of the incident radiation. The role of a diffusely reflecting surface is to obliterate the past history of the incident radiation. In general, a surface intercepting this energy has only a projected view of the surface. Consequently, the energy distribution is a cosine function (the Lambertian cosine law). In contrast, a ray of energy that is specularly reflected has a zero radiation intensity in all directions except at one particular angle from the reflecting surface normal. As shown in Figure 1, this angle is the same as that formed between the incoming ray and the surface normal. In reality, most surfaces reflect energy both diffusely and specularly. The degree of specularity is dependent on such factors as material type, surface finish, application, wavelength, and direction of the incident energy.

The basic radiation relationships applying to this study, which assume no transparent surfaces are:

$$\alpha_{\text{IR}} + \rho_{\text{IR}}^{\text{DIFF}} + \rho_{\text{IR}}^{\text{SPEC}} = 1$$

$$\alpha_{\text{s}} + \rho_{\text{s}}^{\text{DIFF}} + \rho_{\text{s}}^{\text{SPEC}} = 1$$

where

α = surface absorptance

ρ = surface reflectance

IR = infrared wave band

s = solar wave band

DIFF = diffuse component

SPEC = specular component.

The reader should be cautioned that two basic terms are currently in use to define the level of surface specularity. The first is that of specular reflectance, ρ^{SPEC} , as defined by the total, ρ , and diffuse, ρ^{DIFF} , reflectances as follows:

$$\rho^{\text{SPEC}} = \rho - \rho^{\text{DIFF}}$$

where ρ is given for an opaque surface by the equation:

$$\rho + \alpha = 1 \quad .$$

The reflectance values are given either in decimal or percent units.

The terminology used for the second term is usually percent specularity, $\% \rho^{\text{SPEC}}$. It is defined by the reflectance values as:

$$\% \rho^{\text{SPEC}} = \frac{\rho^{\text{SPEC}}}{\rho} \times 100$$

Using these definitions, it is obvious that virtually always

$$\% \rho^{\text{SPEC}} > \rho^{\text{SPEC}}$$

III. PREVIOUS STUDIES

A number of studies have been made previously to investigate the specularity induced effects of the Orbiter radiators. Although none of these studies were directly related to this study, in that they do not give environments for the payload configuration in question, some results were applicable.

In 1976, a study was conducted to assess the effect of changing the deployment angle of the forward radiators [1]. This study examined the relative energy increase in the payload bay volume, below the enclosed payload bay envelope [i.e., $z = 490$ in. (1244.6 cm)], as a result of changing the deployment angle. These data indicated that for a 38° radiator deployment angle the peak specular energy in this envelope was 30 percent greater at a sun angle, α (see Fig. 2), of 70° than at a +z solar inertia (SI) position ($\alpha = 90^\circ$). Unfortunately, this study was done for a radiator shape different from that now used, and for a deployment angle (measured from a reference line created by a line from the hinge point to the door extremity) (see Fig. 2) of 38° rather than the 35.5° angle now being used. No absolute values of specular energy levels were quoted, nor were diffuse to specular comparisons made.

Two studies reported in June 1976 [2,3] examined the effect of radiation trapping within the cavity created by the deployed radiator and door. Analyses were made comparing purely diffuse assumption and specular assumptions. These studies indicated that radiation trapping would occur; this was verified by testing. These studies also showed that with artificial alteration and for a selected range of conditions, a TRASYS I program can be used to predict the thermal performance of a system with specular surfaces [4]. These reports indicated the need for better analytical tools for predicting specular radiation heat transfer.

Hughes Aircraft [5] made a study of the effect of solar loading due to specular reflections off the radiator on the LEASAT payload. This study examined the flux levels on a 120-in. (304.8 cm) diameter cylindrical structure in the Orbiter payload bay volume. Levels of incident energy as high as 1.4 suns were predicted. Earth atmosphere ground tests, run on a 1/10 scale model, indicated that intensities actually reached 1.7 suns. These higher intensity levels were attributed to non-uniformity of the simulated radiator surface causing local concentration. It was not clear if such non-uniformity effects existed in the actual radiators.

Informal communications with a cognizant JSC source [6] indicated that local intensity levels in excess of 500 suns can be analytically predicted at the focal point of the forward radiator contour. However, this source also indicated that the apparent specularly of the "as applied" silver-Teflon on the radiator surface bears a faceted or "orange peel" appearance (see Fig. 3). This observation indicated the overall specularly was less than that of a smooth material sample. Qualitative examination of the radiator surface had borne out this observation, indicating focal point intensities much less than those predicted using purely specular assumptions. However, no definitive data were available with which to corroborate or refute these observations.

Additional studies [6] have recently been completed which examine energy entrapment at a cavity in the radiator near the hinge. At sun inclination angles between 70° and 105° , specularly reflected energy off the radiator can be trapped in this hole creating intensities in the cavity on the order of 2 suns. Further examination of how this cavity energy might affect the payload is warranted. This same source indicates that during door openings/closings, specularly reflected energy passes across the payload bay volume. Reflected intensities of up to 2 suns can irradiate the Orbiter payload volume over its entire length. However, this is a transient condition lasting for only approximately 30 sec.

It has been indicated [6] that a potential exists for covering the forward radiator surface with a more diffuse material. Tentative plans are being made to execute such a modification on later Orbiter vehicles. However, these plans are currently highly tenuous. Also, no data are currently available concerning the material properties. Thus, the consequences of such a change are unknown.

IV. PROBLEM DESCRIPTION

A. IPS/IPS PAYLOAD

For the purposes of illustrating how the Orbiter payload/radiators are configured, a four view photograph mosaic of a typical Spacelab model (1/100 scale) is shown in Figure 4. This depicts a simulated Spacelab mission 2 (SL-2) payload in an on-orbit configuration. Although difficult to determine from the photo the radiators are covered with specular silver-Teflon material. The lower left view shows the relationship of the upward deployed forward radiator to the forward door section and the aft radiator. This figure also pictorially represents the relative size of payload to Orbiter dimensions. A tiltable, payload carrying device, known as the Instrument Pointing System (IPS) capable of being pointed at a solar or stellar target, is a planned payload. The proximity of the IPS and its components to the forward radiator aftmost position for SL-2 is also apparent.

The primary objective of this study is to study the specular energy reflection of the Orbiter forward radiators onto the IPS and its associated experiments. This is of interest primarily due to the elevated position of this hardware, especially the IPS optical sensor package (OSP)/cruciform/experiment combination while the IPS is in a deployed state. (The cruciform is a rigid structure mounted to the IPS to which the various experiment components are attached). However, for certain limited sun angles, other fixed surfaces on the forward most pallets, and the vicinity of the igloo can be irradiated by these radiators. (In addition to the IPS payload, this includes, for limited sun angles, the IPS thermal shroud enclosure and a small part of the forward edge of SL-2 experiment 7 in the position shown in Figures 5 and 6. For Orbiter nose to the sun pitch angles, larger portions of experiment 7 will be irradiated.) Because of this, the thrust of this study was directed at the IPS OSP/cruciform/experiment combination (hereafter referred to as the IPS payload).

The IPS is currently mounted at the Orbiter centerline on pallet 1 for the SL-2 mission (see Fig. 7). The centerline of the structure is located at an x position of 879 in. (2,232.7 cm). This position is in front of the most aft position of the forward radiator at x = 940 in. (2,387.6 cm). The elevation gimbal pivot point is at z = 416 in. (1,056.6 cm). A four-bladed cruciform structure is attached atop the IPS to the IPS adapter ring. The experiment payloads are mounted on this cruciform as shown in Figure 8. In the stowed position the IPS payload (i.e., cruciform/experiment combination) can either be attached to the IPS or separated from it. Separation detaches the IPS payload from the IPS so that significant orbital maneuvering loads are not transmitted to the delicate IPS gimbal. In the separated/stowed position, the IPS payload/IPS ring is positioned 5 in. (12.7 cm) farther from the fixed location IPS gimbals. In the clamped position, a drive motor draws the IPS payload back into the closer position for deployment. In the normal ($\psi = 0^\circ$) deployed position, the base of the IPS payload at the cruciform

is located at $z = 449.5$ in. (1,141.7 cm). The four experiments (i.e., experiments 8, 9, 10, and 11) mounted to the cruciform each has different height and mount positions within their respective cruciform quadrants (see Fig. 8). Currently, the longest is the experiment 10 telescope whose uppermost point is located at a $z = 586$ in. (1,488.4 cm) level when normally deployed.

The IPS can be rolled 360° and/or pitched 120° ($\pm 60^\circ$). For SL-2, the pitch angle is limited to a 40° from the normal cone. (This limit is imposed due to clearance requirements with adjacent equipment.) In a data-taking mode the IPS is pointed at the sun on the sunside of orbital passes. For thermal purposes, it is assumed the IPS line of sight (LOS) is either pointed directly at the sun or stowed. The IPS has a capability to select solar disk coordinates and roll to these positions for science reasons. However, it has no intelligence to allow it to control its position relative to the Orbiter, while pointing at the sun.

As a result of the above SL-2 example case conditions, certain boundaries for this study were established. The primary surface examined during the course of this study was the IPS payload. Sun angles greater than 40° off the xz plane were not considered. Also, since the IPS roll position relative to the Orbiter is an uncontrollable parameter, experiments were all considered to be in the roll position at which the worst specular reflection occurs.

B. APPROACH

The characteristic of specularly reflected energy being dependent on the origin of the incoming ray (as defined by the angle of incidence) complicates the analytical process considerably. Although computer techniques make specular radiation analyses possible, it has yet to be made very practical for large, detailed studies. TRASYS I computes the surface to surface radiation interchange network as well as the total absorbed orbital heating rates on each surface. However, this program lacks the capability to analyze specular surfaces. Energy which is specularly reflected off the radiator upper surface tends to collect at a focus point or region. Consequently, energy levels are highly magnified near this region. The currently used TRASYS I based diffuse Orbiter midsection model assumes the surface of the Orbiter radiators to be formed from a 90° cylindrical section. However, the forward radiator is a much more complicated cusplike shape, tending to "point" energy toward the payload bay area. At the present, a new analysis tool, TRASYS II [7] is available which is capable of analyzing complicated specular 3-dimensional geometries on a limited basis.

The present study addressed the major specular problem, the deployed, forward Orbiter radiators. These radiators, whose locations are defined in Figure 9, are coated with silverized Teflon. According to Reference 8, the degree of specularity of this application of silverized Teflon may range from 96 to 99 percent in the short wave length (solar) energy band.

The Silver-Teflon cover material used on the radiators is classified as a second surface mirror (SSM). The silver is vacuum deposited on the back of the outer Teflon skin. As a protection for the silver, a thin layer of inconel is vacuum deposited over the silver. Finally, an adhesive is applied to the inconel to allow application of the SSM to the structure. In this configuration, since the outer Teflon is transmissive to short wave length energy, the incoming solar energy encounters the highly reflective and low absorptive silver surface. However, since the Teflon is relatively opaque to long wavelength energy, it acts to give the combination a high emittance.

Although the Orbiter to payload ICD indicates a ρ_{SPEC} range between 96 and 99 percent for the silver-teflon surface, some question exists as to its actual specularity. A sample of 5 mil silver-inconel coated Teflon, Sheldahl p/n G401500, was tested by the MSFC Materials and Processes Laboratory for surface properties. The solar absorptance, IR emittance and solar reflectance values were measured for the Teflon side. Absorptance was measured using a Gier-Dunkle mobile solar reflectometer, MS-251 and the specularity was determined using a Beckman Model DK-2A spectrophotometer. Both devices actually measure the reflectance. These measurements are made by placing a 1 x 1 in. sample in an integrating sphere and irradiating the sample's surface with a mercury-xenon lamp. For the specularity determination, 20 measurements of both total and diffuse reflectance are made at wavelength (from 0.27 to 2.7 microns) spacings indicative of equal solar energy increments (using the standard Johnson curve). By this technique, the integrated solar reflectance can be determined with simple averaging of these point measurements. A strip chart output of these data for the silver-Teflon sample is shown in Figure 10 and is tabulated in Table 1. For the diffuse reflectance run, the sample was irradiated at a normal incidence angle. An approximately 1-in. aperture in the 8-in. diameter integrating sphere was located at an equal reflected angle to allow specular energy escape. Using these data, the normal specular reflectance is calculated from the total diffuse component for the solar waveband by using the equations

$$\alpha_s = 1 - \rho_s$$

and

$$\rho_s^{\text{SPEC}} = \rho_s - \rho_s^{\text{DIFF}}$$

For this particular sample, these values [MSFC Letter EH34(79-49), Aug. 1979] were as follows:

$$\rho_s = 0.91$$

$$\alpha_s = 0.09$$

$$\epsilon_{IR} = 0.81$$

$$\rho_s^{DIFF} = 0.10$$

$$\rho_s^{SPEC} = 0.81$$

and from these

$$\% \rho_s^{SPEC} = 89\%$$

As indicated, the value of 89 percent differs somewhat from the minimum expected ICD value of 96 percent. However, this could be caused by a number of potential differences ranging from variations in sample to measuring technique differences. Until these uncertainties are resolved, a 99 percent value is conservatively assumed.

Because of the location of the IPS in the forward part of the Orbiter's payload bay, the radiators can direct solar energy onto the sidewalls of the IPS mounted experiments. Therefore, in general, it was the purpose of this study to determine, in a preliminary form, the differences in the magnitudes of the energy levels on the IPS-mounted experiments as computed assuming both diffuse and specular Orbiter radiators. In particular, the following parameters were investigated:

- 1) Angle of inclination of the payload with respect to the Orbiter's z axis.
- 2) Lateral displacement of payload
- 3) Degree of specularity of the Orbiter radiators.

These parameters are defined in Figure 11. It should be noted from this figure that the heat flux distribution on the deployed IPS equipment is affected by the shape of the radiator surface, the solar inclination angle, and the physical relationship between the radiator and the IPS payload surface.

C. FORWARD ORBITER RADIATOR CONTOUR

Since the contour of the deployed radiator is a dominant parameter affecting the distribution of the solar heat flux on the payload, it was

important that the proper contour be determined. Figure 12 shows the port radiator panels, with the two panels farthest from the viewer making up the port side forward radiator. Four equations describing the aft portion of the deployed forward radiators were obtained from Reference 6. These equations and the resulting plot are shown in Figure 13. The slight discontinuities in the radiator contour at the junctions of the segments defined by each equation may be eliminated by smoothing the plot of the radiator surface angle, θ , as shown in Figure 14. The "smoothed" radiator contour is shown in Figure 15.

V. ANALYTICAL TECHNIQUE

Three analysis tools were used in this study:

- 1) TRASYS II (three-dimensional model)
- 2) TRASYS II ("two-dimensional" model)
- 3) Two-dimensional specular heat flux program.

All of the above assumed:

- 1) Solar constant = 429 Btu/hr ft^2 ($1,353.1 \text{ W/m}^2$)
- 2) Radiator solar absorptance = 0.1
- 3) Payload absorptance = 0.25
- 4) The radiator's degree of specularity to be independent of the angle of the incident energy and local surface irregularities
- 5) Only direct solar (i.e., short wavelength) energy was considered to be specularly reflected from the Orbiter radiators.
- 6) One bounce per ray of solar energy from radiator.

Although the "one bounce" assumption (i.e., energy was not allowed to reflect from one portion of the radiator onto another portion and then to the payload) could be a severe analytical limitation in geometries containing pronounced cavities, it was considered of no consequence for the open radiator and payload geometry of the present study (Fig. 16).

Initially, it was thought that the TRASYS II program would serve as the fundamental analytical tool for this study. A three-dimensional TRASYS II based model was constructed. As shown in Figure 17, the

model considered the port side radiator (179 nodes) and a planar surface (40 nodes) that represented the IPS/cruciform payload. Figure 18 defines the surface geometry of this model. Since the solar vector was always maintained parallel with the planar surface (representing the IPS equipment) in this study, only the section of the radiator that would contribute to energy being specularly reflected on the assumed 11.333×5.584 ft (3.454×1.702 m) planar surface (this represents the projected area of the maximum IPS payload dimensions) was modeled in great detail. The TRASYS II program allows only planar nodes to be considered as specular reflectors. Thus the radiator was modeled using thin, flat segments with either 26 or 101 segments in the y direction. The location of these segments was defined by the smoothed curve shown in Figures 14 and 15. Since the present study was concerned with increases in the total absorbed heating rates over those computed assuming diffuse radiators, it was necessary to include the entire port side radiator length. Energy reflected purely specularly from the radiator surface can be analyzed two-dimensionally. However, because of the diffusely reflected energy component, a three dimensional analysis was required. This allowed comparison of the relative magnitudes of the diffuse and specular energy components.

A "two-dimensional" TRASYS II based model was also constructed for considering strictly specularly reflected energy from the radiators. The use of the "two-dimensional" model over the three-dimensional one (where applicable) resulted in improved computer efficiency. This model's geometry (121 nodes) is shown in Figure 19. (The model was actually a three-dimensional model with extremely thin dimensions in the x direction.)

Both TRASYS II based models had two disadvantages. First, many planar segments were required to model the radiator curvature to minimize reflected ray overlap error (see Fig. 20). As a result of this error in approximating the surface curvature, proper sizing and placement of the absorbing surface nodes for each solar angle would be required to minimize the total error. This would be impractical since it would require that a new model be developed (i.e., generation of new surface/nodal description data) for each solar inclination angle to be analyzed. This would allow the proper location and sizing of the surface nodes to correspond to the bundles of rays reflected from the Orbiter radiator planar segments. However, some method (possibly graphical) would also have to be used prior to this to determine the irradiated IPS payload area (with the reflected solar energy from the radiators) for each solar inclination angle considered. Second, without the careful nodal breakdown of the absorbing surface, the determination of the reflected flux as a function of position on the payload representing plane became a tedious task. This is the result of having to compute the position dependent flux based on heat rate data that were output directly from TRASYS on a nodal basis.

A two-dimensional specular heat flux program was developed for two reasons. First, this program could be used to verify the data

generated from the TRASYS II based models. Second, because of the more general nature of the TRASYS II program, the specular heat flux program could be made more computer efficient as well as be tailored to the output data requirements. For this second reason, the specular heat flux program replaced the TRASYS II based program as the basic analytical tool after it had been established that the two gave comparable results.

The specular heat flux program utilized straight line segments to approximate the radiator curvature. Each segment was characterized by its angle with respect to the horizontal plane (Orbiter's x and y axes) and its average location from the payload bay centerline (\bar{y} , \bar{z}). A line was used to represent the IPS mounted payload. This line was located by its point of origin (y, z) and angle of inclination, ψ . The program geometry is shown in Figure 21. The following equations serve as the basis of this program and may be derived from the geometry shown in Figure 21:

$$A = 20 + 180 - \beta$$

$$\xi = 270 - A - \psi$$

$$y = \cos \left[90 - \tan^{-1} \left(\frac{y_{\text{disp}}}{z_{\text{disp}}} \right) - \psi \right] \cdot \sqrt{(y_{\text{disp}})^2 + (z_{\text{disp}})^2}$$

$$z = z_{\text{pivot}} + \sin \left[90 - \tan^{-1} \left(\frac{y_{\text{disp}}}{z_{\text{disp}}} \right) - \psi \right] \cdot \sqrt{(y_{\text{disp}})^2 + (z_{\text{disp}})^2}$$

$$z_{\text{exp}} = \frac{1}{\sin(180 - \xi)} \cdot \sin \left[\xi - 90 + \tan^{-1} \left(\frac{\bar{z} - z}{\bar{y} - y} \right) + \psi \right] \cdot \sqrt{(\bar{z} - z)^2 + (\bar{y} - y)^2}$$

$$E = (z_{\text{exp}} + z \sqrt{\tan^2 \psi + 1}) \sin \psi + y - z \tan \psi$$

$$C = (z_{\text{exp}} + z \sqrt{\tan^2 \psi + 1}) \cos \psi$$

where:

A = angle of reflected ray

θ = angle of radiator segment

β = solar inclination angle

ξ = angle between reflected ray and payload

ψ = payload inclination angle

z_{exp} = location of reflected ray on payload

y = lower payload location to right of payload bay centerline

z = lower payload location above payload bay centerline

\bar{y} = radiator segment location to right of payload bay centerline

\bar{z} = radiator segment location above payload bay centerline

y_{disp} = lateral displacement of payload

z_{disp} = position of payload above IPS pivot point

z_{pivot} = location of IPS pivot point above payload bay centerline

E = location of reflected ray on payload as measured to the right of the payload bay centerline

C = location of reflected ray on payload as measured above the payload bay centerline.

In addition to the assumptions listed at the beginning of this section, the specular heat flux program also assumed:

- 1) Albedo and earth irradiation to be negligible
- 2) 100 percent specular radiator ($\rho_s^{SPEC} = 100$).

The heat fluxes were calculated by comparing spacing between incoming rays and the same rays when incident in the payload. This computational procedure is explained in Figure 22.

VI. DISCUSSION OF RESULTS

A. RAY TRACINGS

Two techniques were used during this study to determine the map of rays reflected from the forward radiators onto the hypothetical surface. The first is simply by manual plotting of these rays. Figures 23 and 24 show these plots for a fixed IPS and a sun-tracking IPS, respectively. The two-dimensional specular heat flux program is capable of machine plotting reflected rays from the radiator. These rays are plotted in Figure 25 for various solar inclination angles. (Since these rays were used in the calculation of local heat fluxes, as a computation convenience, the spacing of incoming rays was not the same for all portions of the radiator contour.) Figure 25 clearly illustrates that there are areas above the deployed forward radiators where the reflected solar energy is concentrated. This is the result of the concave nature of the radiator contour. Although no attempt will be made at present to quantify this energy level, Figure 26 identifies the regions of the highest ray concentrations for the various solar inclination angles considered.

Figure 27 shows the imbalance in specular irradiations from opposite side radiators created by pure vehicle roll (i.e., no pitch) with respect to the sun. This figure depicts the strike path of rays reflected from both starboard and port radiators on the hypothetical fixed plane at the Orbiter centerline (i.e., xz plane). From this plot, it can be seen that reflections completely miss the payload bay volume [i.e., $z > 490$ in. (1,244.6 cm)] at the centerline when in a +z SI attitude. However, because of the elevated position of the deployed IPS payload, some of these experiments are irradiated. As the sun vector angle increases, reflections from the sun side radiator cover more of the payload bay volume until an angle of approximately 20° is reached. At this angle the entire payload bay is irradiated down to the top of the fuselage sidewall [i.e., $z = 419.5$ in. (1,065.5 cm)]. As the angle increases further, the radiator contour actually begins to block some reflection causing the irradiated surface limit to again move upward. Comparing this to the anti-sun-side radiator irradiation, the imbalance in specular reflection from the two radiators is obvious. As the angle increases the rays from the anti-sun-side radiator move rapidly upward, so that at approximately 20° the lowest position of rays is above the highest possible projection of the most elevated IPS experiment. In regard to the IPS experiments, this figure is somewhat misleading. The experiments are actually located on a platform so that they are never at the Orbiter centerline even at +z SI. Also, since the current SL-2 mission planning requires that the IPS LOS be always directed at the sun when deployed, the path of rays on the experiments differs from that on a fixed position plane. Figure 28 shows the path for rays for a sun tracking plane.

B. SOLAR FLUX DETERMINATION FROM TRASYS II OUTPUT DATA

Using the "two-dimensional" TRASYS II based model, the data shown in Figure 29 were generated assuming 100% specular radiators. The data plotted in this figure is short wavelength energy (i.e., solar). This same energy, which originated directly from the sun, was reflected by the radiators onto the payload. Throughout the remainder of this report, the term "solar" in connection with energy, heat rates, or heat fluxes is used in this sense. It does not include albedo or reflected solar energy from other sources. These data apply to a solar inclination angle of 90° (payload inclination angle of 0°). The payload was represented by a narrow plane placed 2.792 ft (0.851 m) (maximum radius of IPS payload) from the center of the IPS cruciform. This position is representative of the IPS cruciform baseplate outer edge. As was characteristic of the TRASYS II generated heat rates, which resulted from specularly reflected energy from non-planar geometries, the data were oscillatory. This may be ascribed to the ray overlap error mentioned earlier. This error was most pronounced at localized regions of the payload plane. (This apparent instability in the TRASYS II analysis output is a major source of concern.) Although local oscillations occurred in the data, it is easily verified by hand calculations that the total energy reflected on the payload as calculated using TRASYS II is accurate. As such, the total energy as predicted by TRASYS II was used to determine the local IPS payload heat fluxes.

To use the local heat rate data for predicting local flux intensities, a method for smoothing the data was required. These data may be smoothed by simply adding the heat rates for several nodes and plotting the sums. This has been done for the data in Figure 29 and is shown in the smoothed form in Figure 30. Note that the data have been smoothed by adding the heat rates for two adjacent nodes for one case and grouping the heat rates for four nodes in the second case. It can be seen from Figure 30 that the four-node grouping gives the smoother curve.

To determine heat flux as a function of location on the IPS payload, an additional curve was generated. This curve, shown in Figure 31, is a plot of the cumulative absorbed solar heat rate as a function of the distance away from the base of the IPS payload. This curve was drawn using the data points shown in Figure 30 for the four-node grouping of heat rates. The derivative of this curve was computed using $\Delta Q / \Delta Z_{exp}$ as an approximation. Dividing the derivative by the width of the payload plane [0.1667 ft (0.0508 m) for the "two-dimensional" model] gave the heat flux as plotted in Figure 32.

C. PAYLOAD INCLINATION ANGLE

Using the "two-dimensional" TRASYS II model, the heat flux on the payload plane for the payload inclination angle of 0° was determined (Fig. 32). Additional cases were run for various payload inclination

angles between -15° (no energy is reflected on the IPS payload for angles exceeding -20°) and 40° (the IPS tilt limit). The payload was kept parallel to the sun's rays. The solar inclination angle ranged from 105° to 50° for the cases studied. The nodal heat rate data for these new cases are plotted in Figures 33 through 40. The local heat fluxes on the IPS payload which were generated from the data in Figures 33 through 40 (by the method described in para. B of this section) are shown in Figures 41 through 48.

The two-dimensional specular heat flux program was used to verify the data generated by the TRASYS II based program for a varying solar inclination angle. These data are shown in Figures 49 and 50 for all inclination angles which were under consideration. For a direct comparison with the TRASYS II produced data, Figure 51 compares the IPS payload local flux data generated for a 0° payload inclination angle. As can be seen from the figure, the data are very comparable considering that the TRASYS II data were obtained using directly output nodal heat rate data values.

Table 2 summarizes the data obtained for the various payload inclination angles studies (these data are also plotted in Figure 52). The maximum local solar flux on the payload was found to be 76.0 Btu/hr ft^2 (239.7 W/m^2) and was located 4.6 ft (1.4 m) from the cruciform baseplate at a 40° payload inclination angle (payload parallel to the sun's rays); however, the payload was found to absorb the greatest total amount of solar energy [2800 Btu/hr (820.4 W)] at an approximate 14° payload inclination angle. As shown in Table 2 and Figure 52, the total energy level reflected on a single side of the IPS payload decreases as the payload inclination angle becomes more negative. It must be realized that although one side of the IPS payload would have no energy reflected onto it from the radiators at a payload inclination angle of -20° , the opposite side (operating at a $+20^\circ$ angle) would receive 2620 Btu/hr (767.7 W) [for an assumed area of 63.3 ft^2 (5.88 m^2)]. This is illustrated in Figure 53.

D. LATERAL LOCATION OF PAYLOAD SURFACES

In an effort to determine the amount of flux reduction that can be expected on payload surfaces closer to the centerline of the cruciform, two cases were analyzed to compare with the case of maximum lateral displacement [2.792 ft (0.851 m)] used in the previously discussed cases in which the solar inclination angle (as well as the payload angle) was varied. These two cases considered the plane representing the payload surfaces to be placed at the center of the cruciform and half the distance between the center and maximum displacement (Fig. 54). For these cases, the solar inclination angle was held constant at 90° . The flux data generated for the cases under consideration are shown in Figure 55. As is seen in the figure, a surface that is at the cruciform centerline has a maximum flux of approximately 80 percent of that same surface

placed its maximum distance from the centerline [2.792 ft (0.851 m)]. However, as one moves away from the cruciform baseplate in the z_{exp} direction, this difference approaches zero. An average difference between minimum and maximum surface displacement may be taken to be about 10 percent. Thus in regard to solar energy reflected from the radiators onto the IPS payload surfaces, it is clear that the lateral position of the surfaces on the cruciform does not strongly influence the heat flux level on the surfaces.

E. DEGREE OF RADIATOR SPECULARITY

As a result of the apparent lack of data on the properties of the silverized Teflon as applied to the Orbiter radiators, the effect of the degree of radiator specularity ($\% \rho^{SPEC}$) on the magnitudes of the heat flux reflected onto the IPS experiments was examined. The three-dimensional TRASYS II based model was used for this task since it was not possible to generate accurate diffusely reflected energy data with a two-dimensional model. Once again, the baseline configuration for this study was taken to have a solar inclination angle of 90° , and the plane representing the IPS experiments was placed 2.792 ft (0.851 m) from the payload bay centerline in the direction of the radiator analyzed. Four cases were considered — 0, 50, 75, and 100 percent degree of specularity. The resulting absorbed solar flux data are shown in Figure 56. Note from the figure that the maximum solar flux, considering a 100 percent specular radiator, is over six times greater than the maximum flux value with a completely diffuse radiator ($\% \rho^{SPEC} = 0$). The maximum flux produced with a 75 percent and 50 percent specular radiator was 82 percent and 67 percent, respectively, of the maximum value with a 100 percent specular radiator (see Fig. 57). Thus, as a result of the increase in the diffuse component of the reflected energy (as the degree of radiator specularity decreases), the heat flux level does not decrease directly in accordance with a reduction in specularity.

VII. FUTURE STUDY PLANS

A number of questions remain unanswered in regard to specular reflections and their environment effects. In particular, the technique for handling large sophisticated geometries needs to be improved. TRASYS II seems to have good fidelity in regard to total energy reflected when considering the entire integrated field of incident and reflected energy. However, when examining local influences, the data appear to be highly dependent on the surface geometry/node grid size selected. Even when a fine node spacing is selected, some instabilities in heating rates are exhibited. Where accurate local surface environment definition is required, this discrepancy is significant.

Inherently, a combination specular/diffuse analysis requires additional calculation steps which increase the amount of computer time required as compared to a purely diffuse analysis. Added to this is the fact that small surface node sizes required to accurately calculate local heat rates increase in size of the computer model.

It is obvious from this that other techniques must be studied. In particular, a Monte Carlo radiation analysis program [9] is available, and its possible application to the present problem needs to be examined. This program uses a completely different specular analysis scheme from the traditional technique incorporated in TRASYS II. In any event, further examination of other techniques for analyzing large specular/diffuse systems will be investigated. Finally, the effect of Orbiter pitch angle should be examined. Although worst case thermal environments due to specular reflections occur at conditions defined herein, other skewed sun angles are probable for the currently planned missions.

VIII. CONCLUSIONS

The shape and specularity of the upper surfaces of the forward radiators of the Orbiter cause high energy densities to occur in the forward payload volume above the top edge of the fuselage sidewall. These densities occur when the Orbiter's +z axis is pointed in the direction of an energy source (i.e., the sun) with the forward radiators in their deployed configuration. Because of the highly directional nature of this energy reflected from the radiators, the payload surfaces in and above the cargo bay which face the radiators are primarily affected.

Data were generated to assess the impact that specular Orbiter radiators have on the tiltable payloads. These data were generated using TRASYS II based models and a two-dimensional specular heat flux FORTRAN program.

Although TRASYS II was used in the generation of these new data, the data did not result from a detailed analysis on the order of that performed earlier using TRASYS I with the assumption of diffuse Orbiter radiators. The primary differences in these data and a more complete environmental study are as follows:

- 1) Exact equipment geometries were not used.
- 2) Radiation exchange and trapping resulting from interequipment reflections were not considered.
- 3) Energy exchanges with other SL-2 surfaces were neglected.
- 4) Albedo and earth IR energies were not generally accounted for.

5) Specific equipment surface properties were not used.

Based on the assumptions given in this report, the solar oriented case absorbed heat rates on tilttable payloads are, in general, much higher when the Orbiter radiators are considered to be specular rather than diffuse. As an example, the following data (from additional, supplemental analyses) are given for a 0° payload inclination angle at orbital noon:

	Total Flux (Diffuse Radiators)	Total Flux (Specular Radiators)
Maximum Flux, Btu/hr ft ² (W/m ²)	34 (107.2)	93 (293.3)
Average Flux, Btu/hr ft ² (W/m ²)	32 (100.9)	52 (164.0)

These data apply to a deployed, white IPS payload flying a -40° Beta angle, 216 n.mi. (400 km) +z solar inertial orbit. These data indicate that when considering specular Orbiter radiators, the maximum total flux and average flux on the IPS's 11.333 ft (3.454 m) high payload can increase 173 percent and 63 percent, respectively, when compared to diffuse radiators. In computing total flux, all three components of energy normally associated with orbital heating analysis were considered. These components are direct solar, albedo, and earth irradiation. Also this total flux considers energy reflections among the surface geometry. However, it must be remembered that these values apply at only one point in the orbit. On an orbital average basis, the heat flux is only 47 percent higher when specular radiators are considered. Due to the large mass and heavily insulated configuration of most equipment, this orbital average value is probably more illustrative of the overall effect of radiator specularity.

The methods used in this study to analyze solar energy reflected from the Orbiter radiators onto the IPS payload gave very comparable results (using smoothed TRASYS II based model output data). Although the two-dimensional, specular heat flux program was much more computer efficient than the TRASYS II based models, its usefulness was limited to simple, two-dimensional geometries. TRASYS II had two disadvantages in its use as a tool to analyze specular energy reflections. First, the present study showed that the nodal (i.e., local) heat rates calculated using a TRASYS II based model were not very accurate as output directly by the program. The heat rate data for a series of adjacent nodes on the IPS payload oscillated about the curve describing the actual local heat rate over the node group. Although the data were capable of being "smoothed," the tedious process by which this was accomplished would prove to be a very formidable task for a larger, more detailed analysis. The second disadvantage to using the TRASYS II based models was the large amount of computer time required.

REFERENCES

1. Cansler, H. T.: Shuttle Forward Panel Optimum Deployment Angle Determination Study for Solar Inertial Attitude. Report No. TN272-1652, Northrup Services, Inc., Huntsville, Alabama, June 1976.
2. Clawson, J. F.: Radiator Cavity Specularity Study. Internal Letter SEM-ITA-76-195, Rockwell International, Houston, Texas, July 1976.
3. Scheps, P. R. and Howell, H. R.: The Effect of Radiation Trapping within the Specular Cavity Formed by the Shuttle Forward Radiators and Payload Bay Door. ASME paper 76-ENAs-55, July 1976.
4. Thermal Radiation Analysis System (TRASYS I) User's Manual. MCR-73-105, Martin-Marietta Corporation, Denver, Colorado, May 1973.
5. Belchem, R. C.: Higher than Predicted Solar Reflections Off the STS Radiator. Document 4132.15/664, Hughes, Culver City, California, May 1979.
6. Jaax, J.: verbal/written communications. Johnson Space Center (EC-12), Houston, Texas, October and November 1979.
7. Thermal Radiation Analysis System (TRASYS II) User's Manual, MCR-73-105 (Rev. 2), Martin-Marietta Corporation, Denver, Colorado, June 1979.
8. Shuttle Vehicle/Spacelab ECS/Thermal Interfaces. Document No. ICD-2-05201, (Rev. B), Johnson Space Center, Houston, Texas, December 1975.
9. Net Energy Verification and Determination Analyses (NEVADA) Users' Manual. Turner Associates, Brea, California, March 1979.

TABLE 1. SPECULAR REFLECTANCE DATA FOR SILVER-TEFLON
(TEFLON SIDE)

WAVELENGTH (MICRONS)	SOLAR REFLECTANCE (PERCENT)	
	DIFFUSE	TOTAL
0.337	15.5	61.0
0.399	15.4	82.9
0.441	14.1	89.0
0.474	13.0	91.1
0.506	12.0	92.5
0.540	11.1	93.0
0.575	10.3	94.0
0.613	9.8	94.0
0.653	9.4	95.5
0.698	9.2	96.0
0.748	7.9	98.5
0.805	7.3	99.0
0.871	7.0	99.0
0.949	6.5	99.2
1.042	6.3	99.5
1.153	6.0	99.5
1.296	5.7	100.0
1.501	5.4	100.0
1.851	5.1	100.0
2.789	5.0*	20.0*
INTEGRATED REFLECTANCE (PER CENT) →	9.1	90.2

NOTE: INTEGRATED SPECULAR REFLECTANCE = $(90.2 - 9.1)\% = 81.1\%$

* ESTIMATED

TABLE 2. CHARACTERISTICS OF SOLAR ENERGY REFLECTED FORM THE FORWARD RADIATORS FOR VARIOUS PAYLOAD INCLINATION ANGLES

INCLINATION ANGLE (DEG.)		IPS PAYLOAD					
PAYLOAD	SOLAR	MAXIMUM FLUX, BTU/HR. FT ² (W/M ²)		MAXIMUM FLUX, LOCATION * FT (M)		TOTAL ENERGY, ** BTU/HR (W)	
-20	110	0.0	(0.0)	-		0	(0.0)
-15	105	38.3	(120.8)	10.45	(3.19)	139	(40.7)
-10	100	53.0	(167.2)	7.20	(2.19)	879	(257.6)
-5	95	64.2	(202.5)	4.92	(1.50)	1425	(417.5)
0	90	70.7	(223.0)	3.23	(0.98)	1917	(561.7)
10	80	63.8	(201.2)	0.70	(0.21)	2639	(773.2)
20	70	52.9	(166.8)	3.35	(1.02)	2620	(767.7)
30	60	62.0	(195.5)	6.07	(1.85)	2166	(634.7)
40	50	76.0	(239.7)	4.60	(1.40)	1680	(492.3)

* WITH RESPECT TO THE CRUCIFORMS BASEPLATE

** ASSUMING 3.454 X 1.702M. FT PLANE TO REPRESENT PAYLOAD

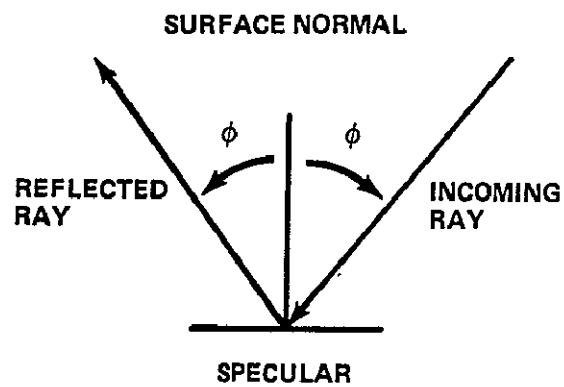
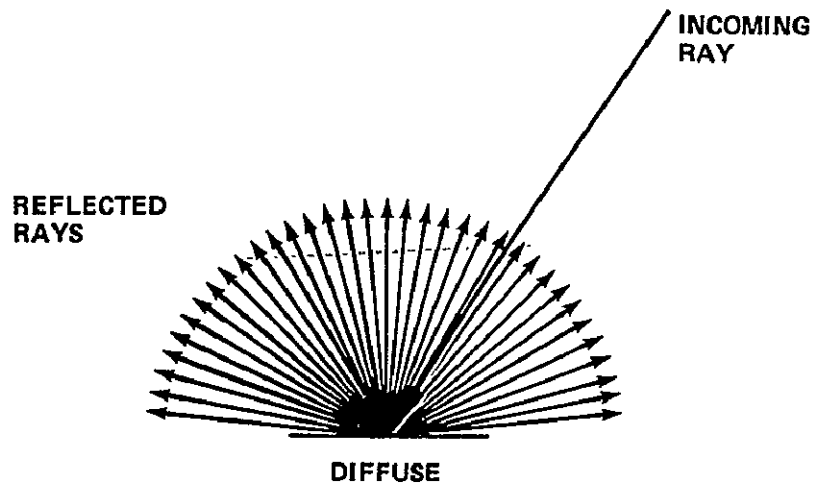


Figure 1. Two dimensional radiation reflection from diffuse and specular surfaces.

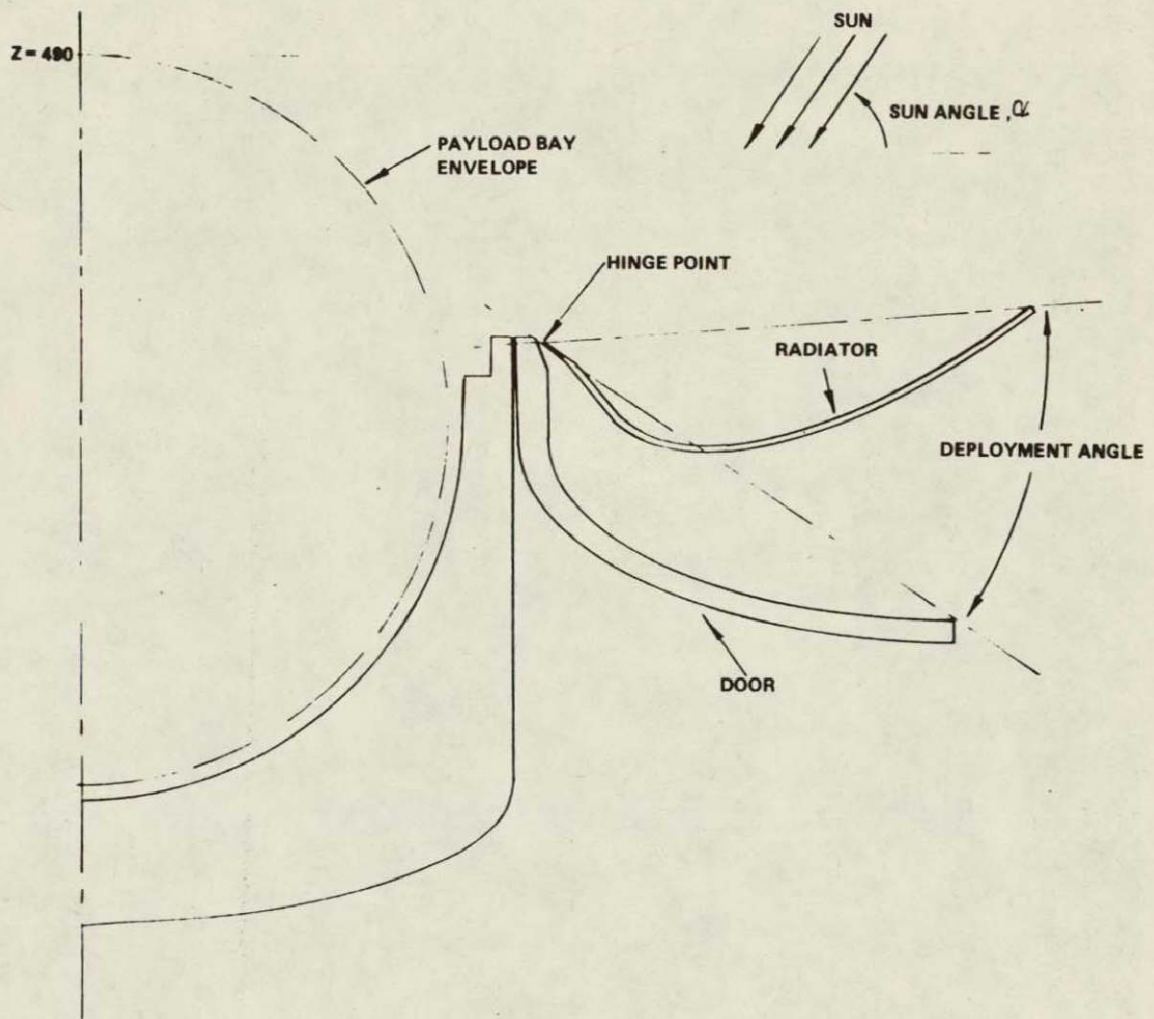
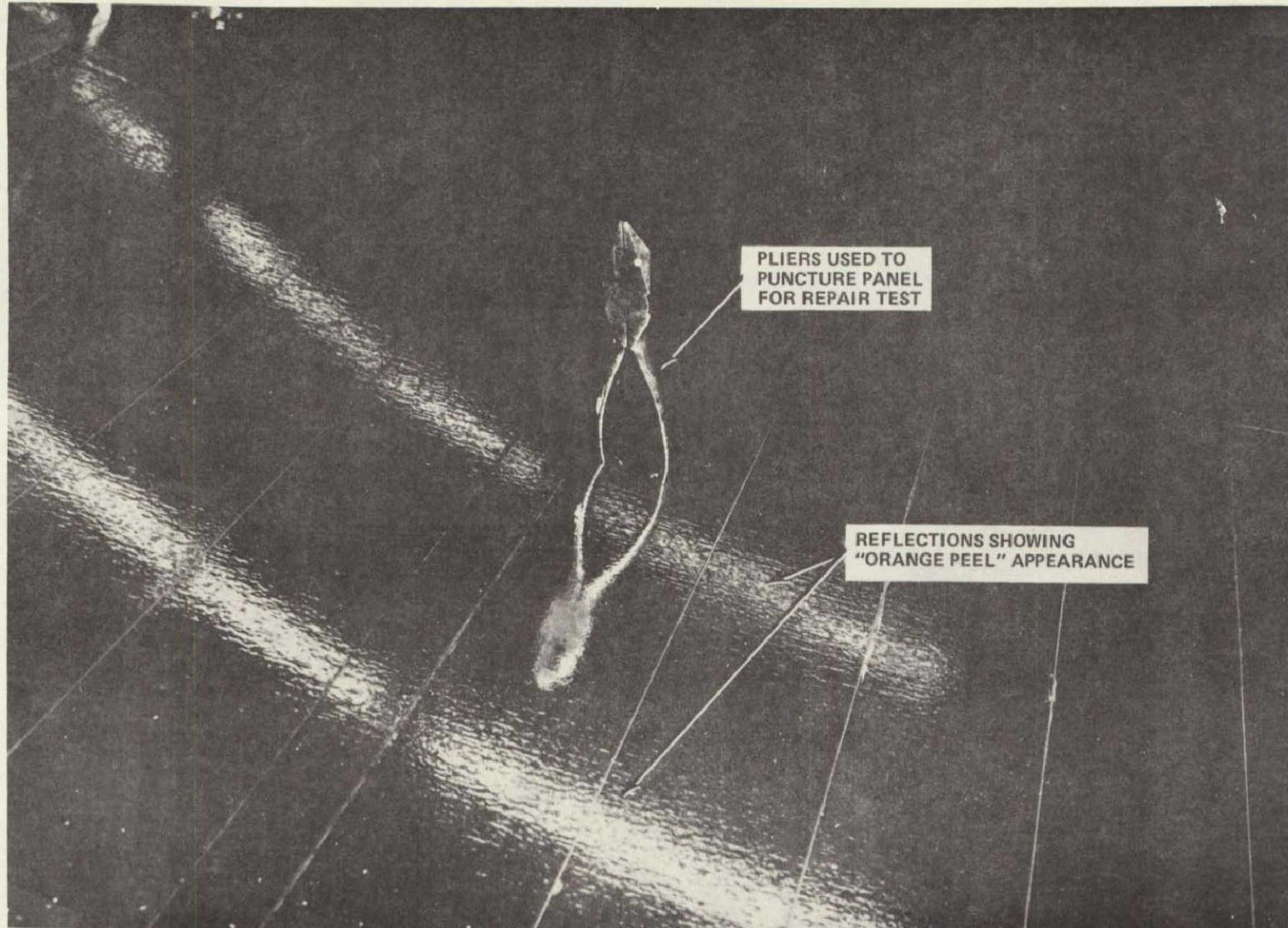


Figure 2. Orbiter geometry and nomenclature used in Northrup study (reference 1).

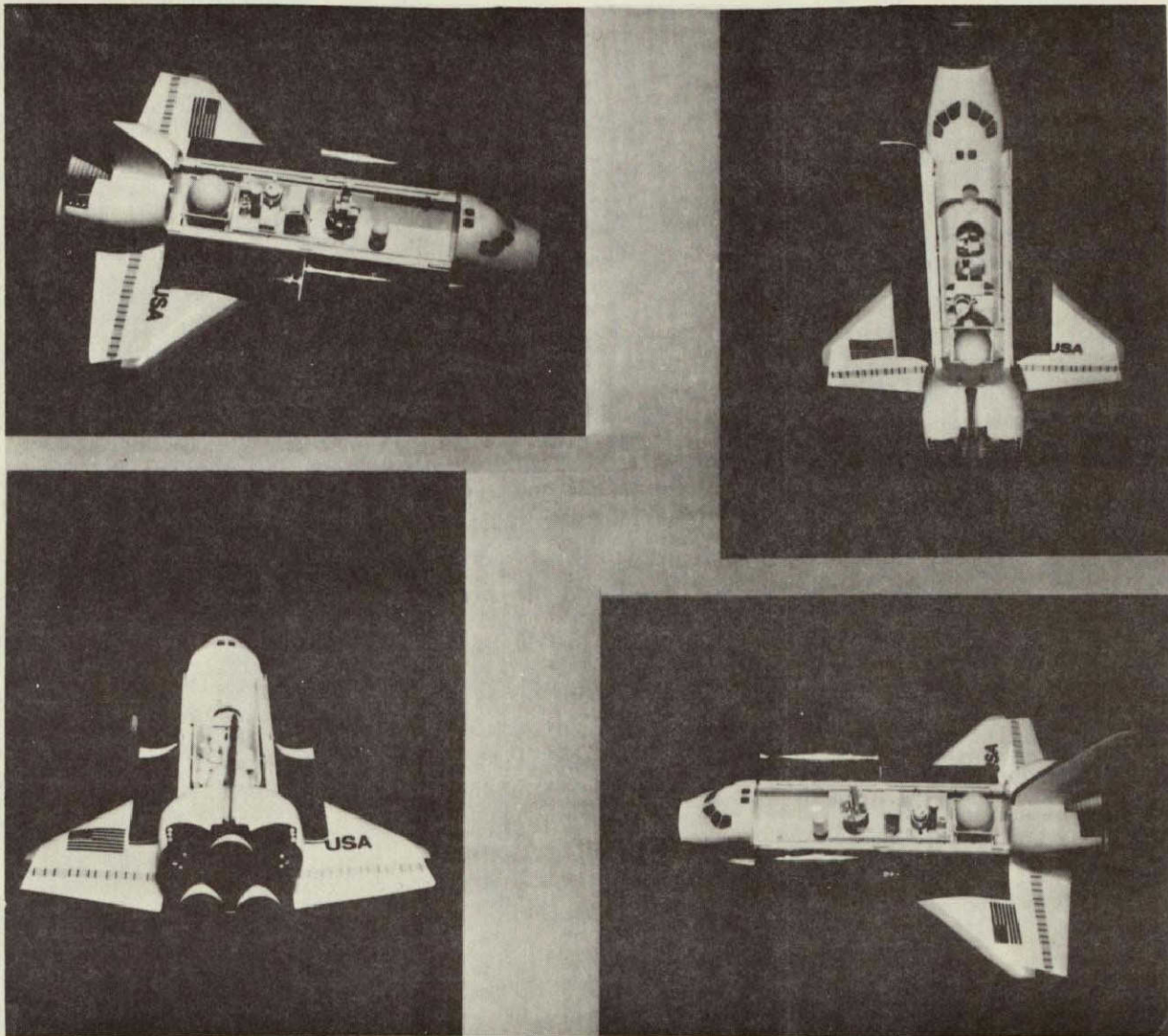


PLIERS USED TO
PUNCTURE PANEL
FOR REPAIR TEST

REFLECTIONS SHOWING
"ORANGE PEEL" APPEARANCE

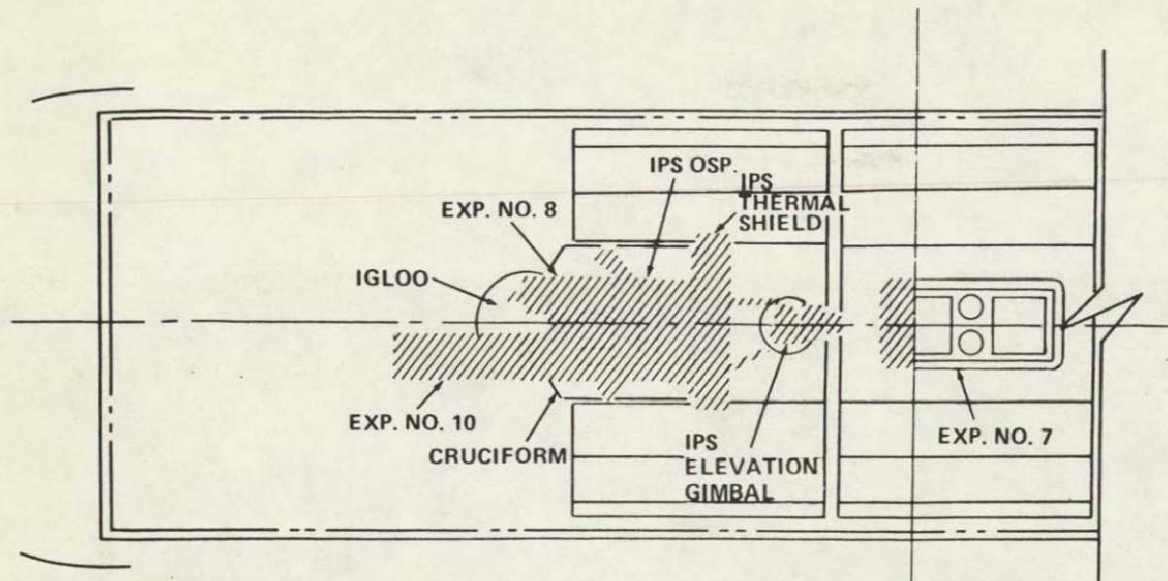
Figure 3. Closeup view of Orbiter radiator panel.

ORIGINAL PAGE IS
OF POOR QUALITY



ORIGINAL PAGE IS
OF POOR QUALITY

Figure 4. Scale model of Orbiter with SL-2 payload configuration.



NOTE: NORMAL IRRADIATION
ZONE OF FORWARD RADIATORS
CROSSHATCHED

← FORWARD

NOTE: STATION NUMBERS ARE GIVEN
IN INCHES (CM.)

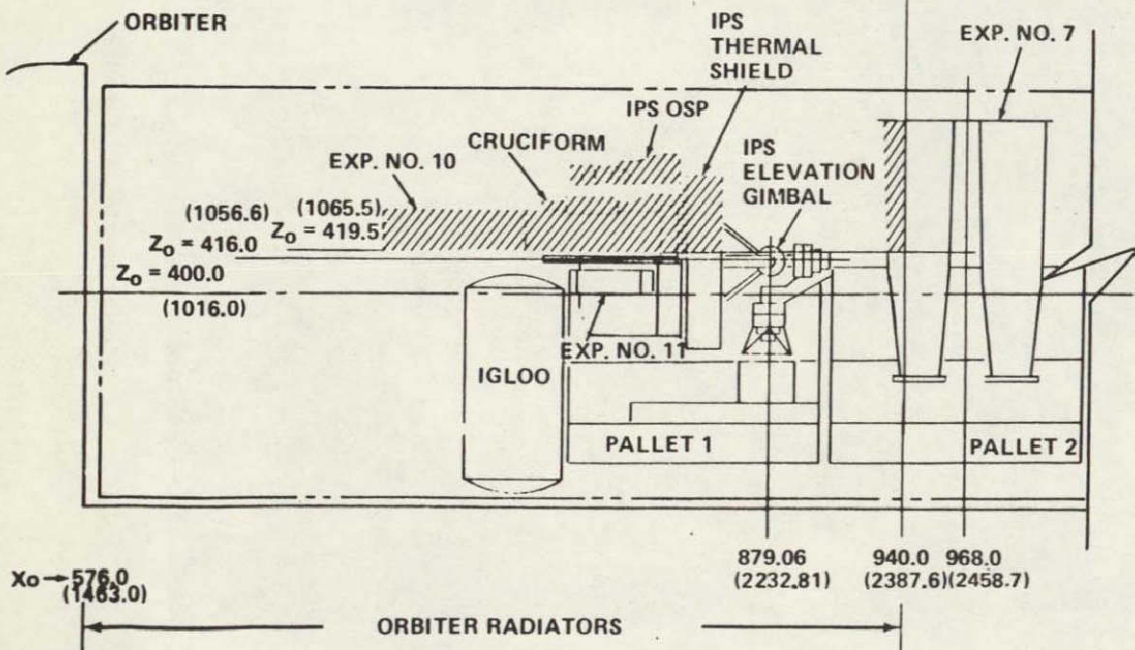


Figure 5. SL-2 payload irradiated by forward Orbiter radiators in stowed configuration.

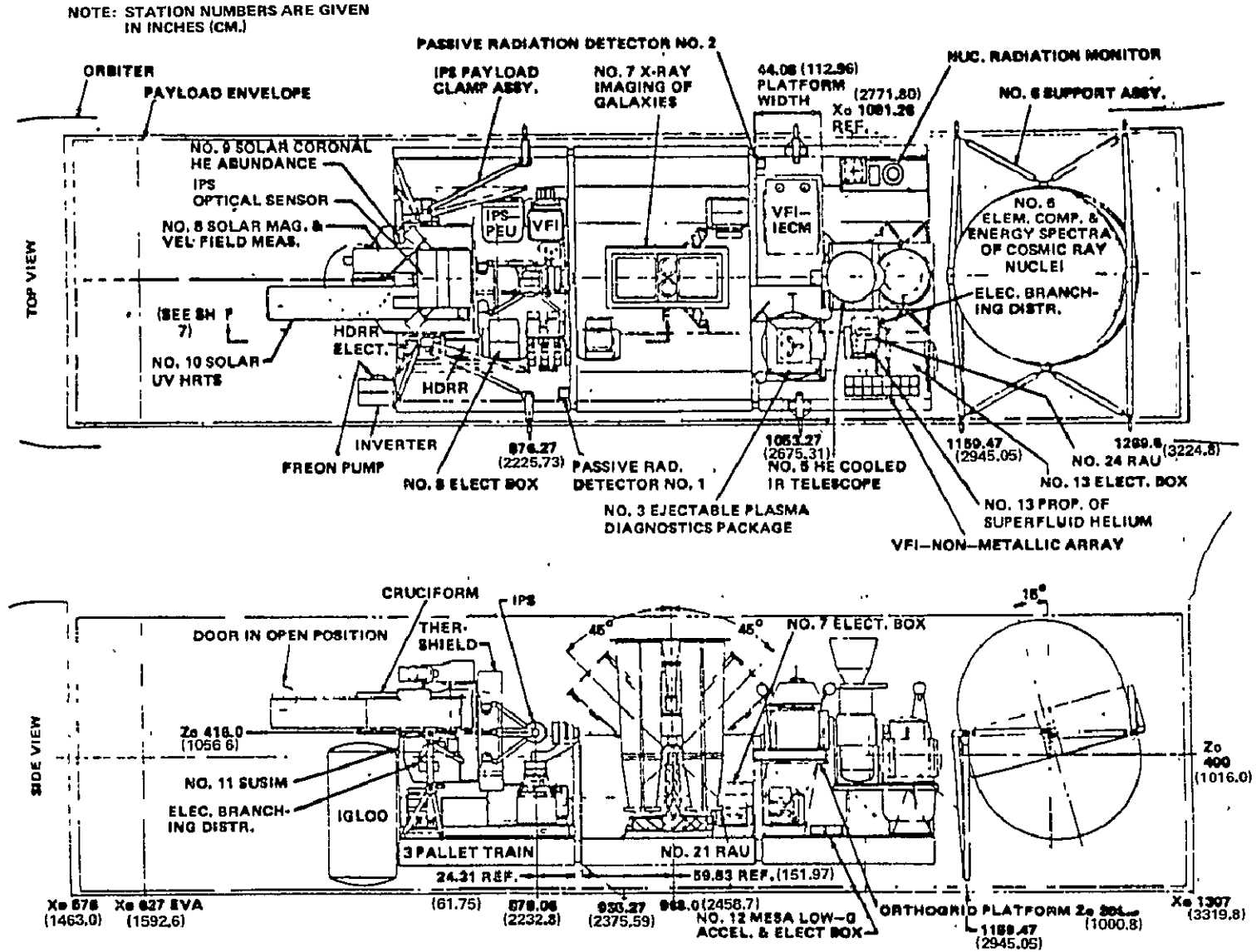


Figure 7. Overall payload configuration, SL-2.

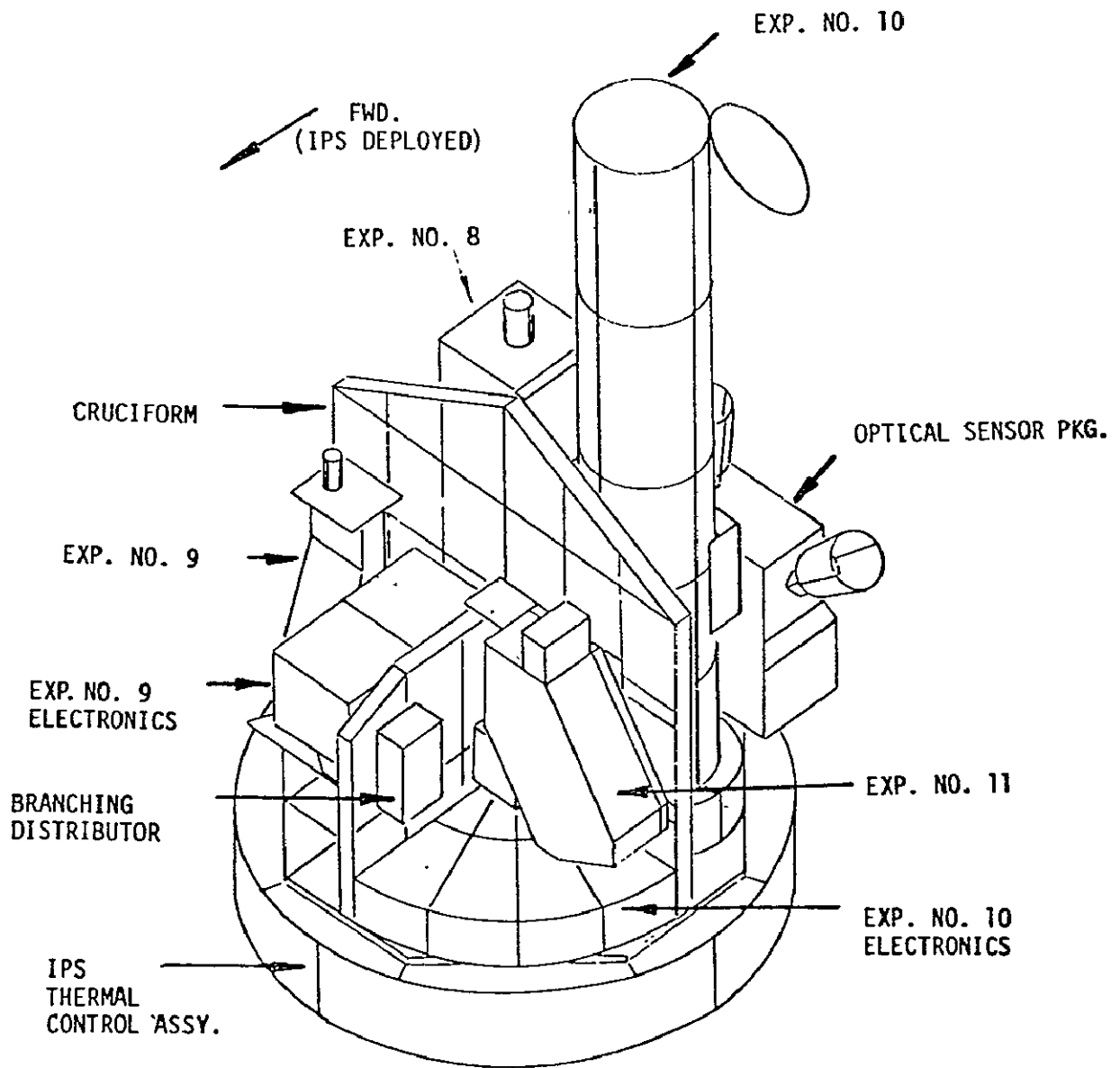


Figure 8. Cruciform/experiment configuration.

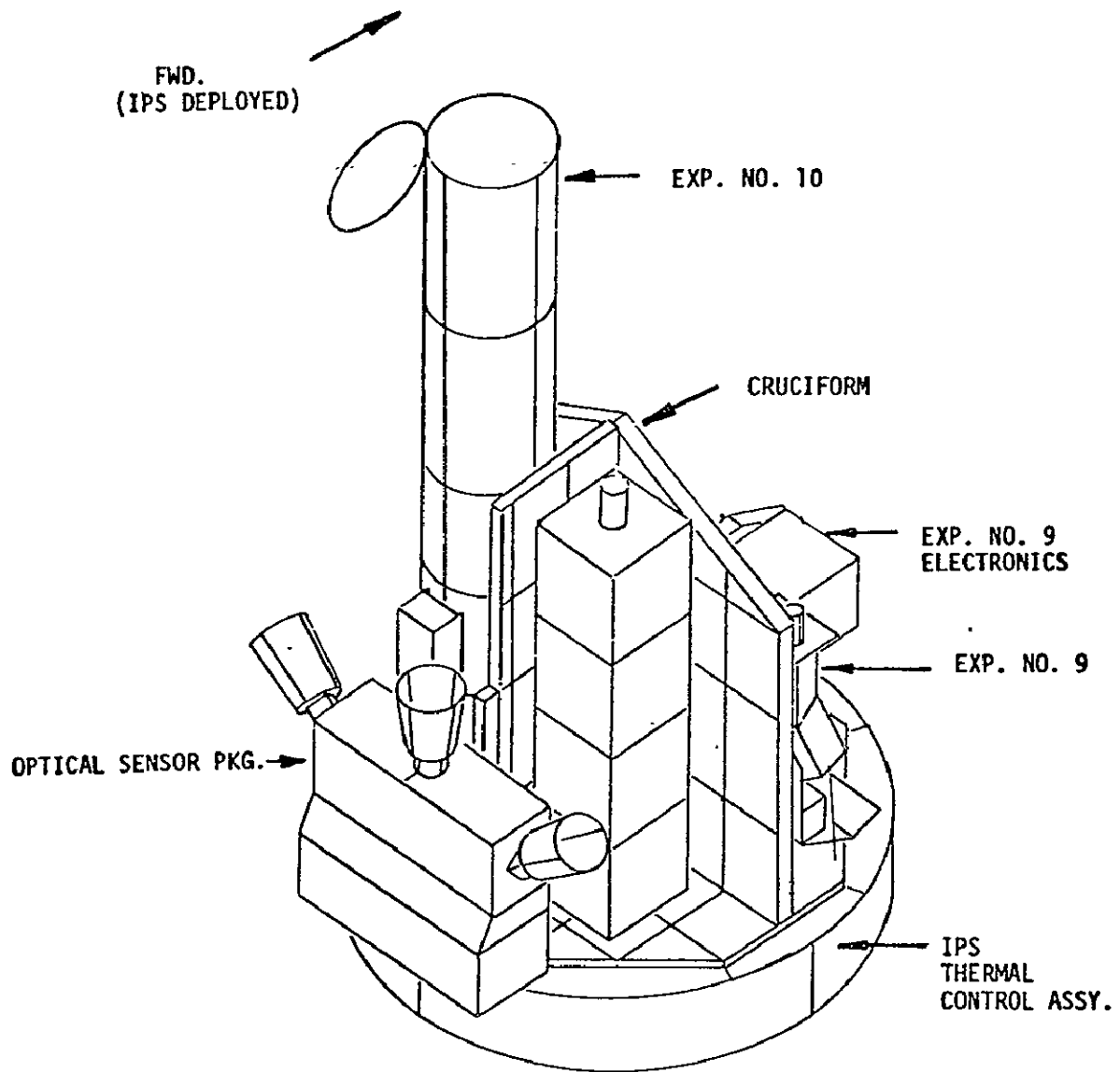


Figure 8. (Concluded).

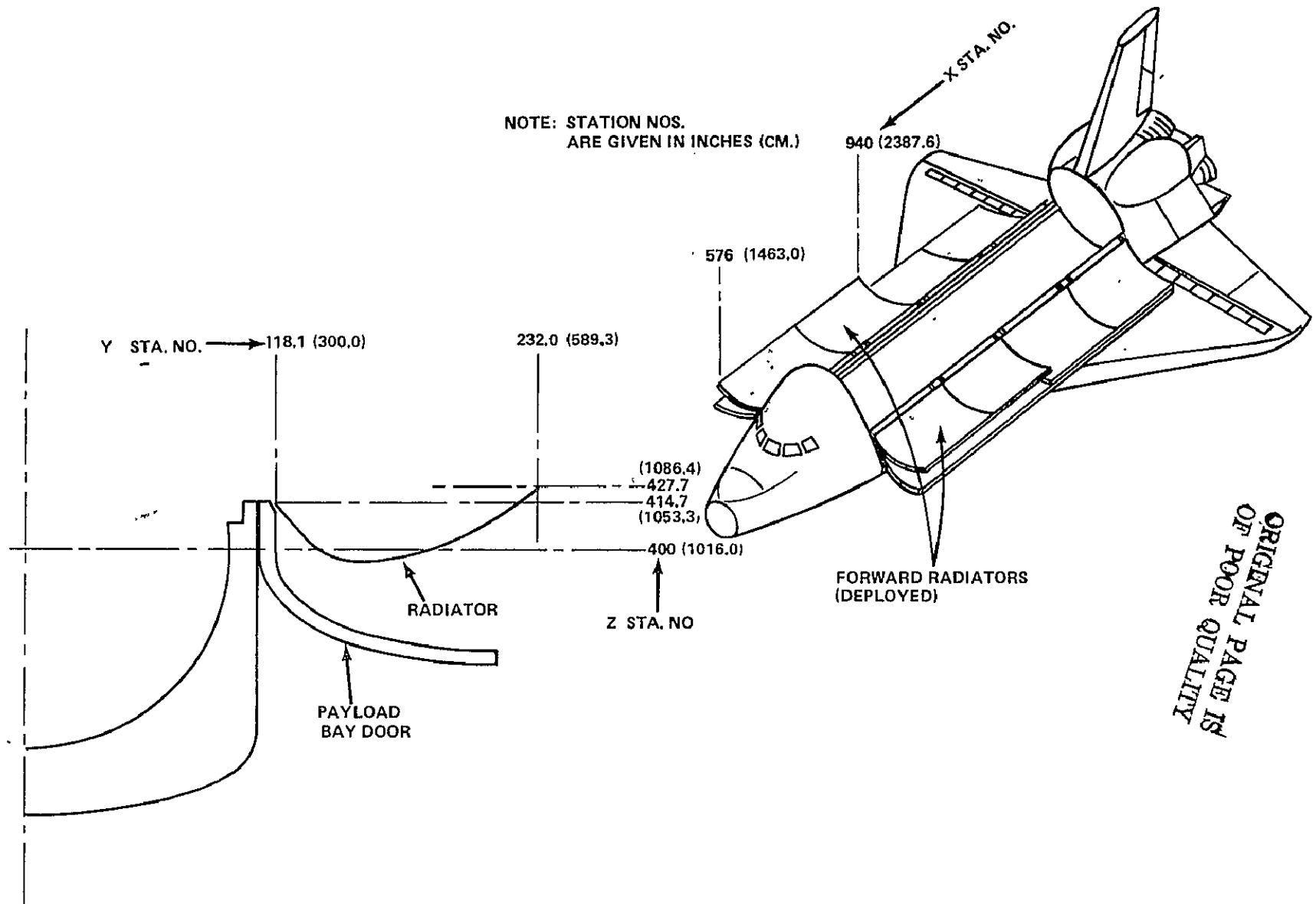


Figure 9. Deployed forward Orbiter radiators.

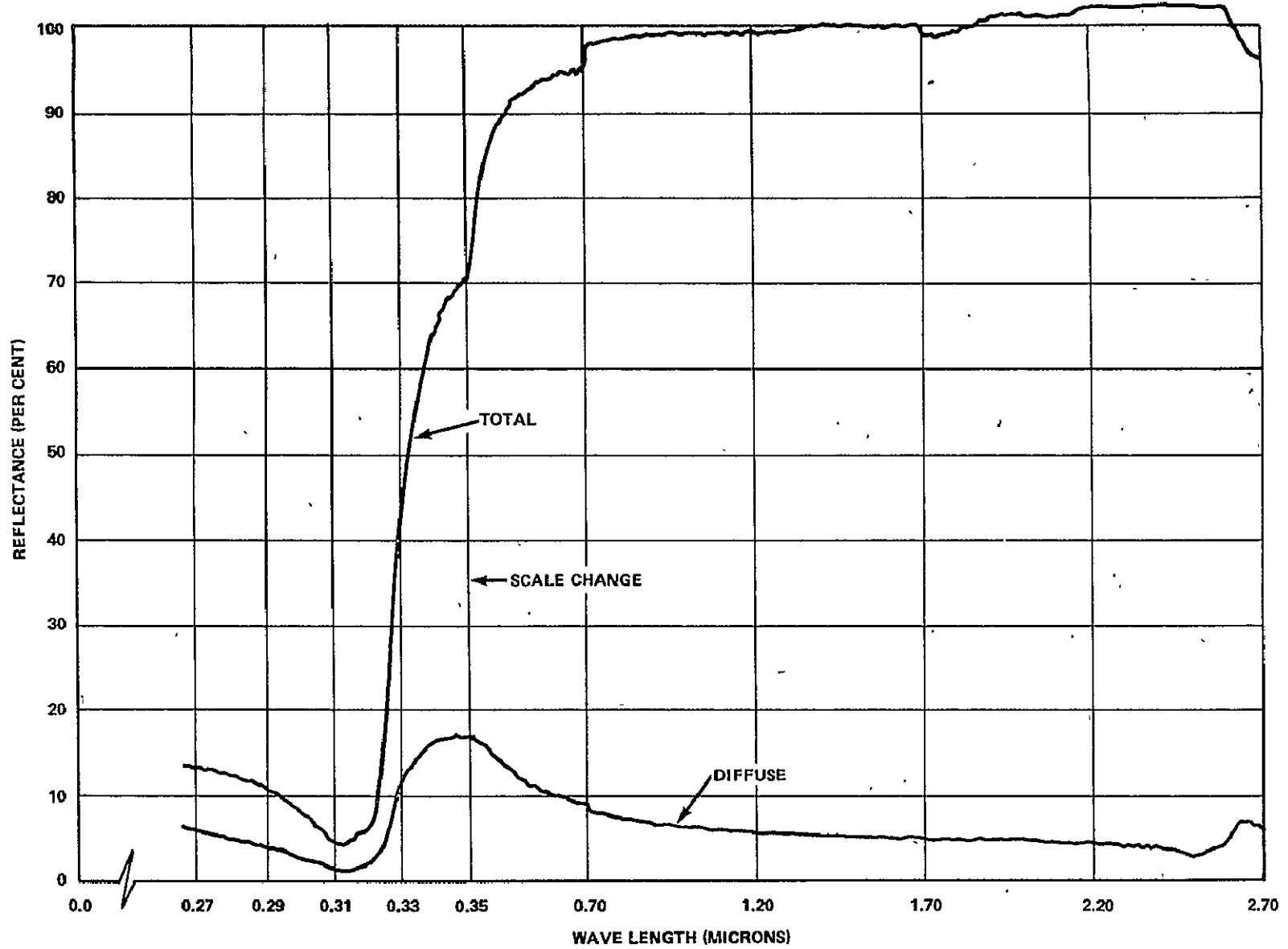


Figure 10. Solar reflectance versus wavelength for silver-Teflon sample.

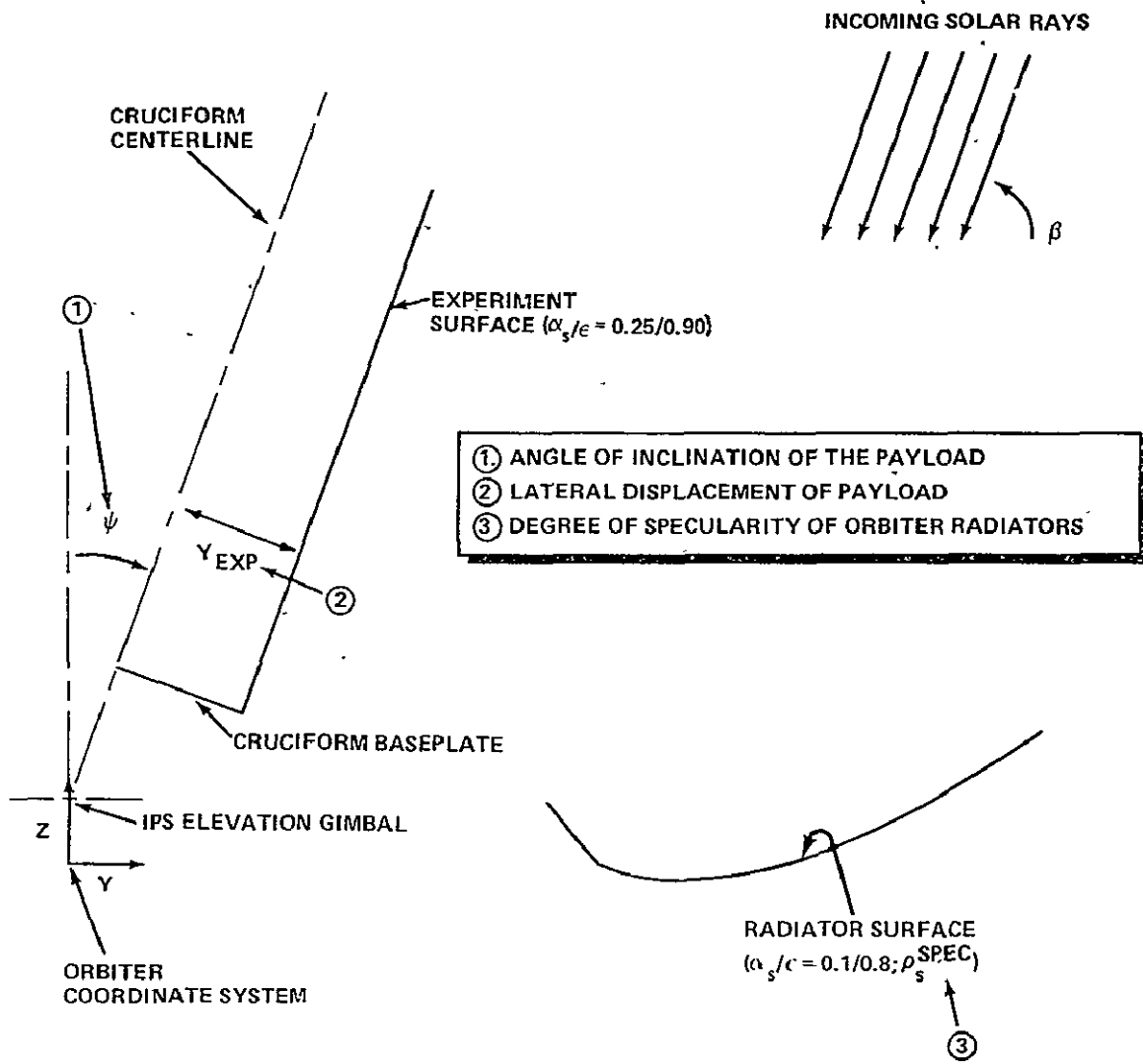


Figure 11. Parameters investigated in specular radiation study.

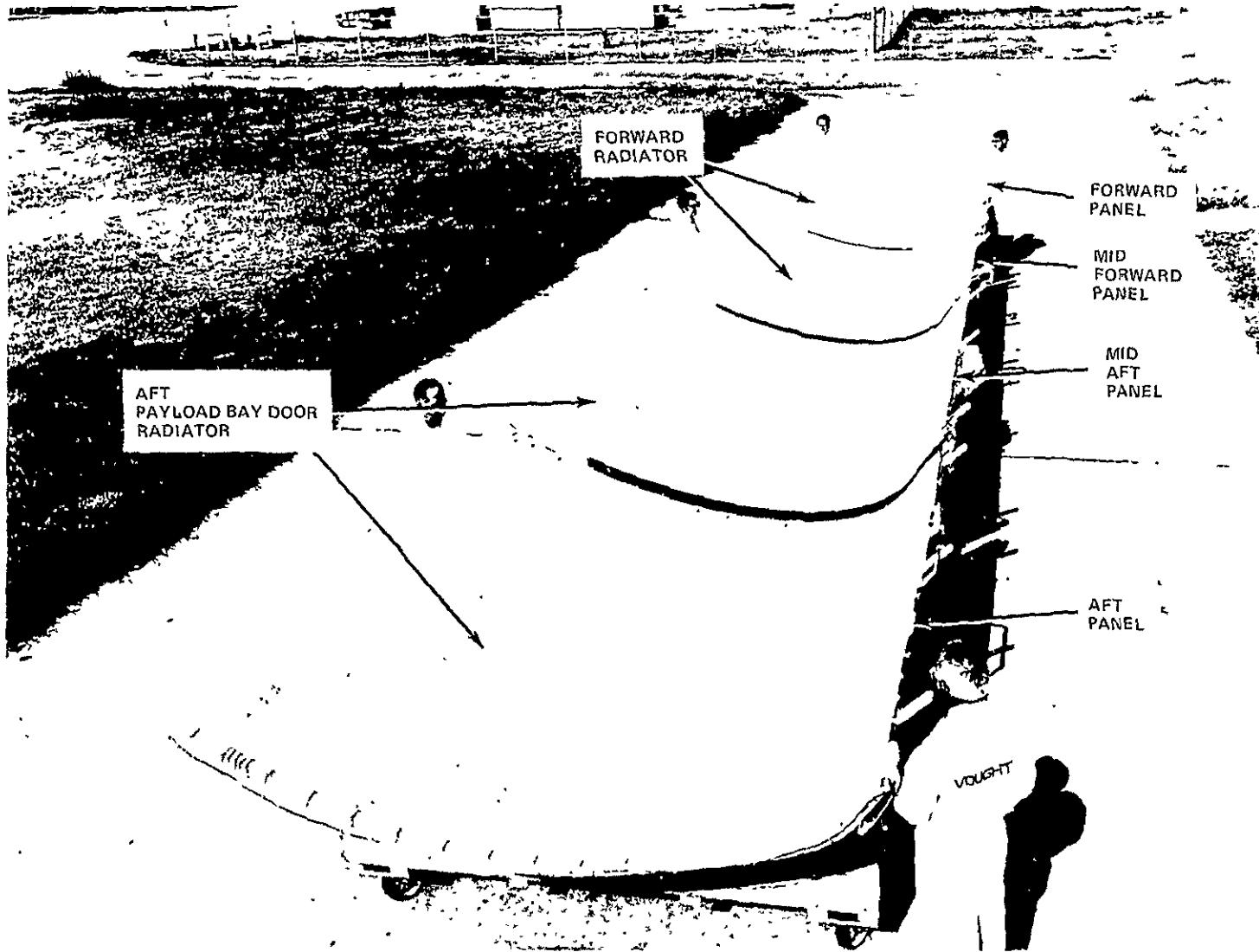


Figure 12. Orbiter port radiator panels.

ORIGINAL PAGE IS
OF POOR QUALITY

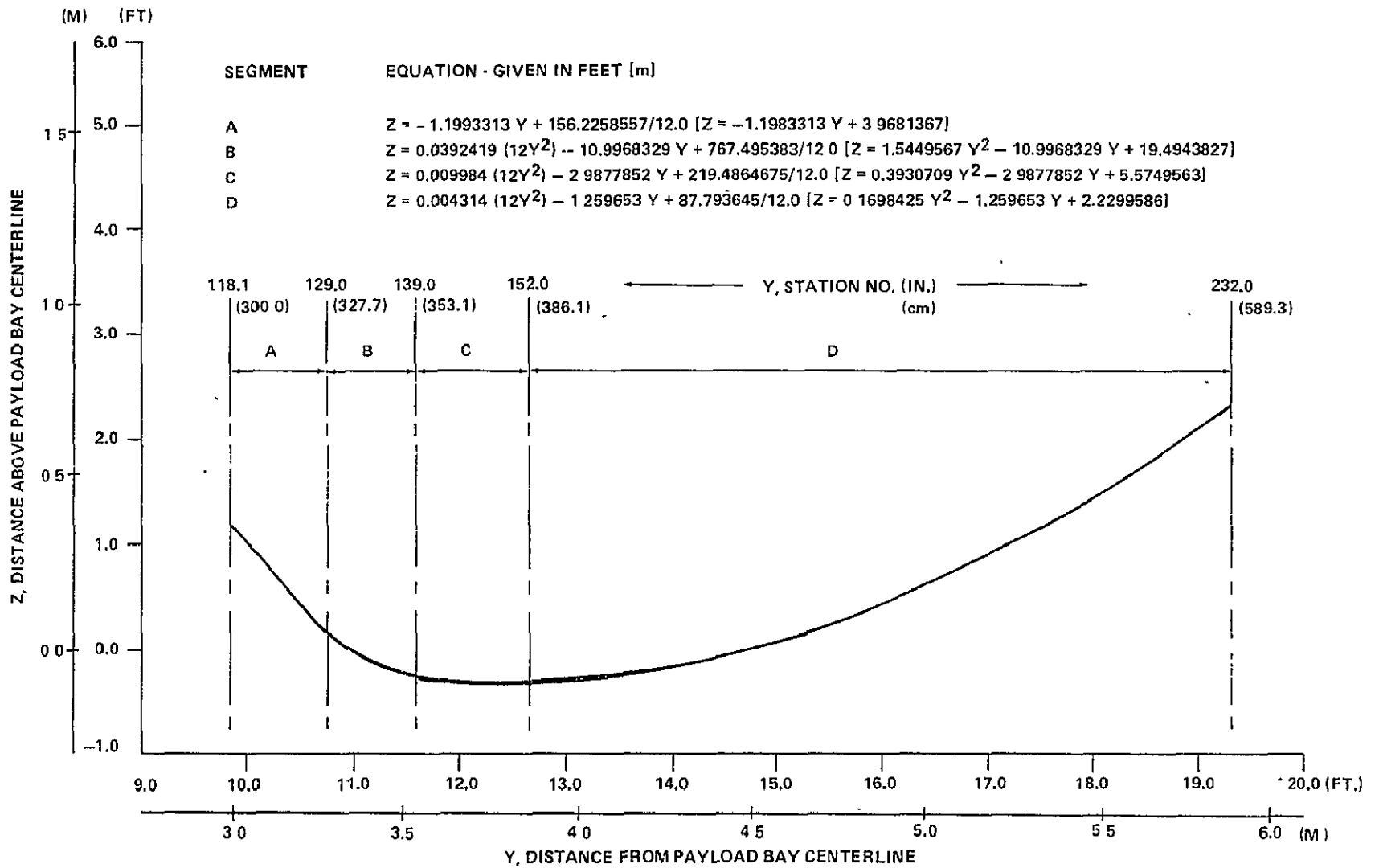
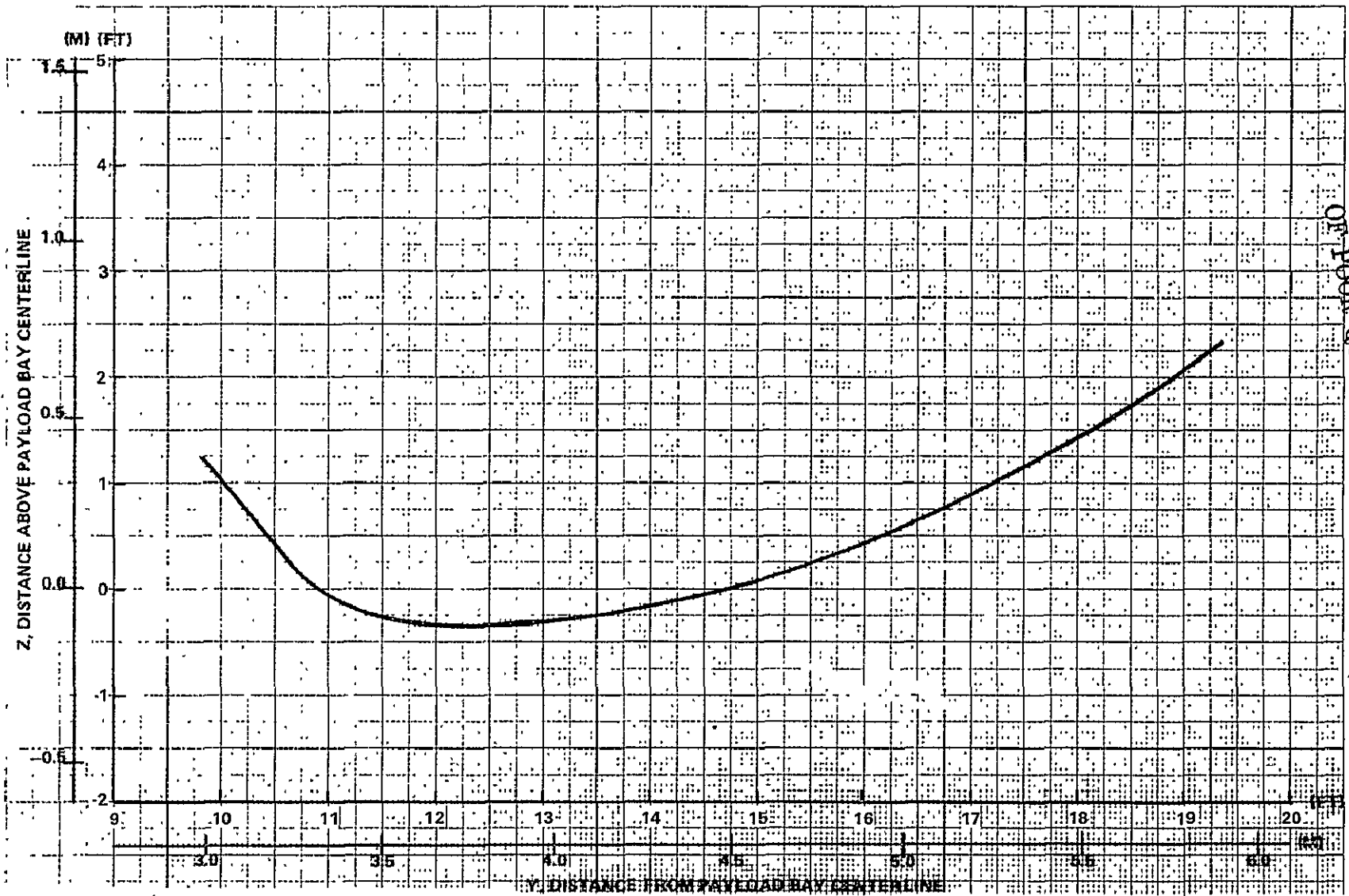


Figure 13. Forward Orbiter radiator contour (mid forward panel) as defined by Rockwell supplied equations.



ORIGINAL PAGE IS
OF POOR QUALITY

Figure 15. "Smoothed" contour of forward Orbiter radiator (mid forward panel).

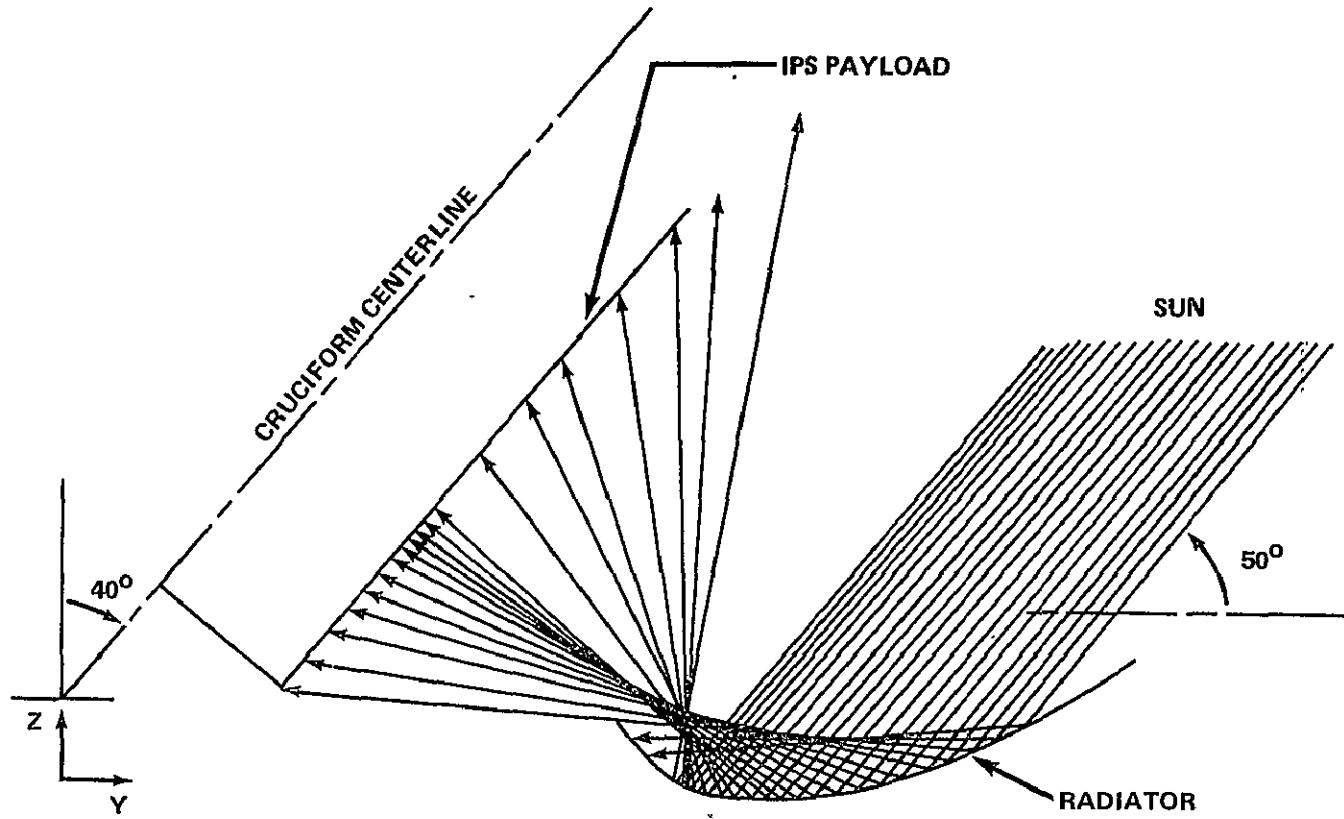


Figure 16. Energy reflected from radiator for configuration studied that created narrowest cavity.

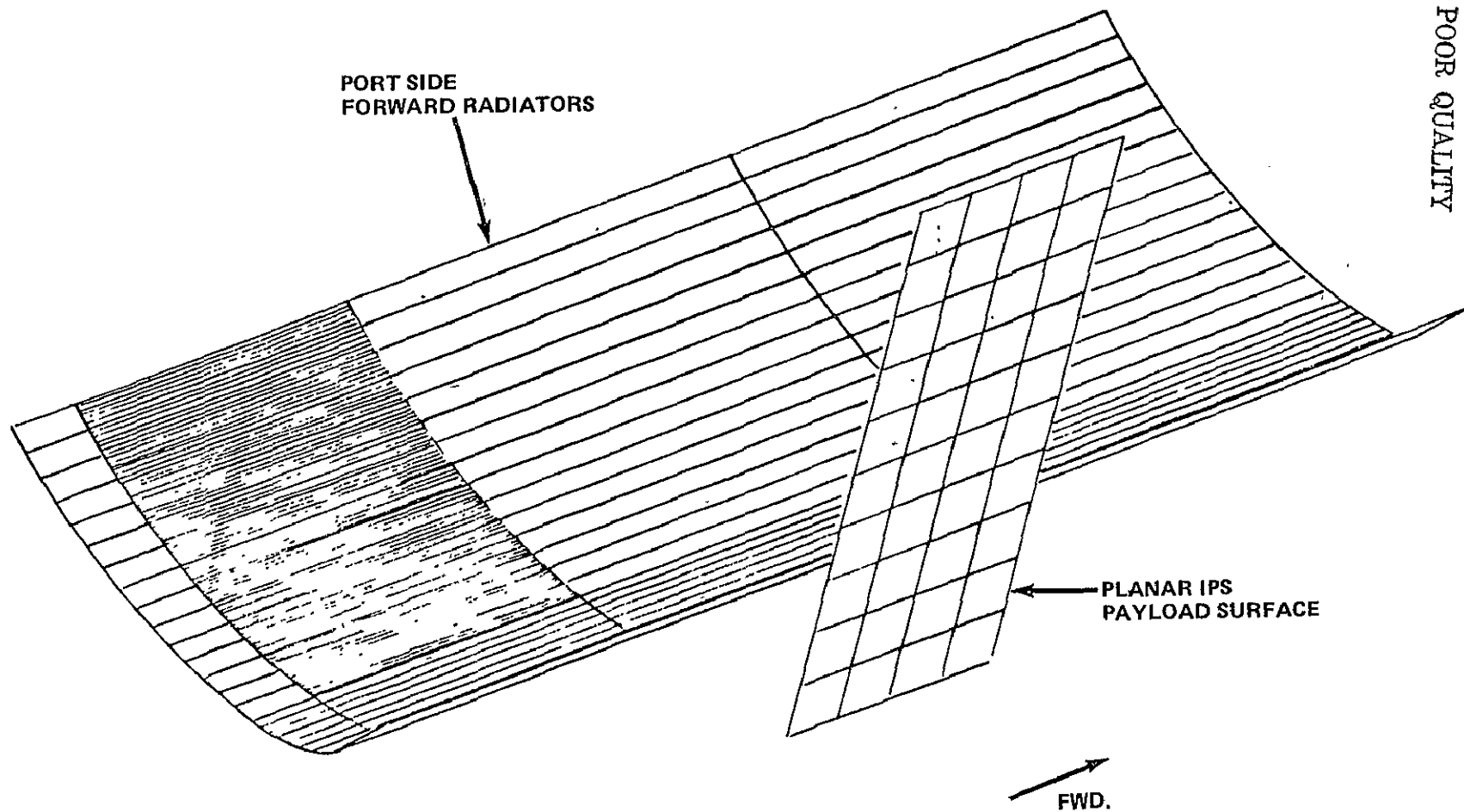


Figure 17. Three-dimensional TRASYS II based model.

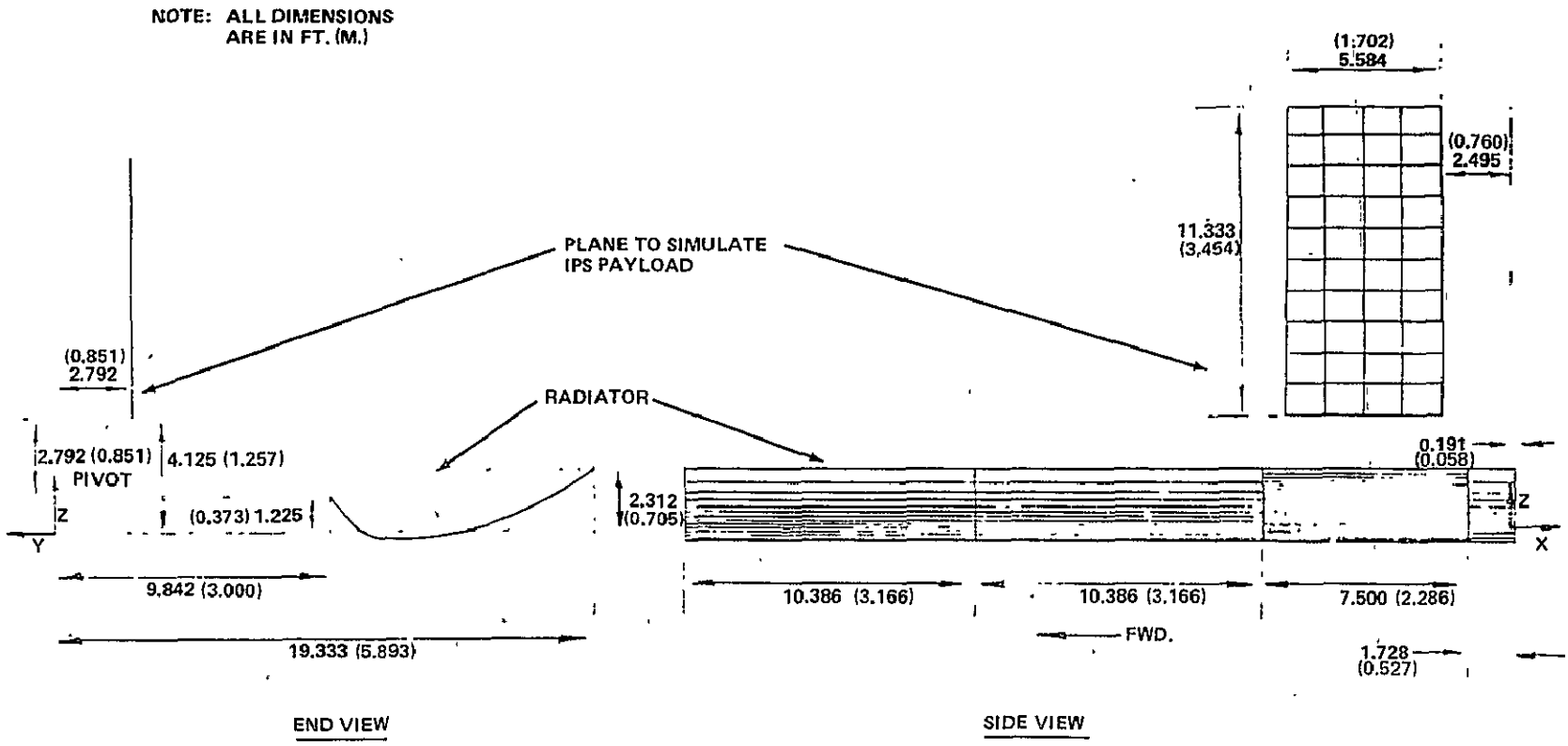


Figure 18. Geometry used in three-dimensional TRASYS II based model.

- NOTES:
- ALL DIMENSIONS ARE IN FT. (M.)
 - GEOMETRY AS VIEWED ALONG X AXIS IS SAME AS SHOWN IN FIGURE 18

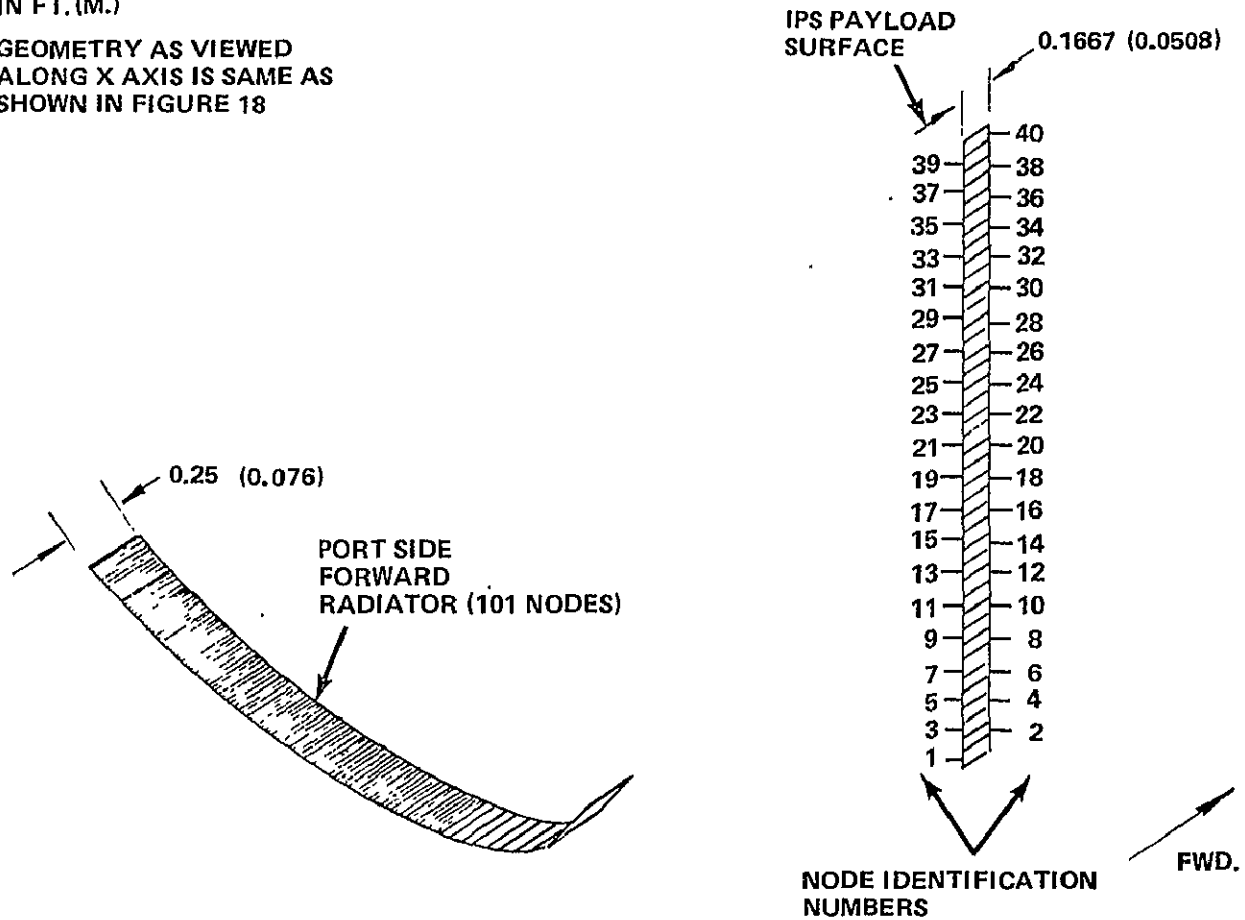


Figure 19. "Two-dimensional" TRASYS II based model.

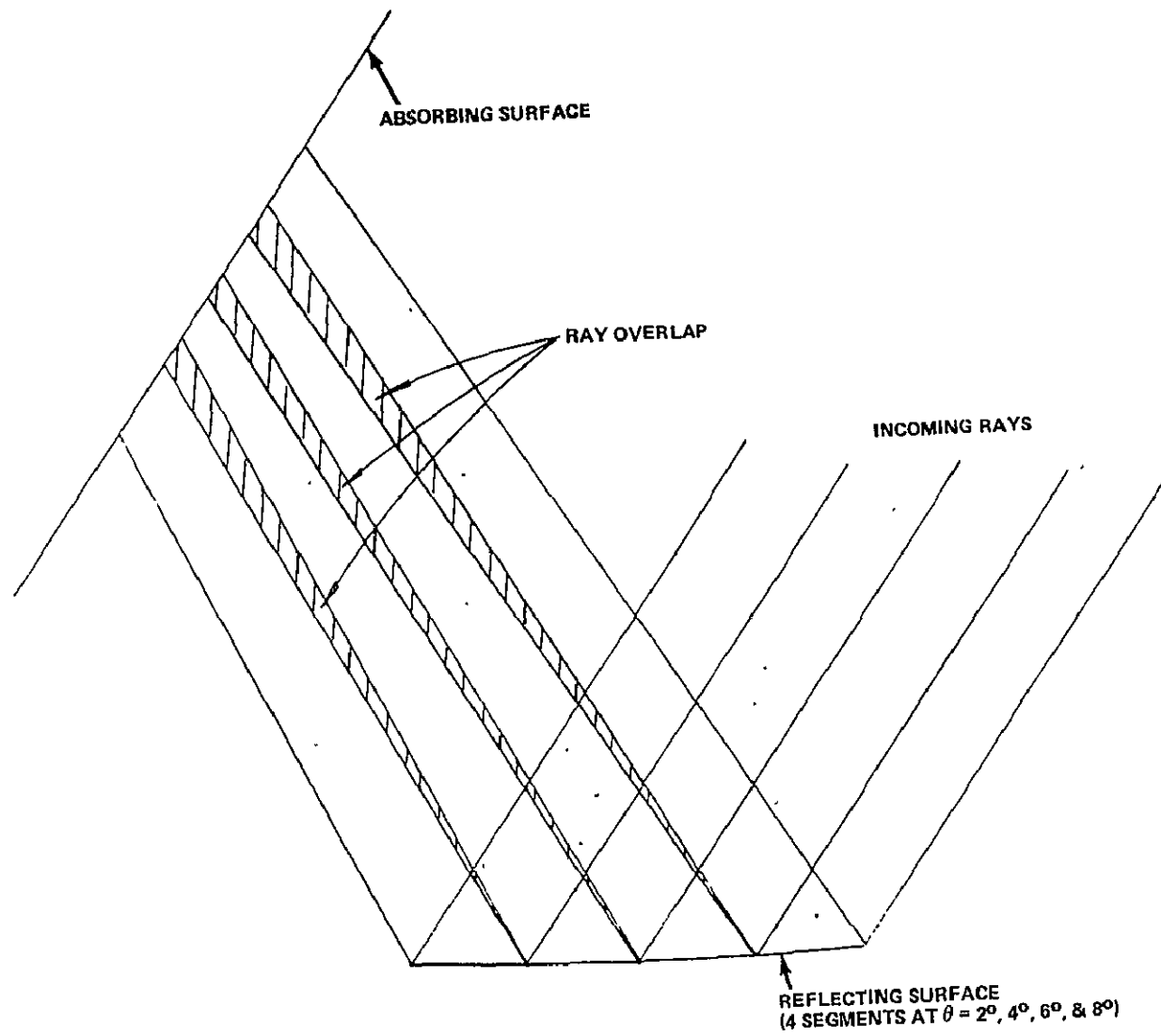


Figure 20. Reflected ray overlap characteristic of TRASYS II based models.

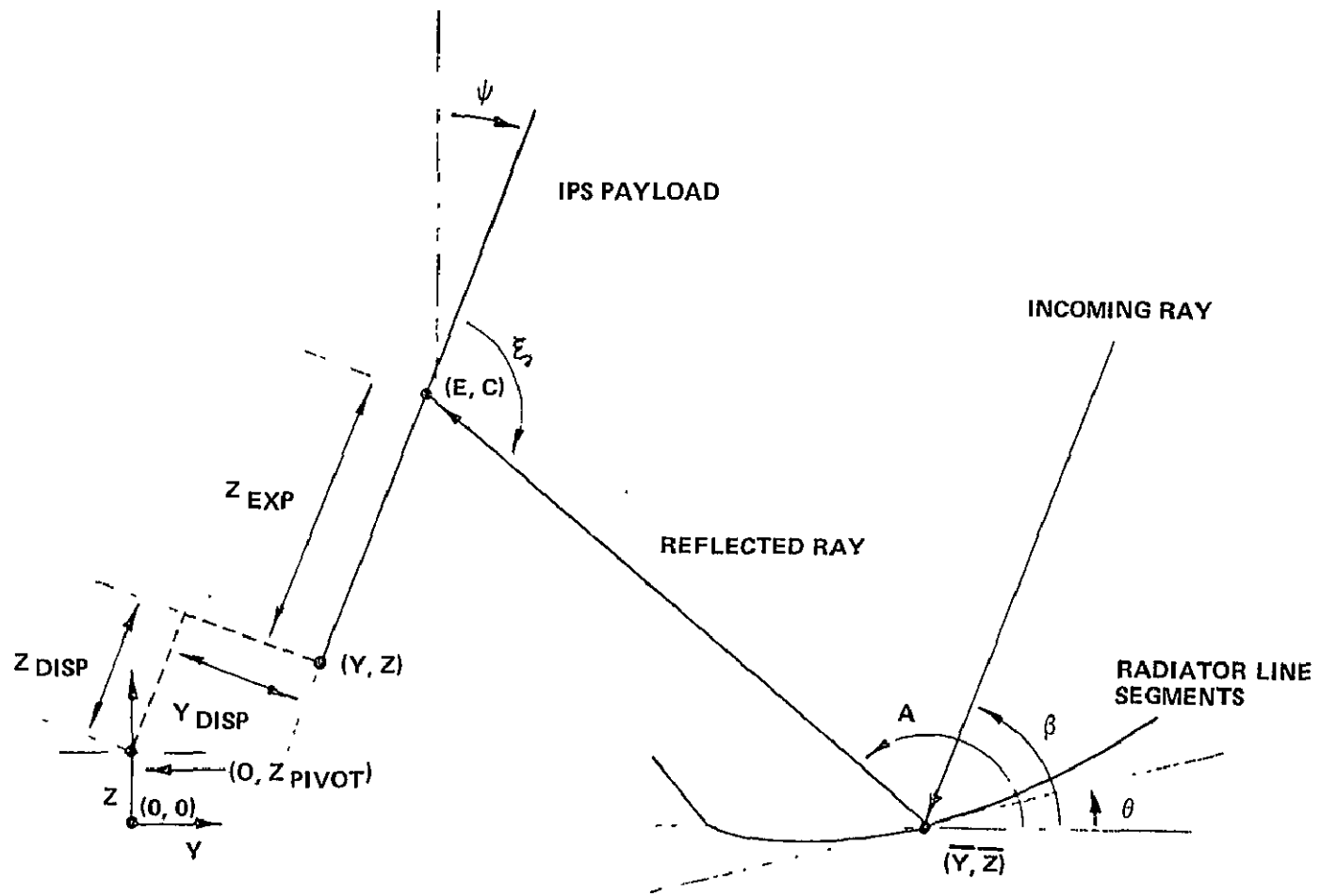
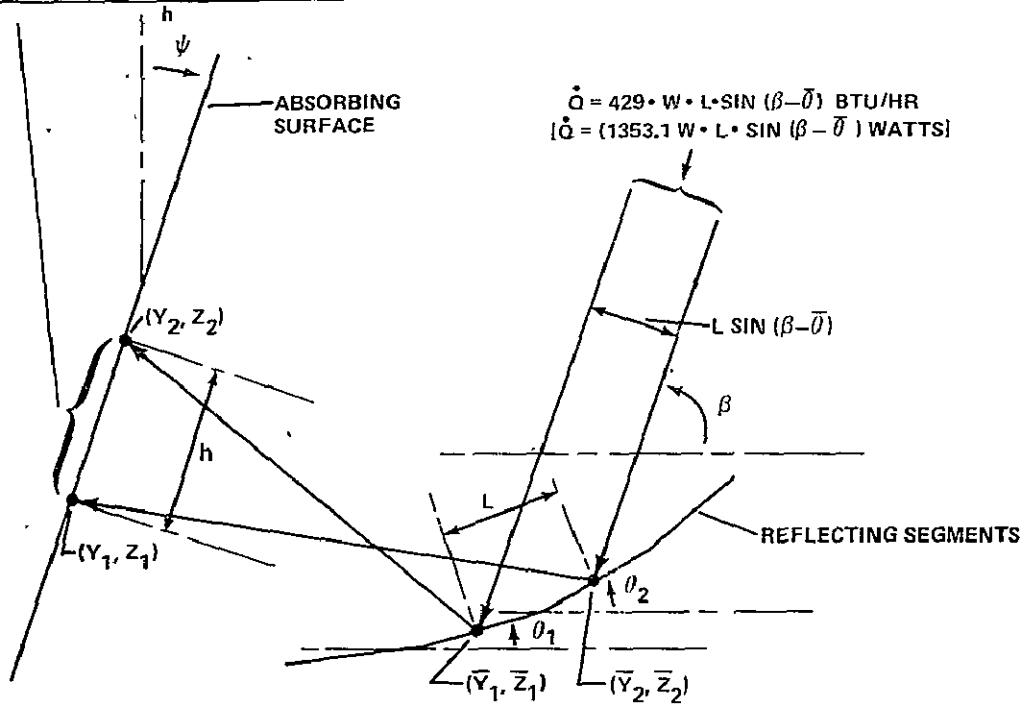


Figure 21. Two-dimensional specular heat flux program geometry.

NOTE: $\alpha = 0.25$ (ABSORBING SURFACE)
 $\rho = 0.90$ (REFLECTING SEGMENT)

$$\dot{Q}/a = \frac{(429) (0.25) (0.9) L \cdot \sin(\beta - \bar{\theta})}{h} \text{ BTU/HR} \cdot \text{FT}^2$$

$$[\dot{Q}/a = \frac{(1353.1) (.25) (.9) L \cdot \sin(\beta - \bar{\theta})}{h} \text{ W/M}^2]$$



NOTES:

- $L = \sqrt{(\bar{Y}_2 - \bar{Y}_1)^2 + (\bar{Z}_2 - \bar{Z}_1)^2}$
- $\bar{\theta} = (\theta_1 + \theta_2) / 2$
- W = WIDTH
- $h = \sqrt{(Y_2 - Y_1)^2 + (Z_2 - Z_1)^2}$

Figure 22. Heat flux calculation in the two dimensional specular heat flux program.

ORIGINAL PAGE IS
OF POOR QUALITY

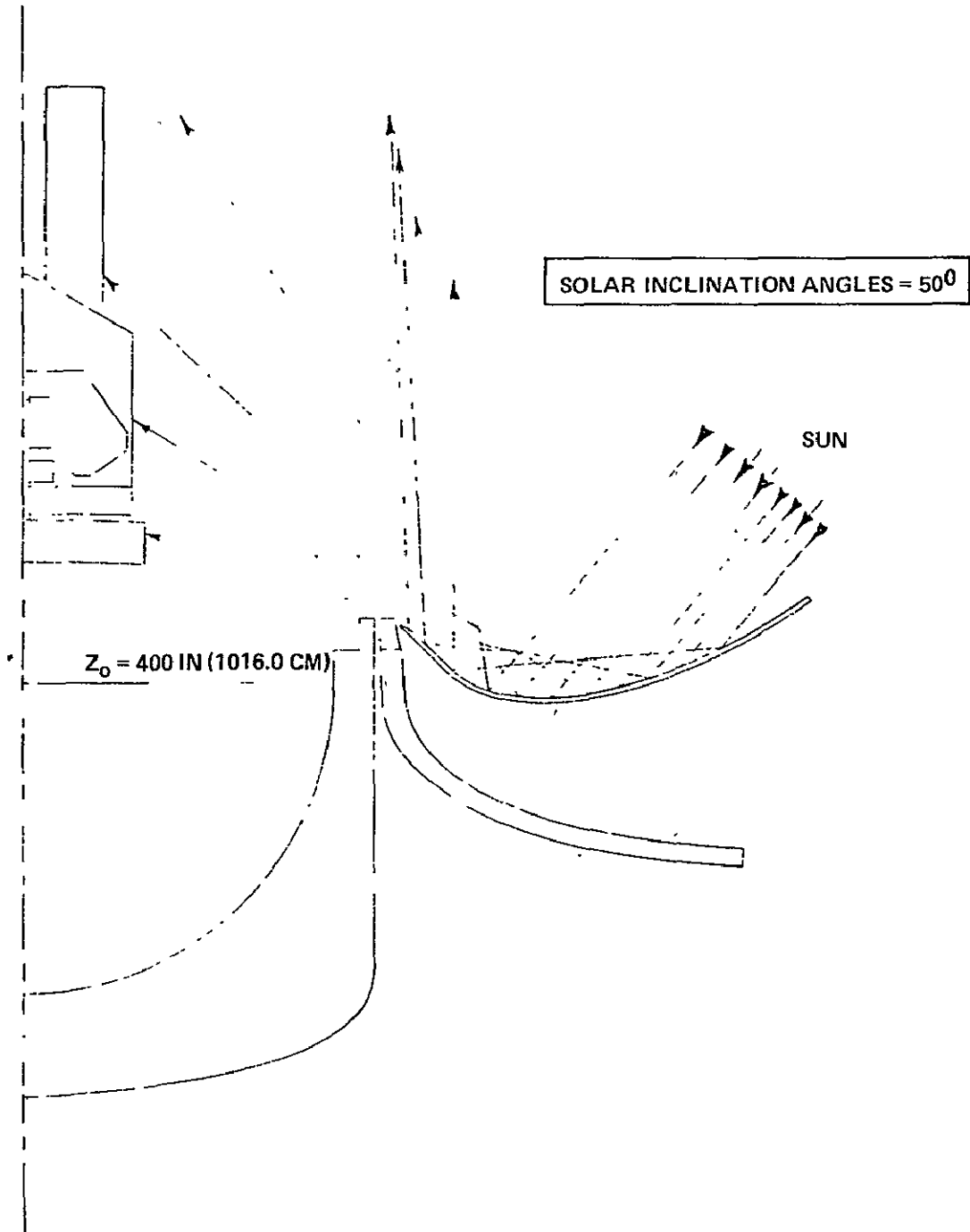


Figure 23. Manual tracings of reflected solar rays from the Orbiter radiator; fixed IPS.

ORIGINAL PAGE IS
OF POOR QUALITY

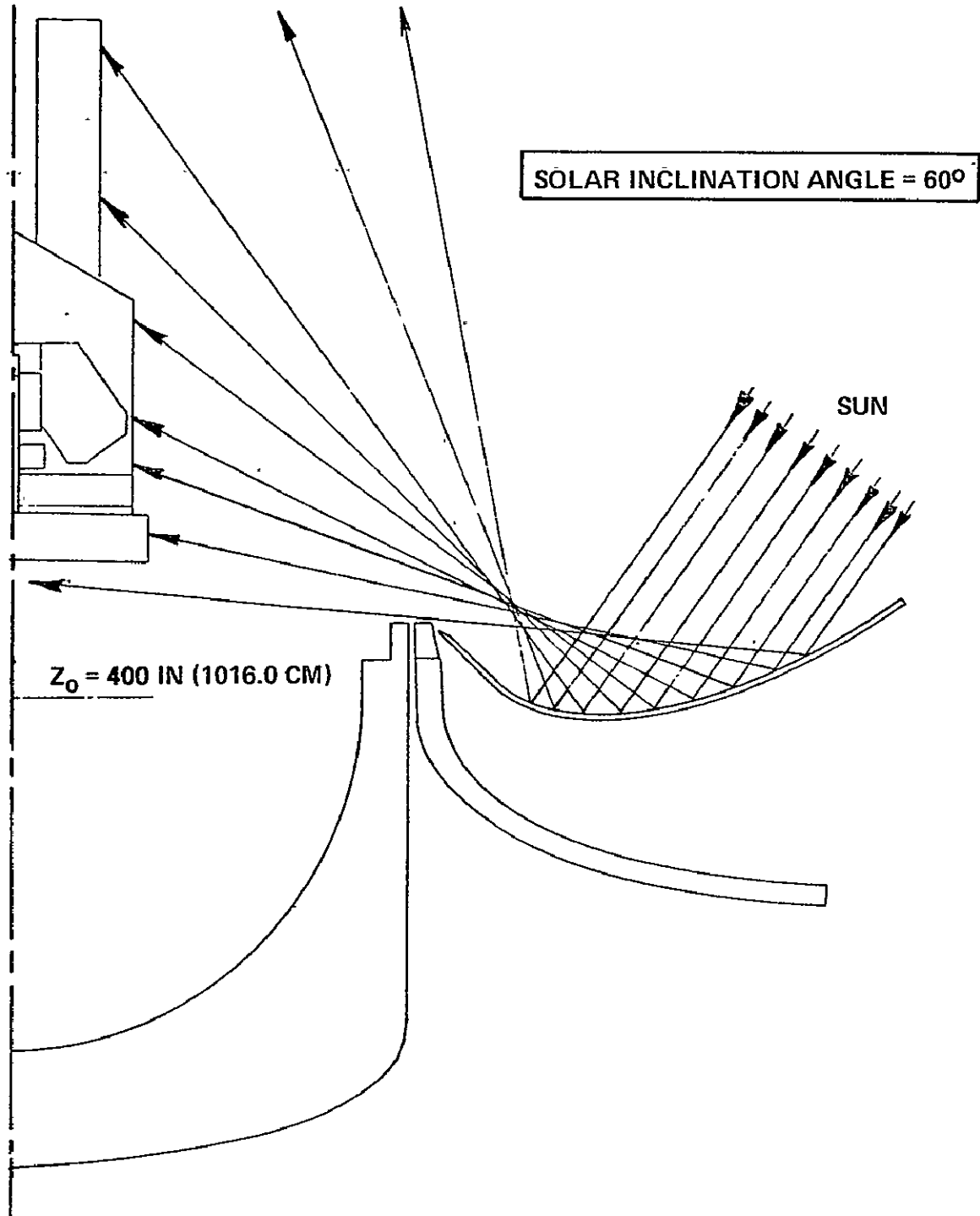


Figure 23. (Continued).

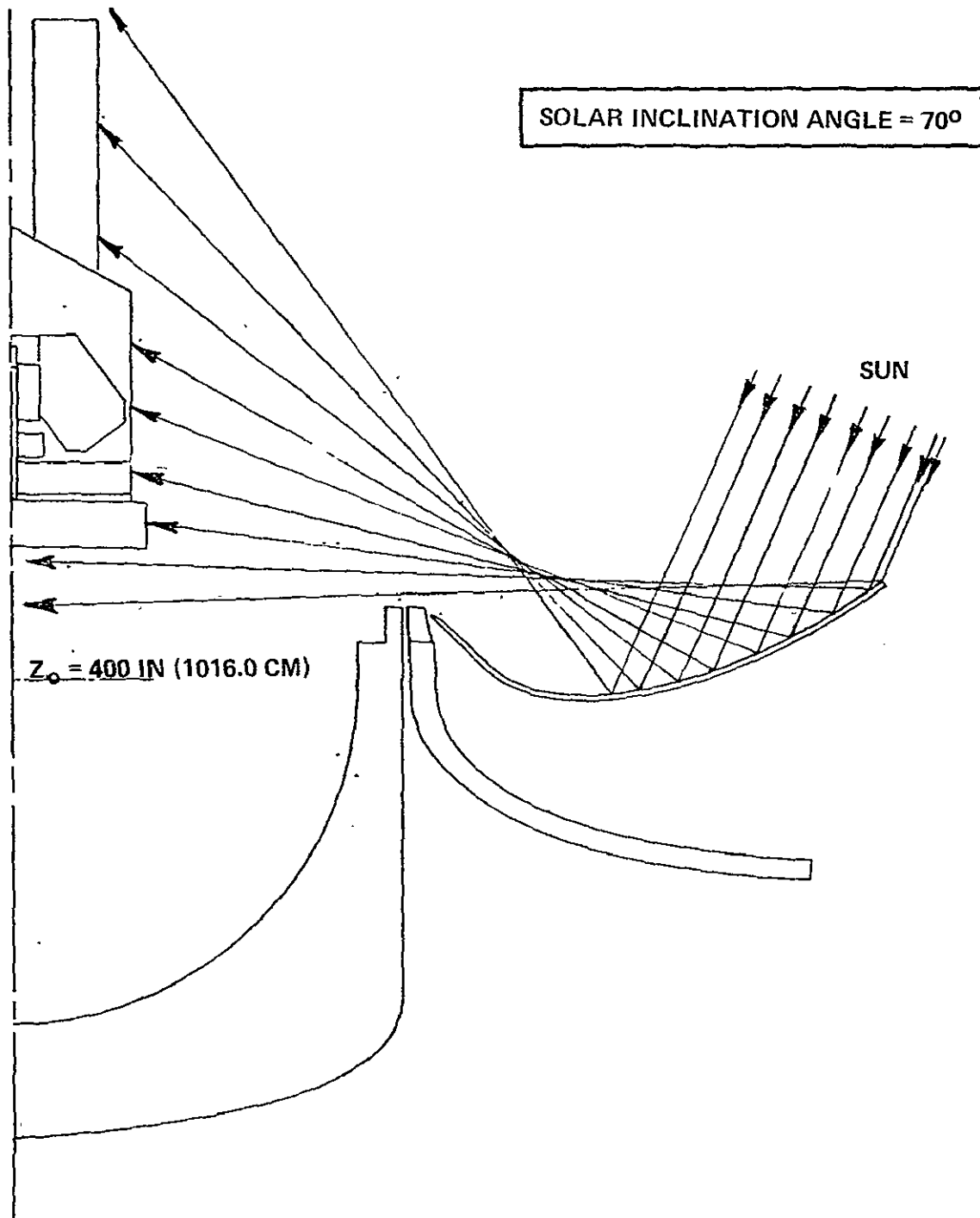


Figure 23. (Continued).

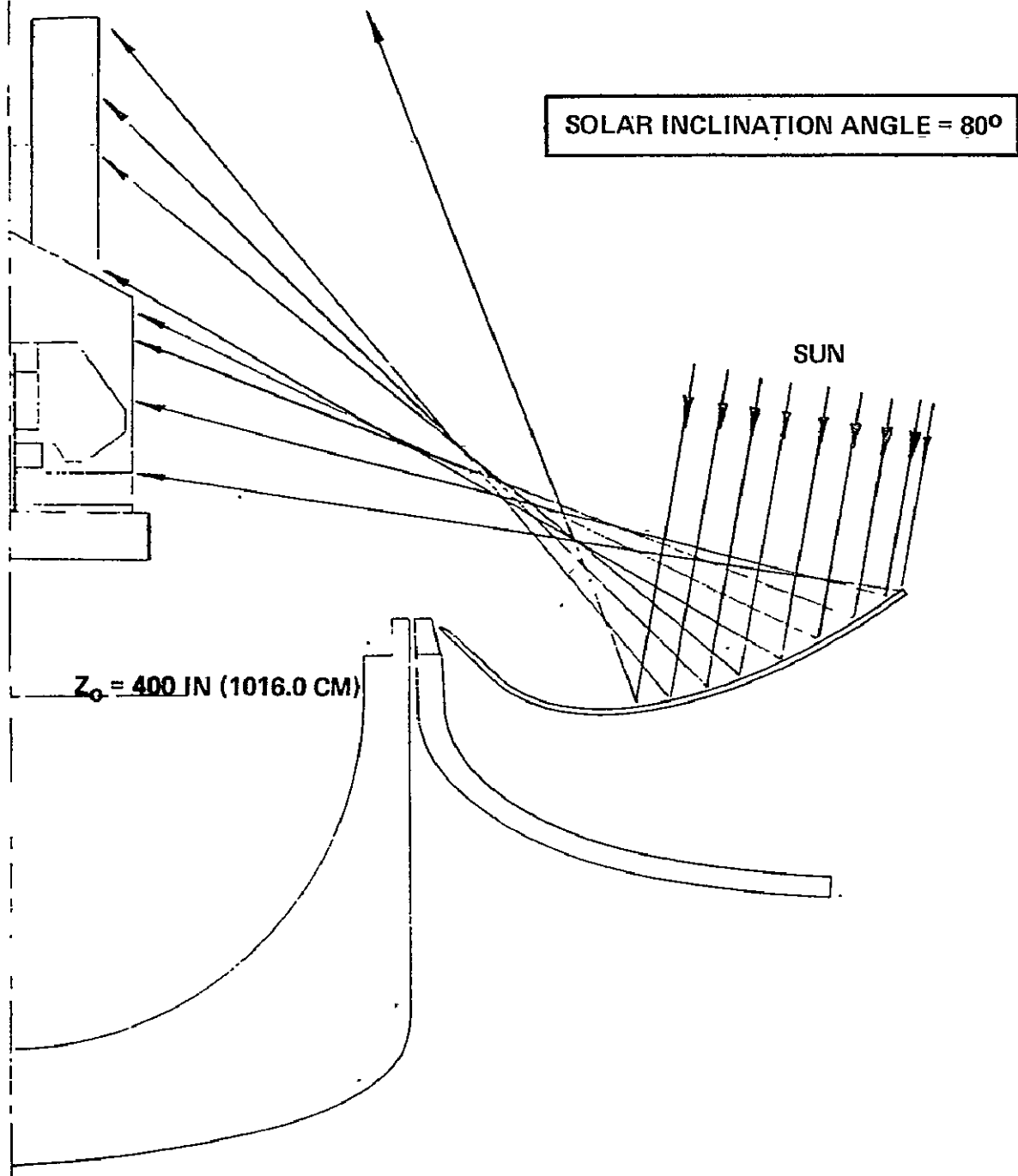


Figure 23. (Continued).

ORIGINAL PAGE IS
OF POOR QUALITY

SOLAR INCLINATION ANGLE = 90°

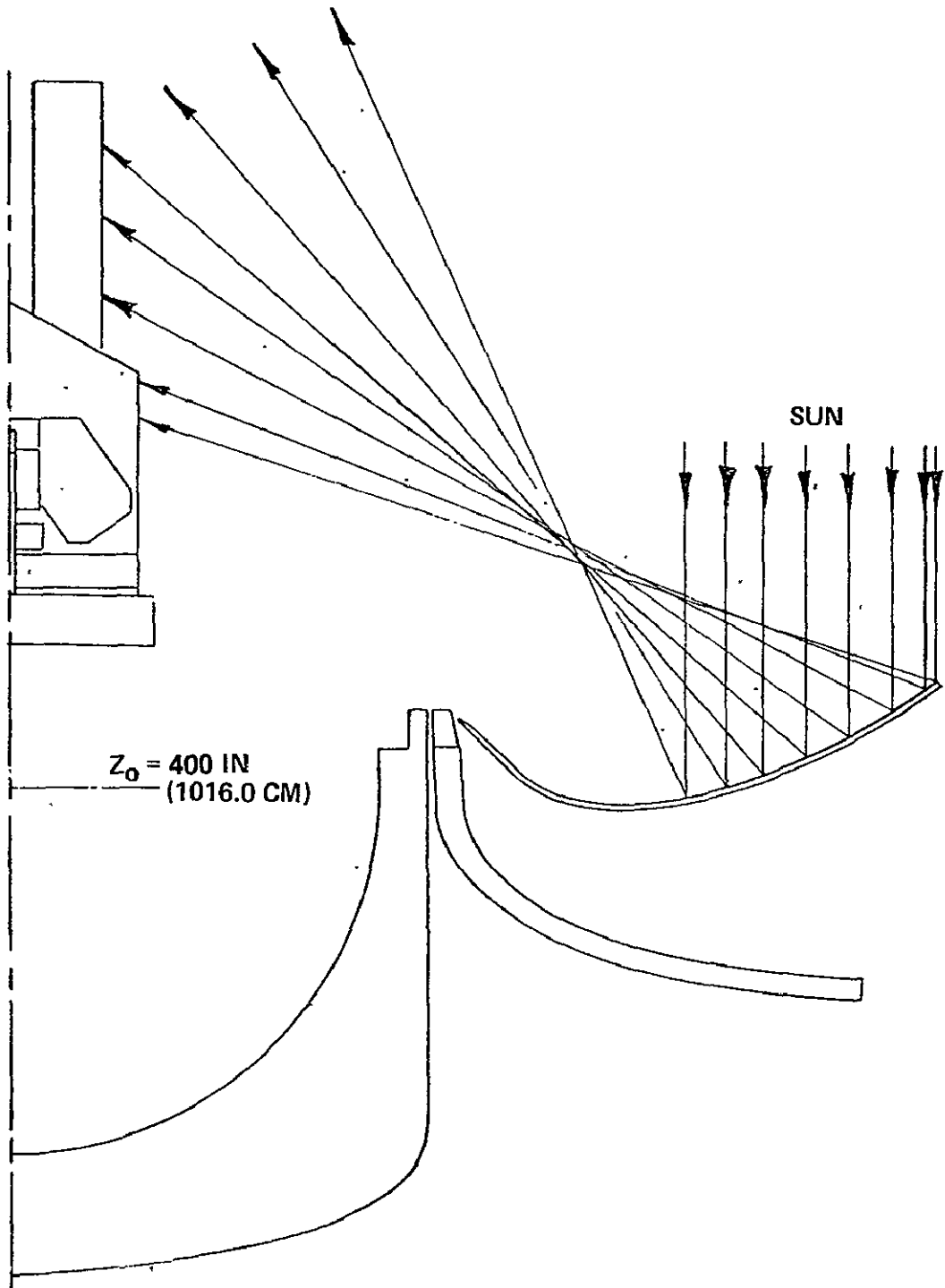


Figure 23. (Continued).

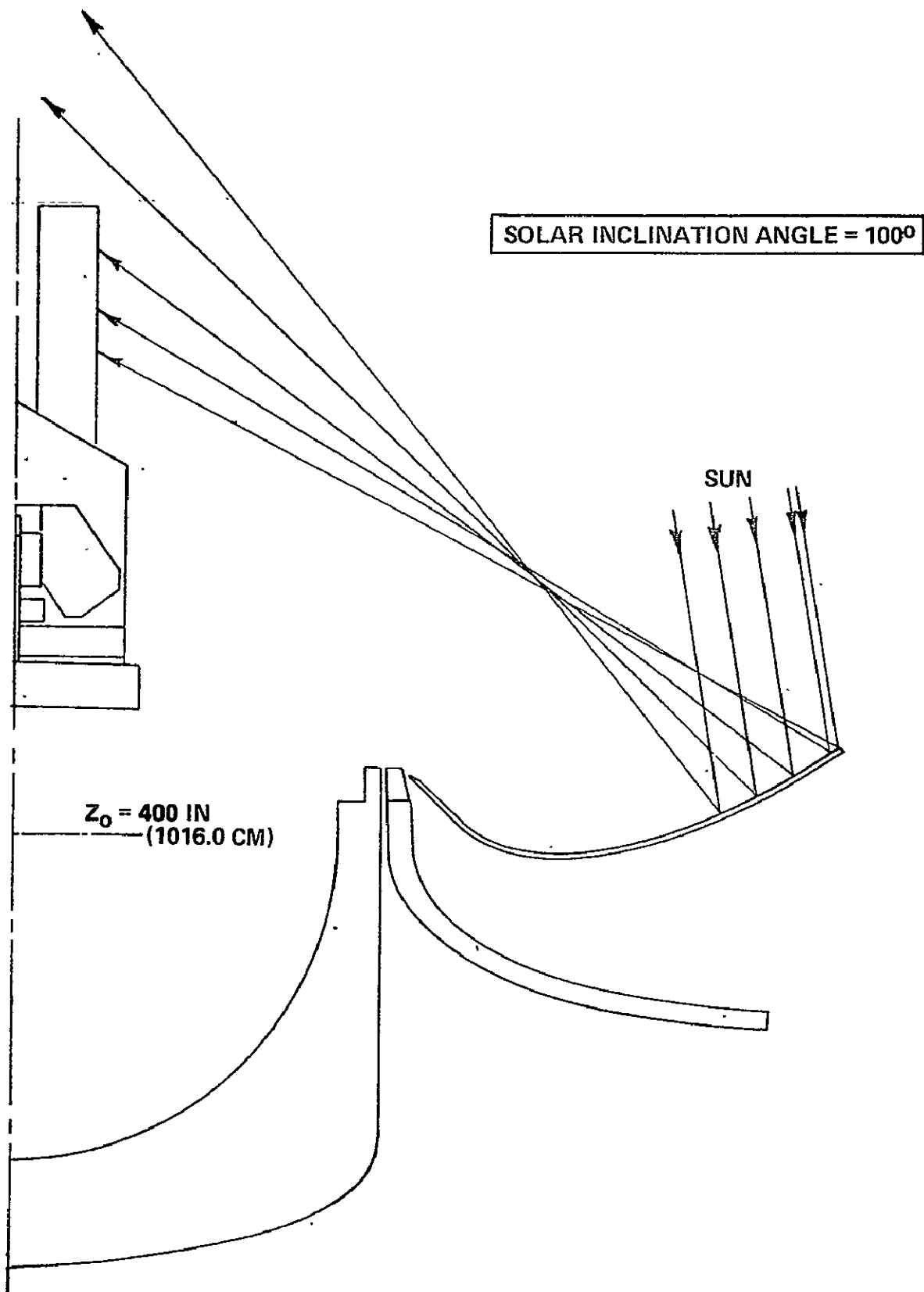


Figure 23. (Concluded).

ORIGINAL PAGE IS
OF POOR QUALITY

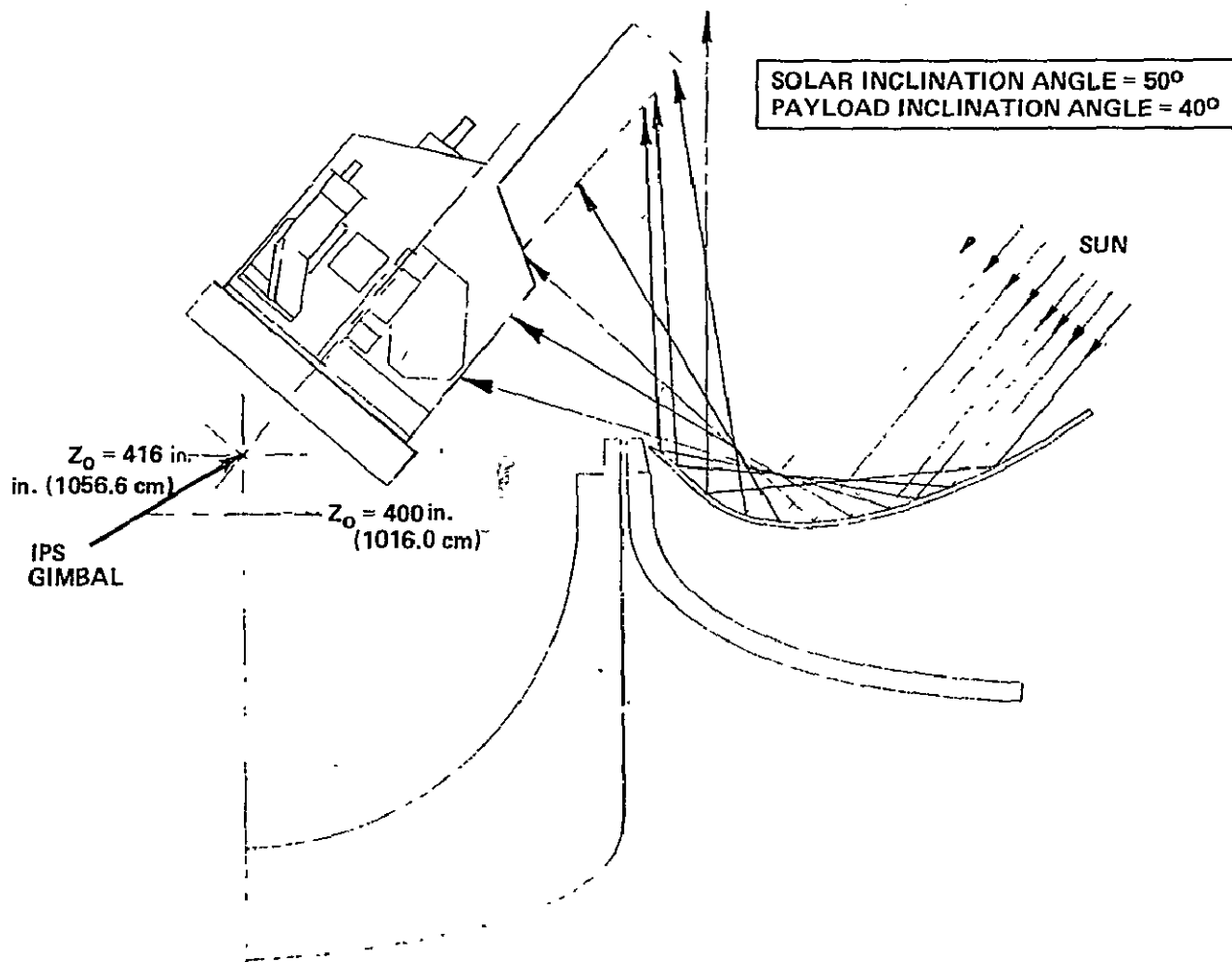


Figure 24. Manual tracings of reflected solar rays from the Orbiter radiator; sun-tracking IPS.

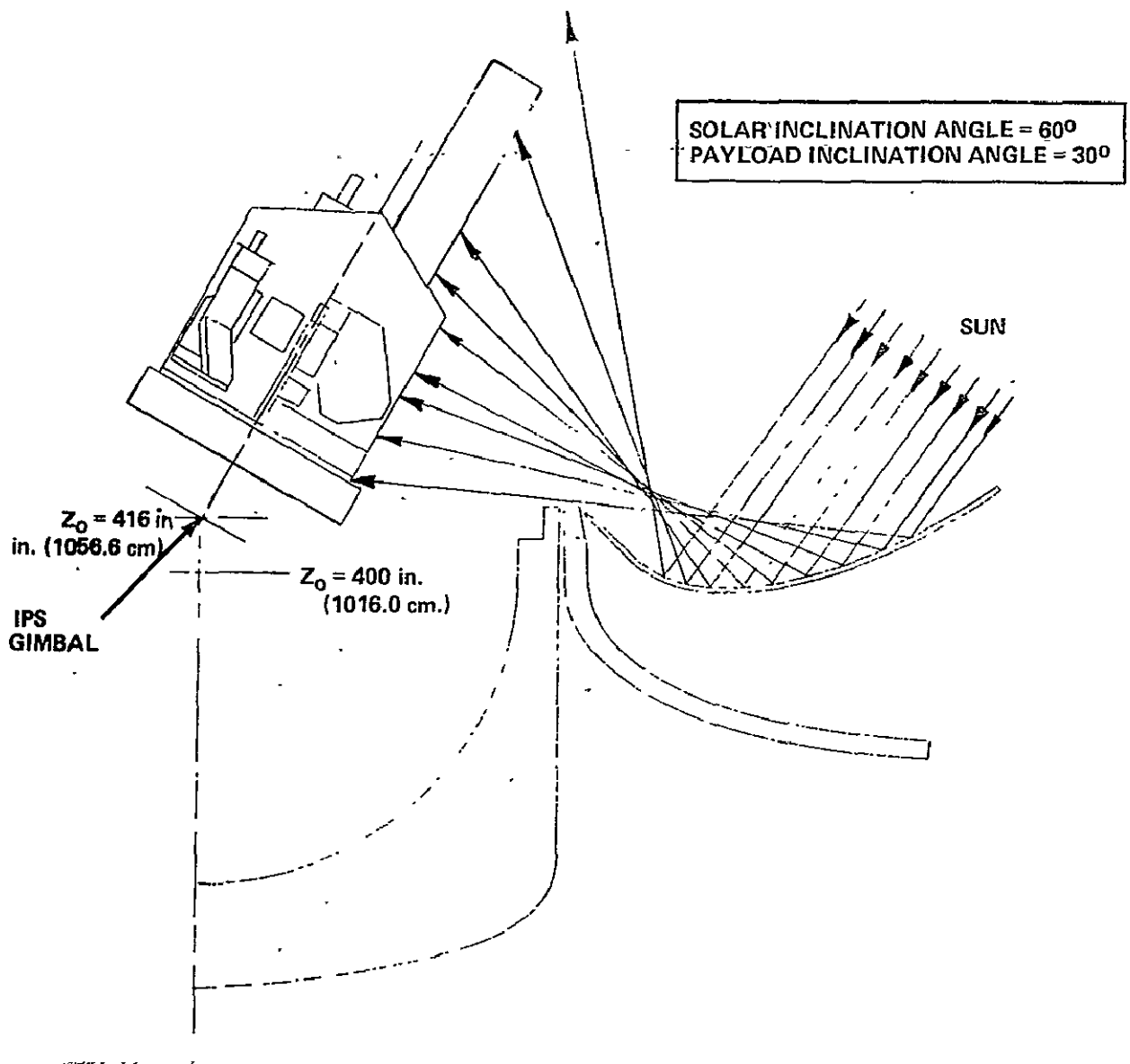


Figure 24. (Continued).

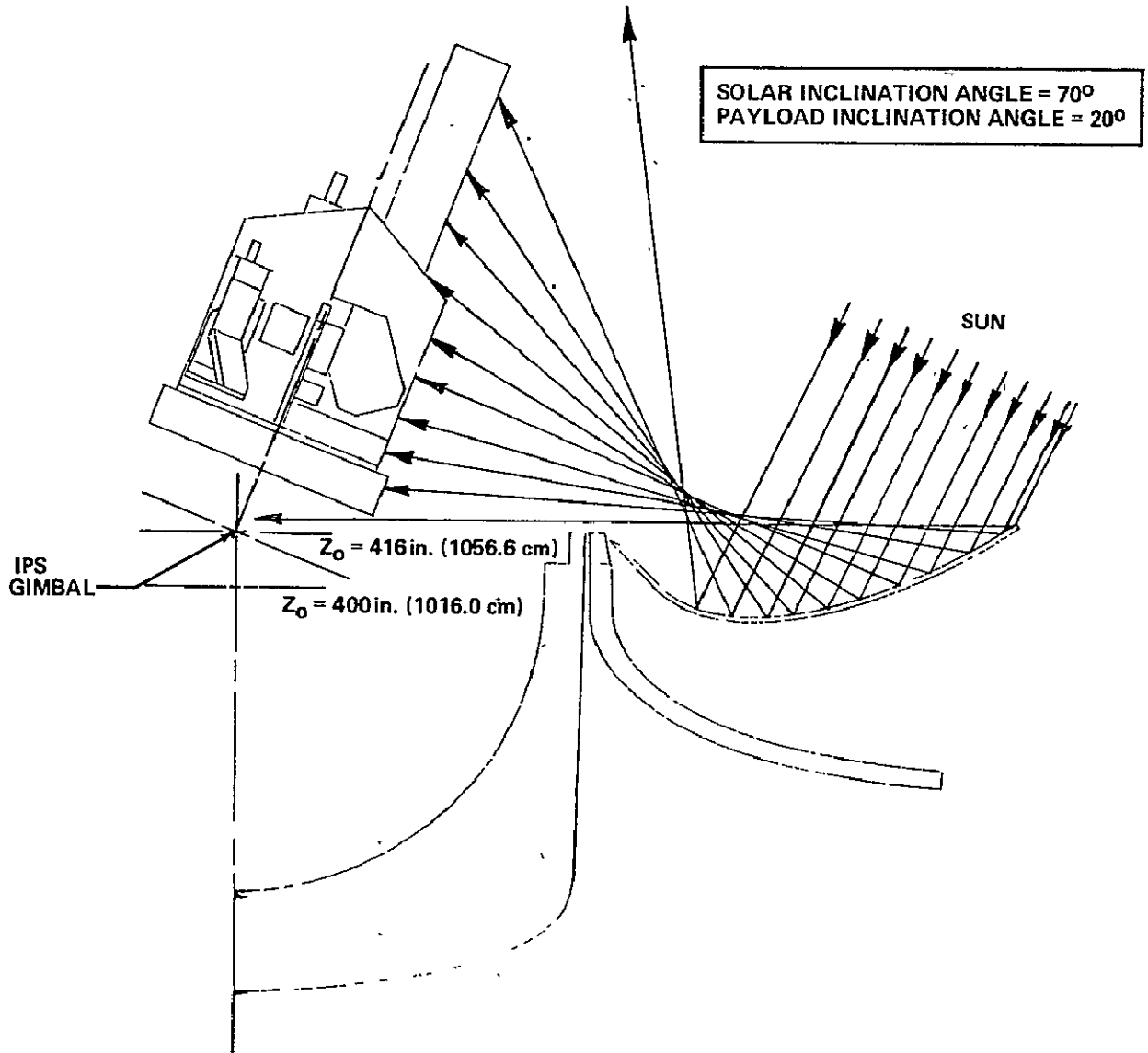


Figure 24. (Continued).

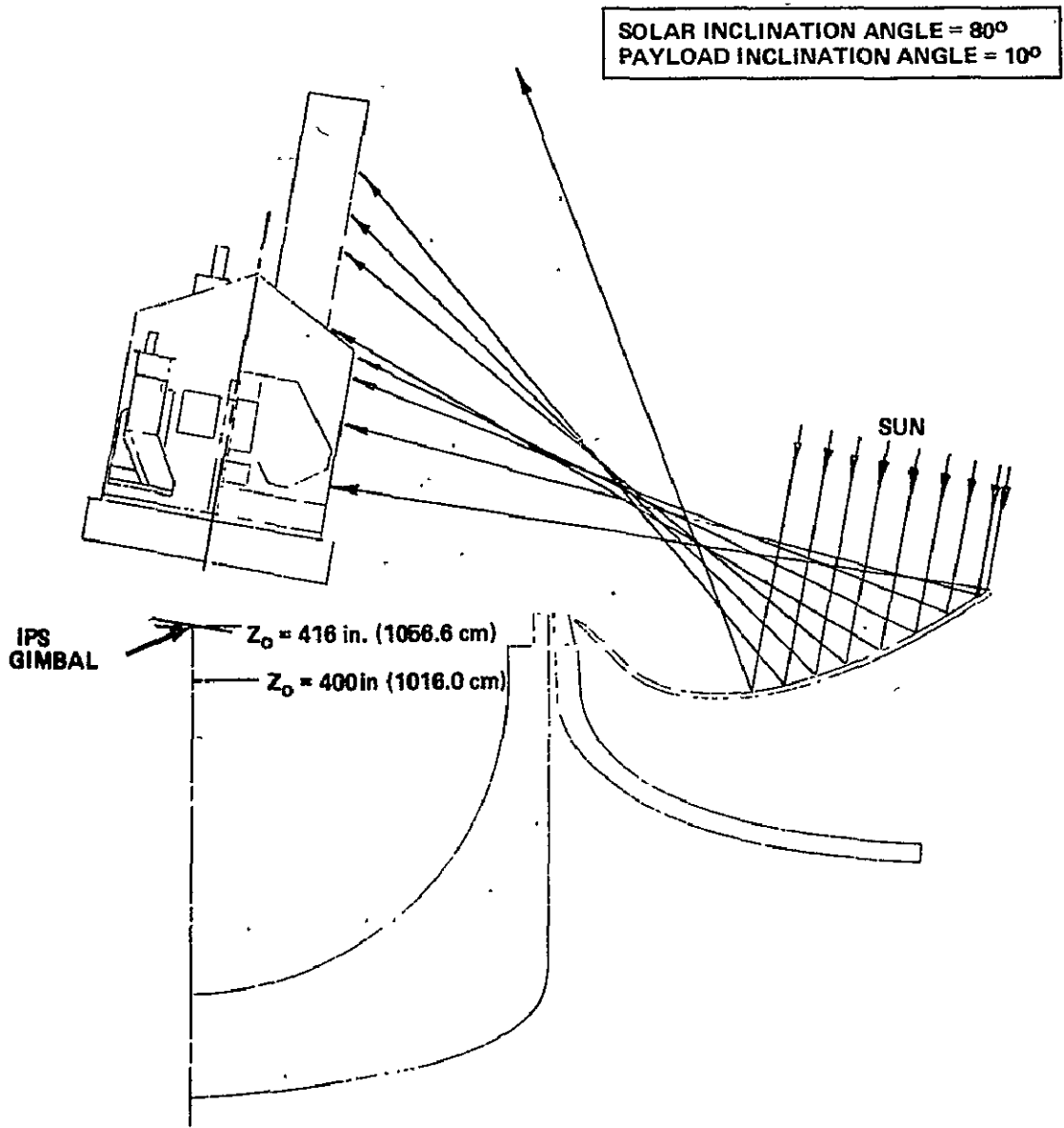


Figure 24. (Continued).

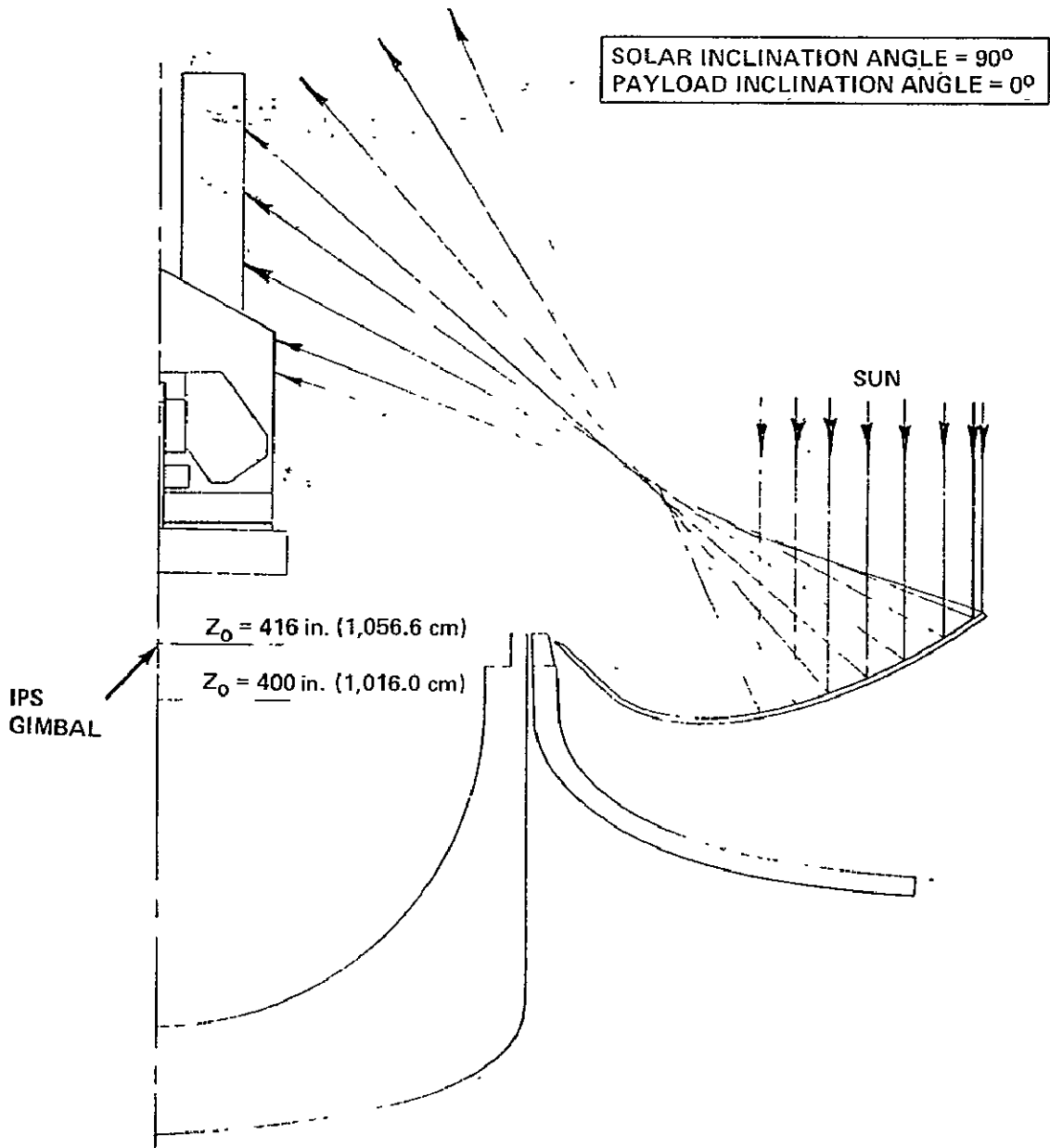


Figure 24. (Continued).

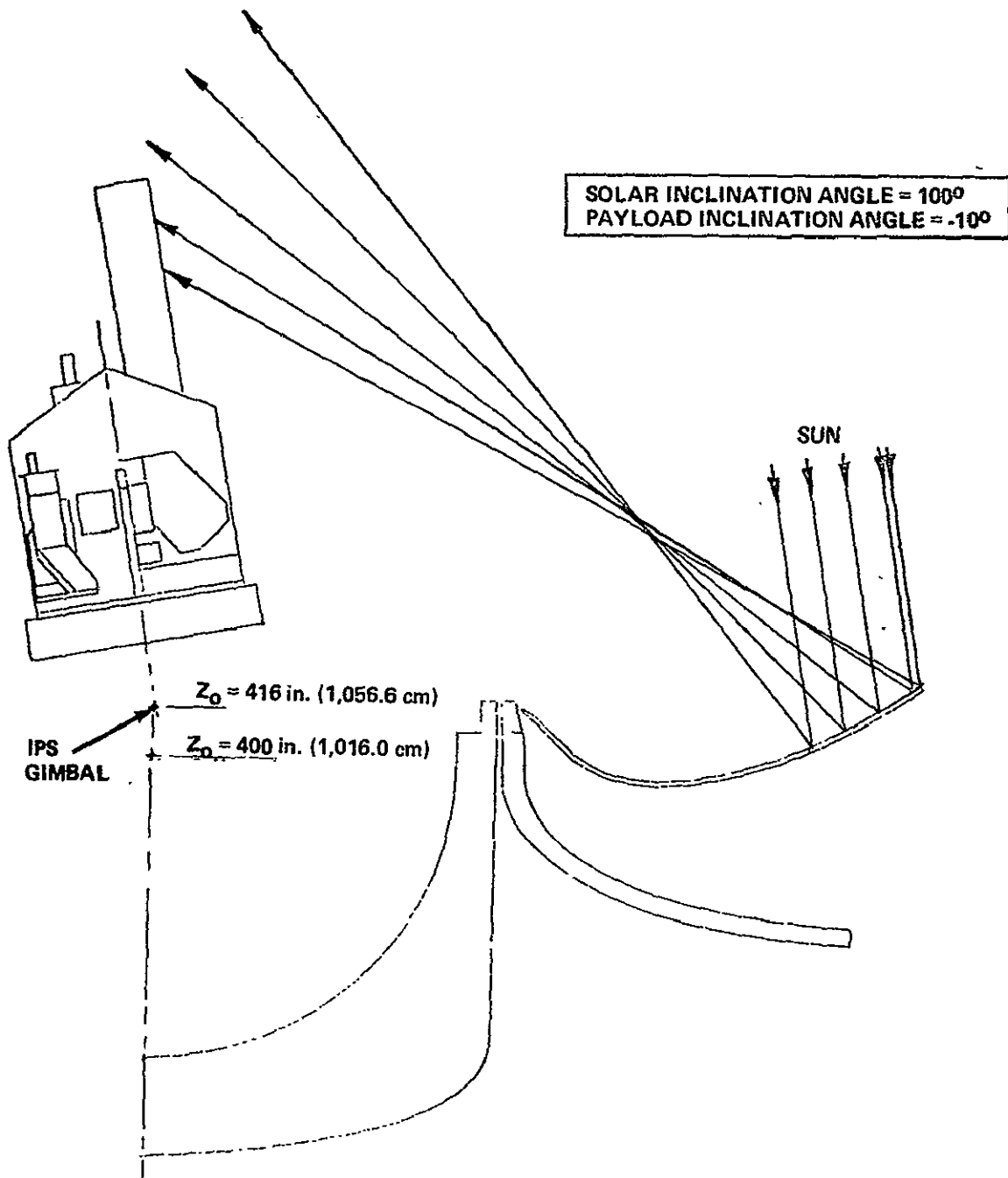
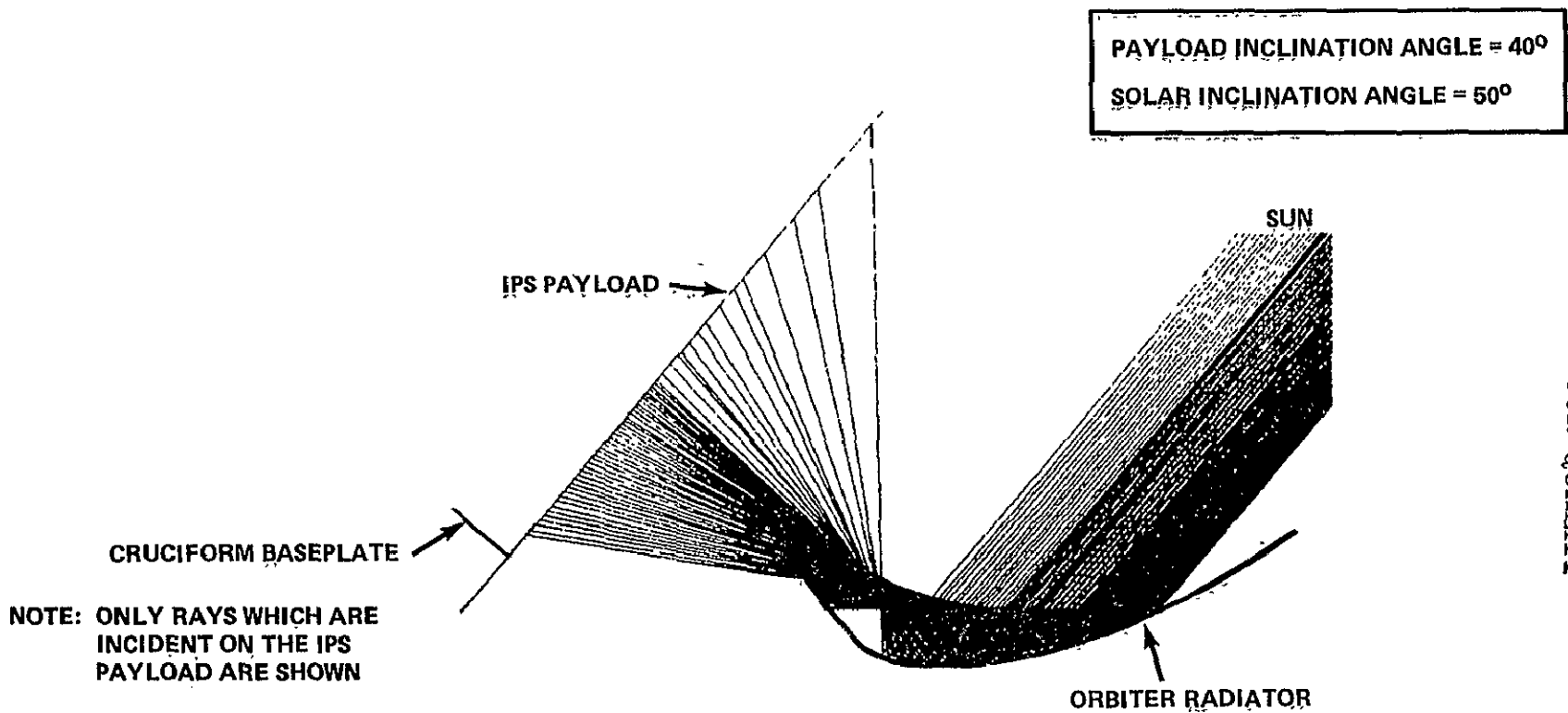


Figure 24. (Concluded)..



ORIGINAL PAGE IS
OF POOR QUALITY

Figure 25. Tracings of reflected solar rays from the Orbiter radiator as generated using the two dimensional specular heat flux program.

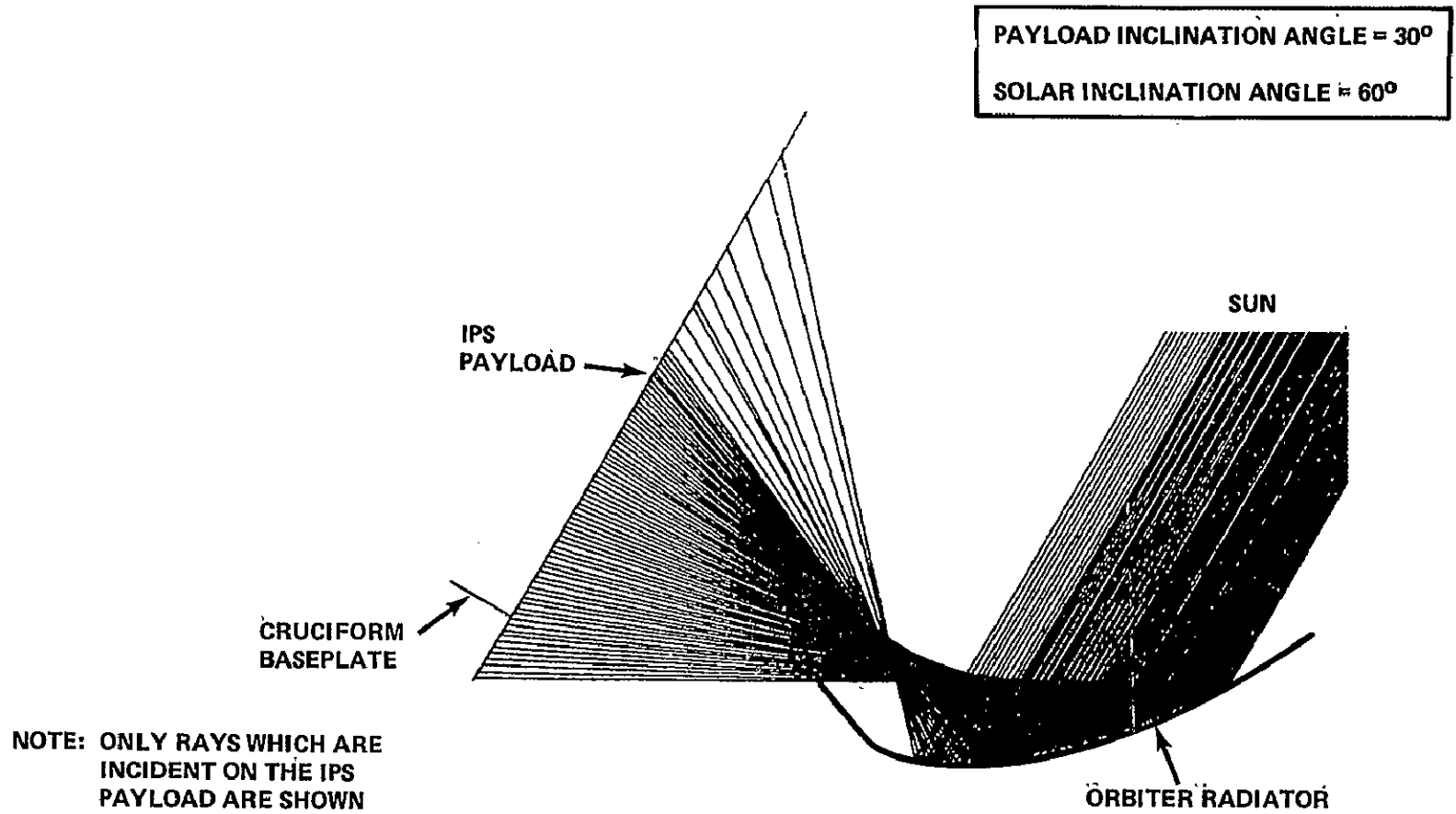


Figure 25. (Continued).

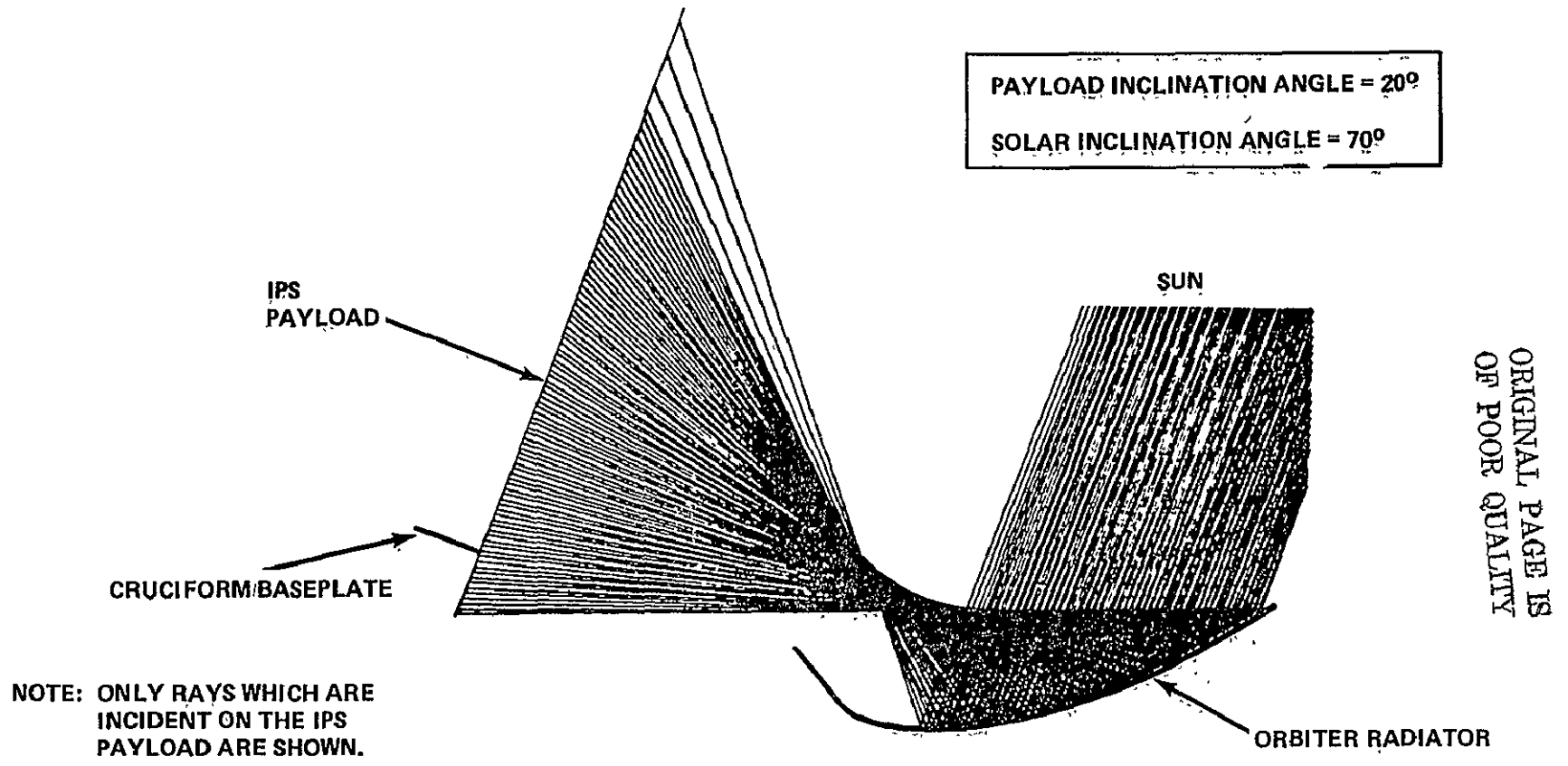


Figure 25. (Continued).

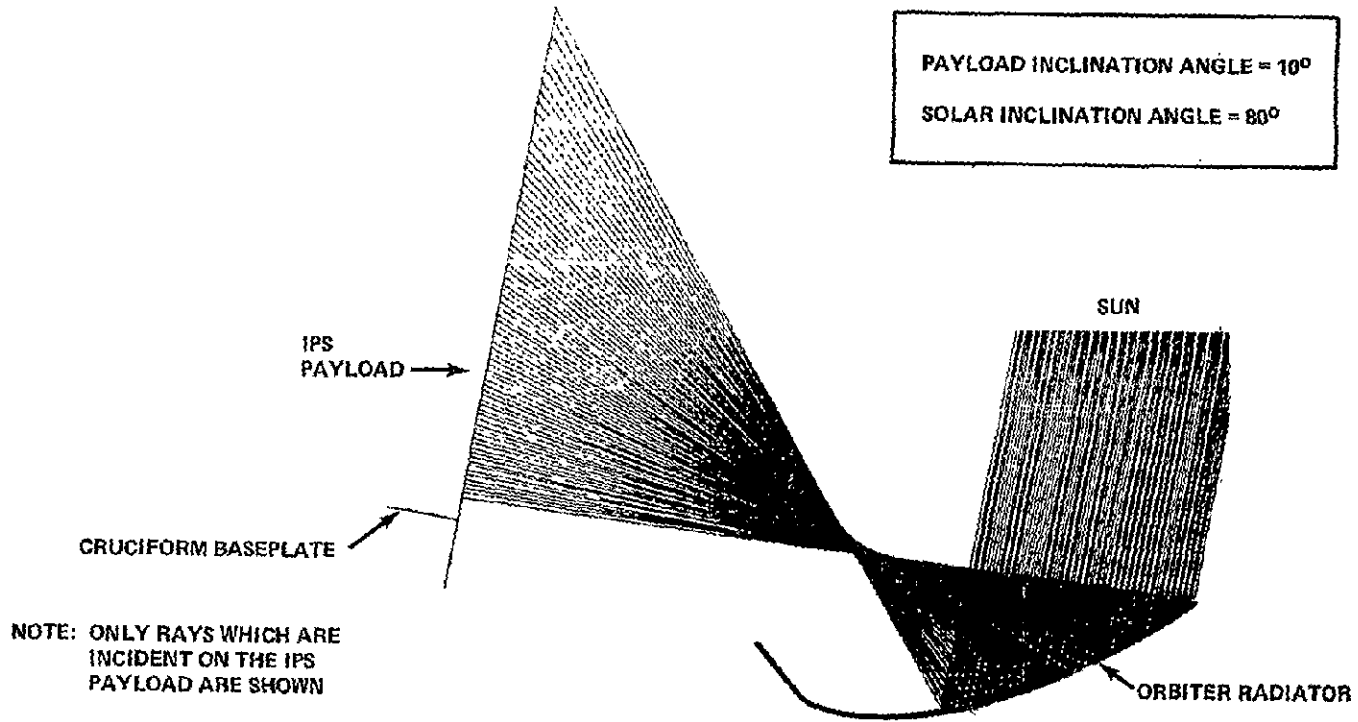


Figure 25. (Continued).

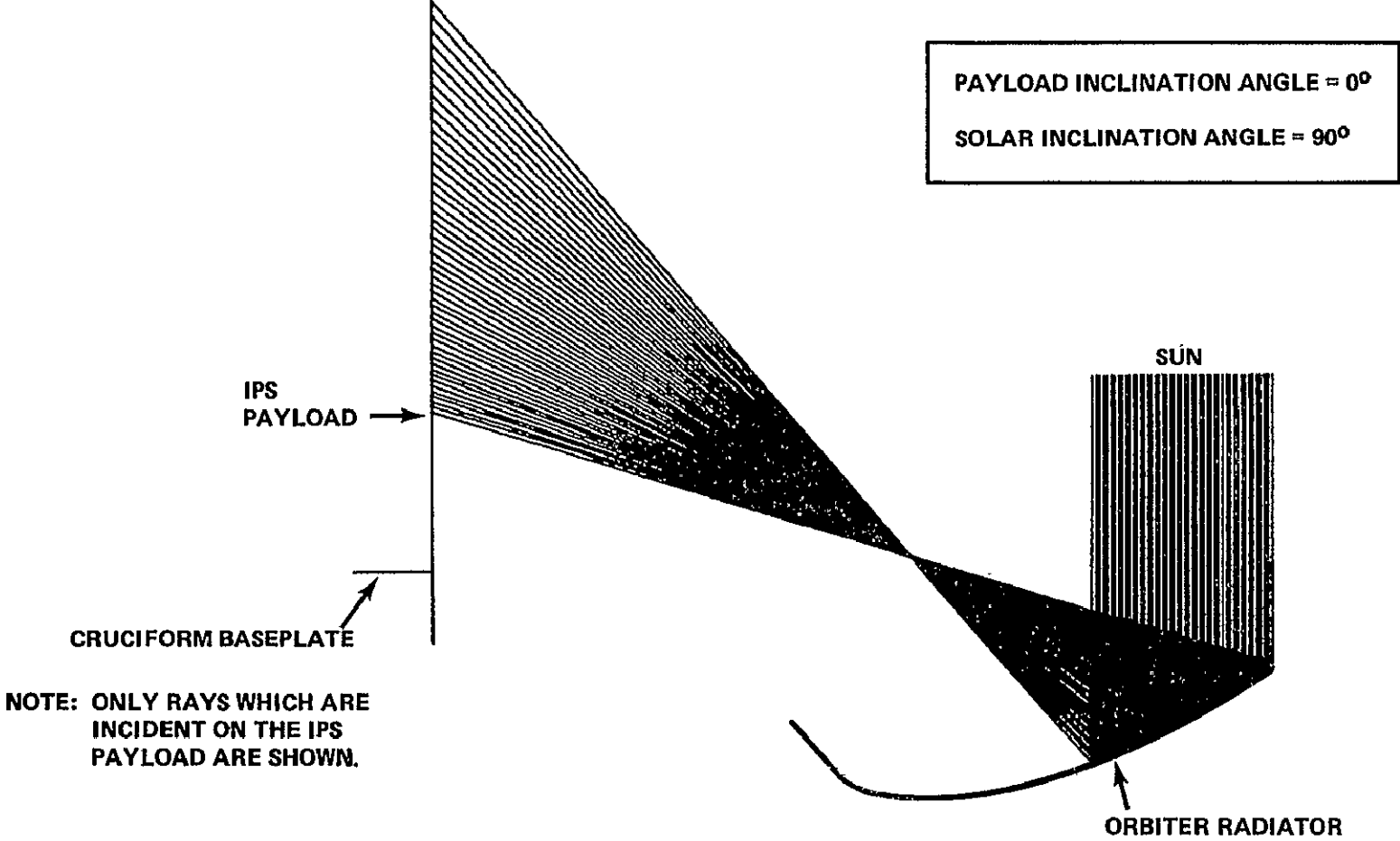


Figure 25. (Continued).

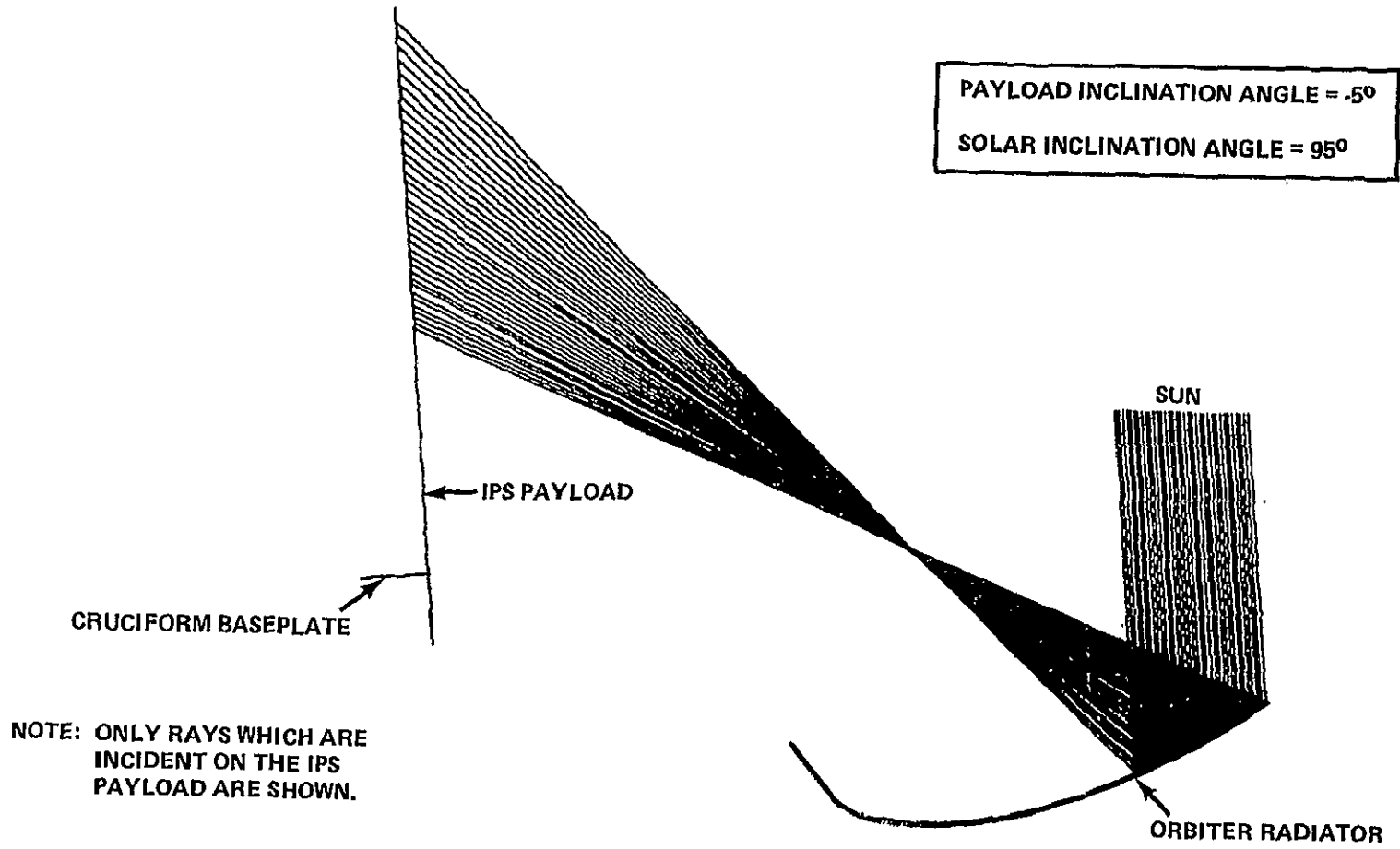
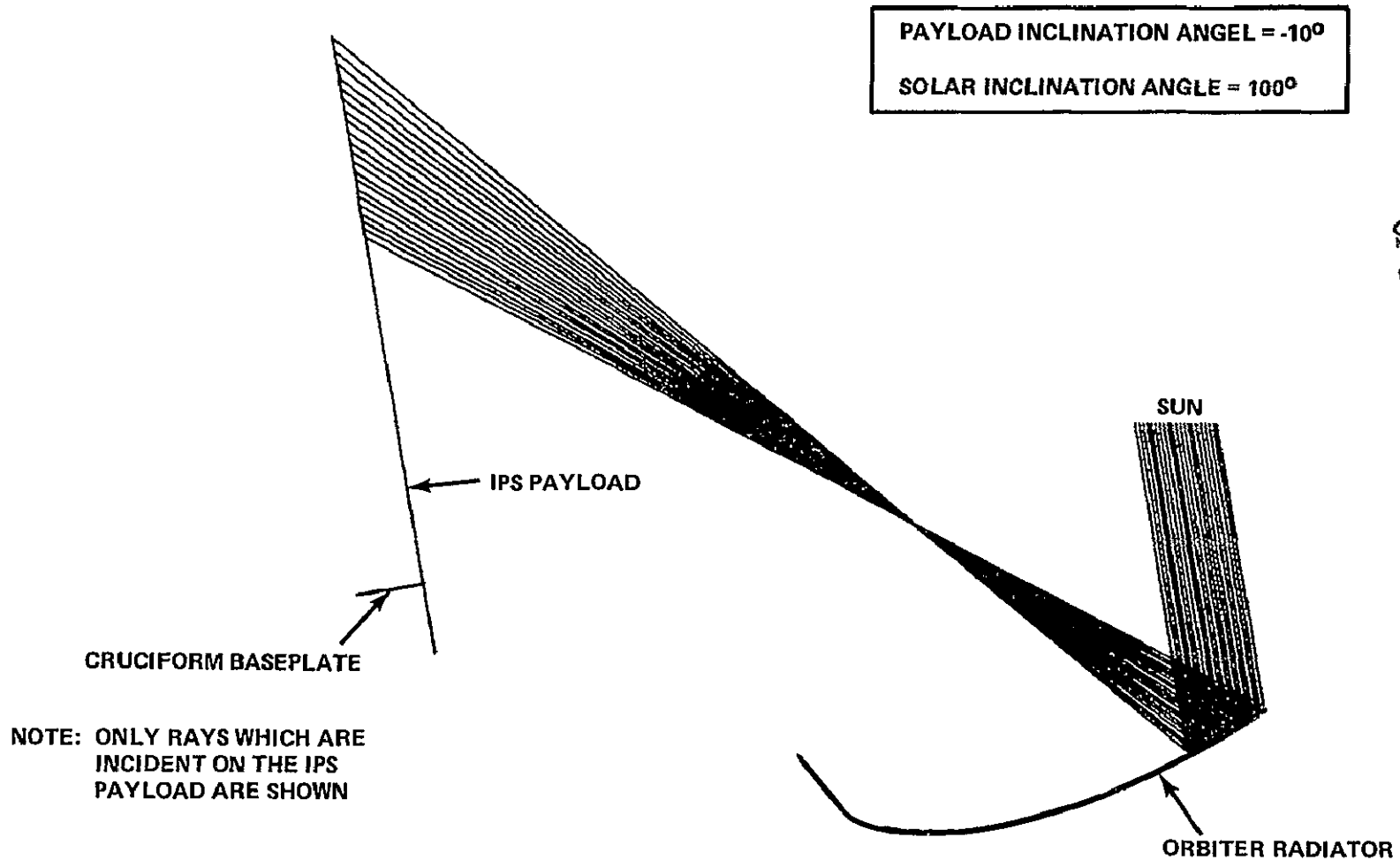


Figure 25. (Continued).



ORIGINAL PAGE IS
OF POOR QUALITY

Figure 25. (Continued).

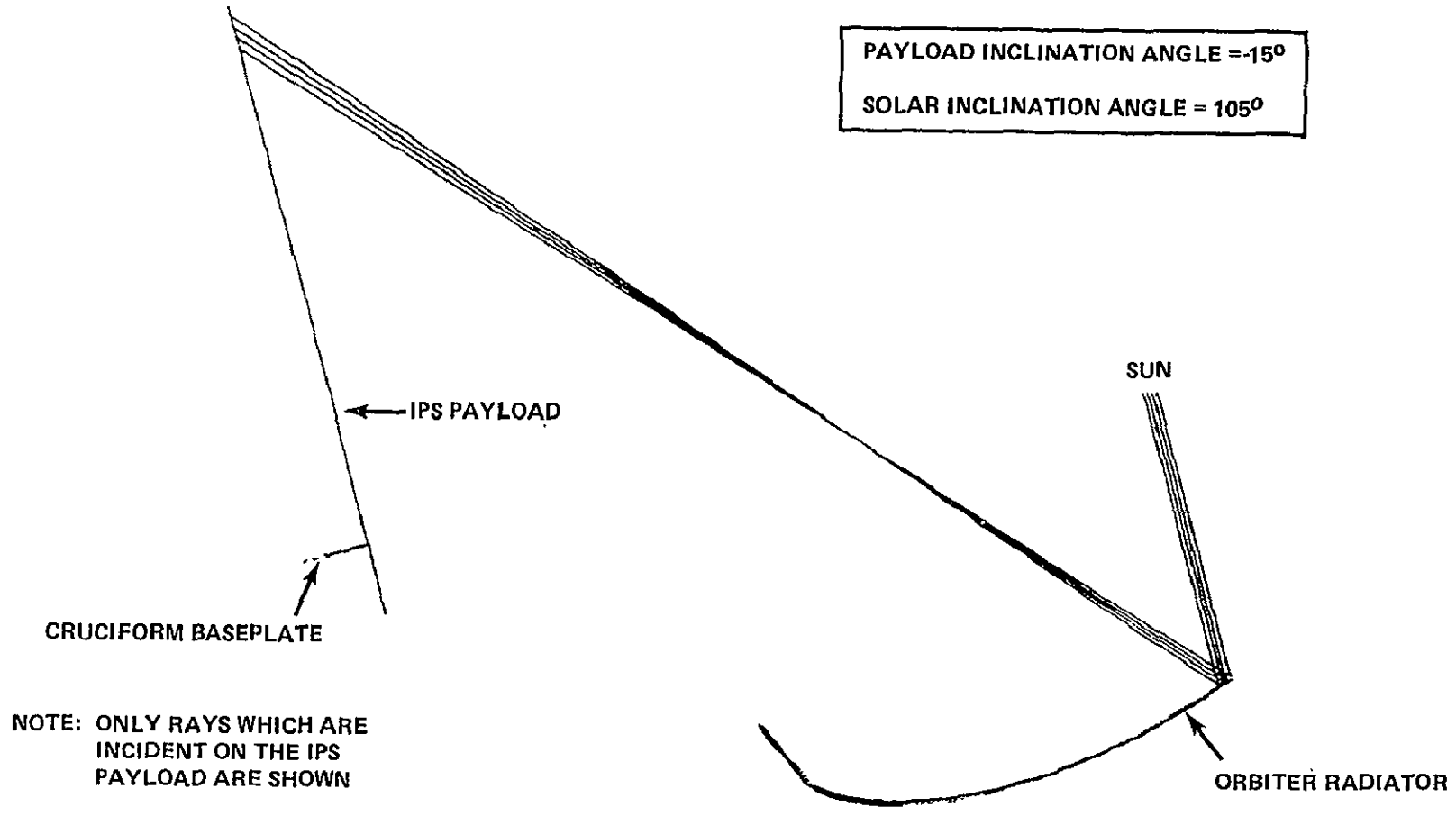
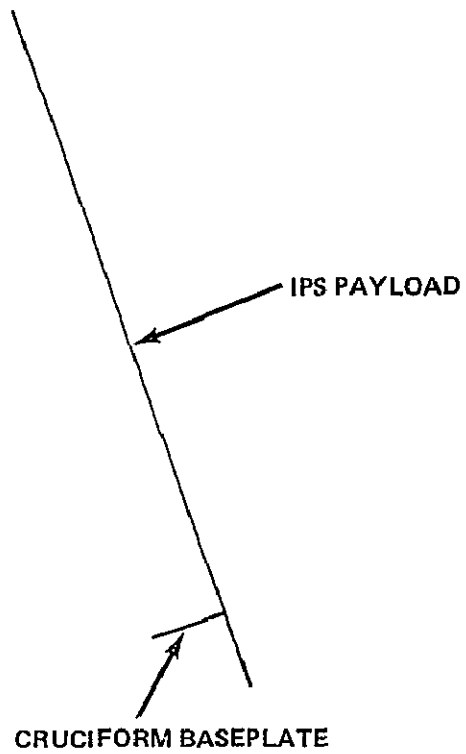
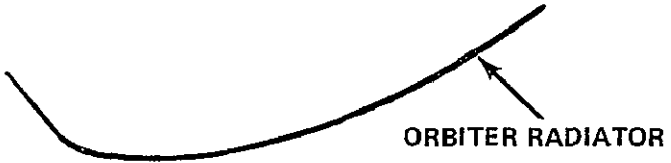


Figure 25. (Continued).



PAYLOAD INCLINATION ANGLE = -20°
SOLAR INCLINATION ANGLE = 110°

(NO ENERGY IS REFLECTED ON
THE PAYLOAD FROM THE RADIATORS)



NOTE: ONLY RAYS WHICH ARE
INCIDENT ON THE IPS
PAYLOAD ARE SHOWN

Figure 25. (Concluded).

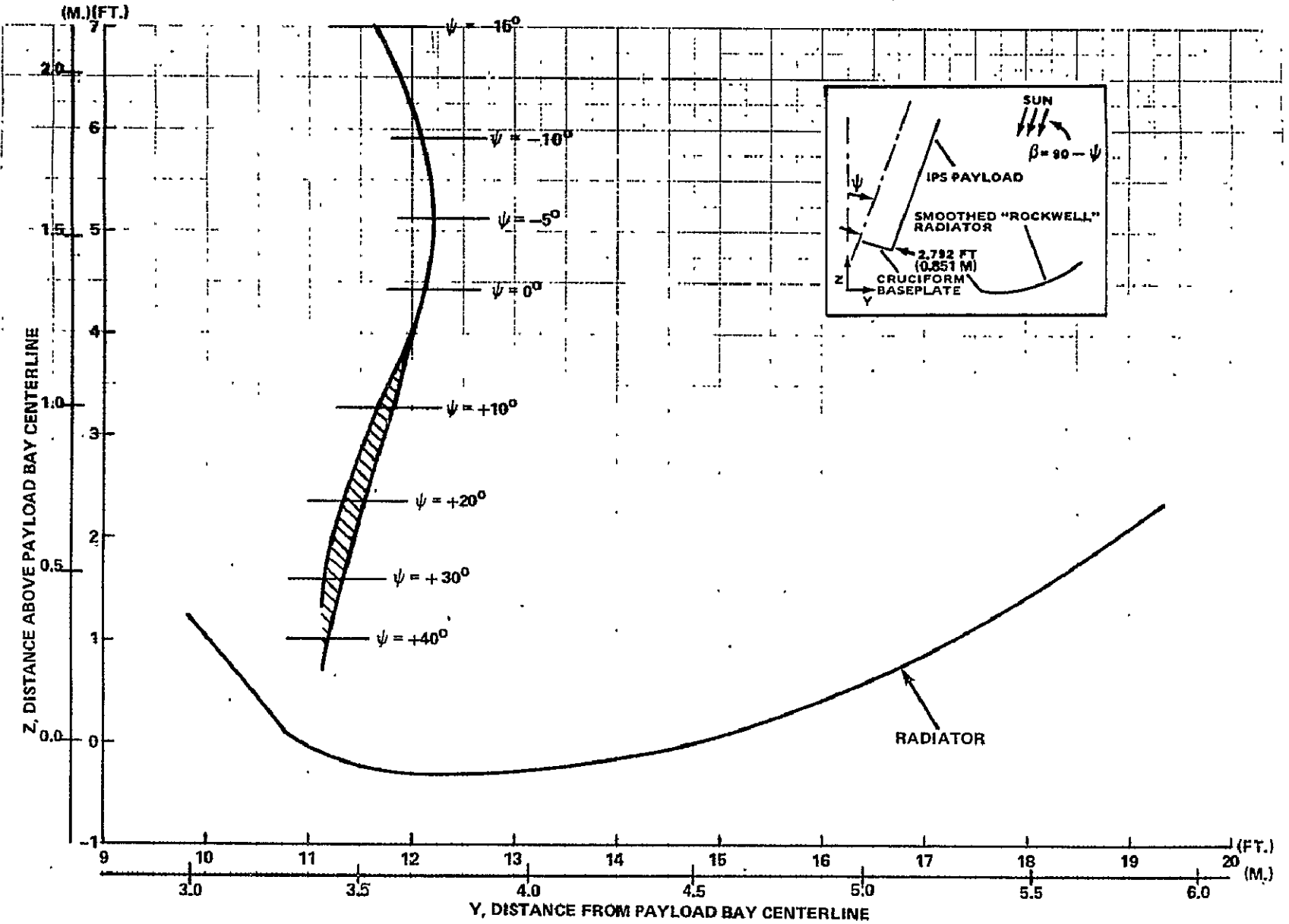
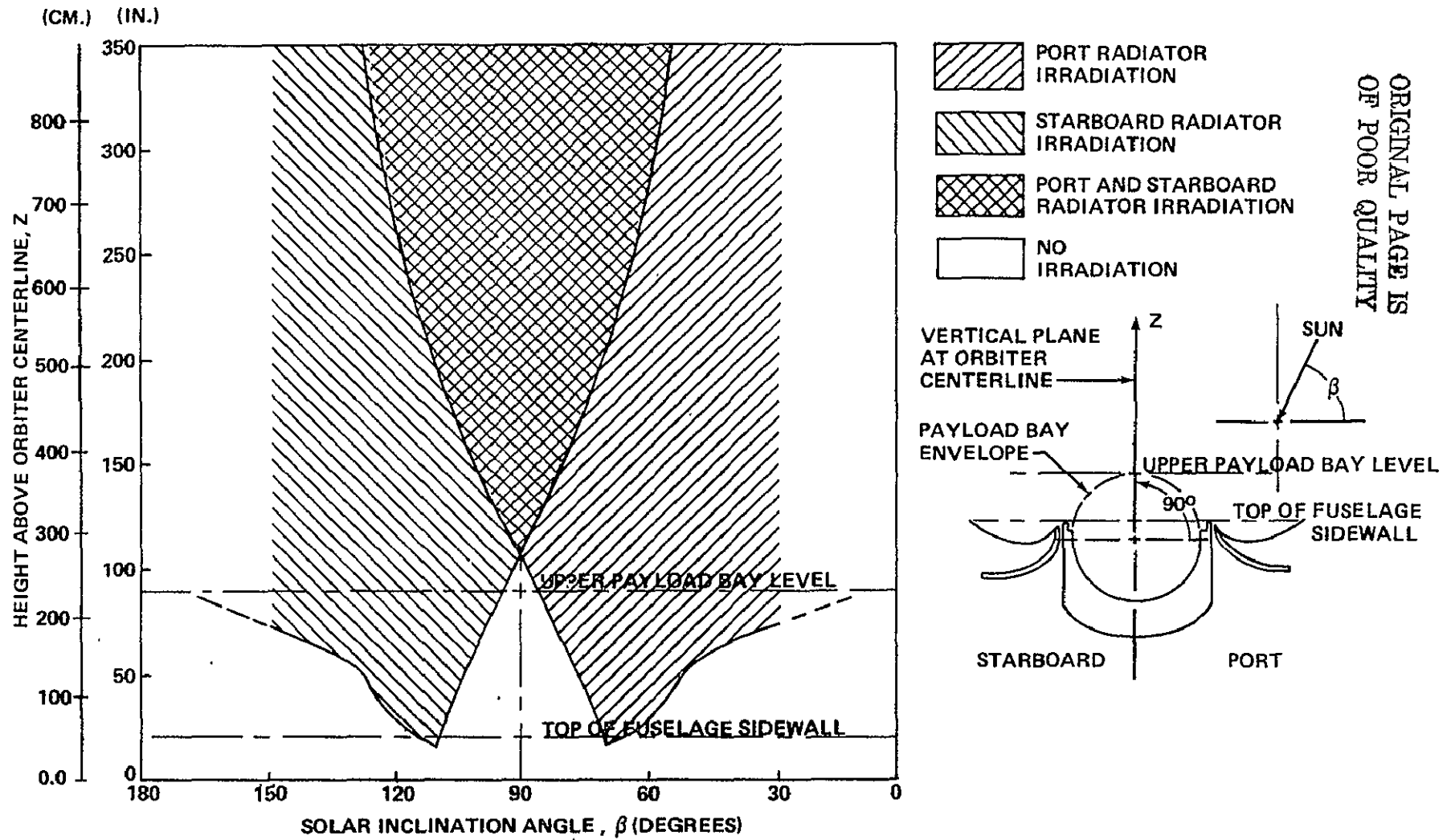


Figure 26. Areas of highest solar ray concentration (focal region) above the deployed forward Orbiter radiator.



ORIGINAL PAGE IS
OF POOR QUALITY

Figure 27. Projection of specular energy reflections from radiators to vertical plane at Orbiter centerline.

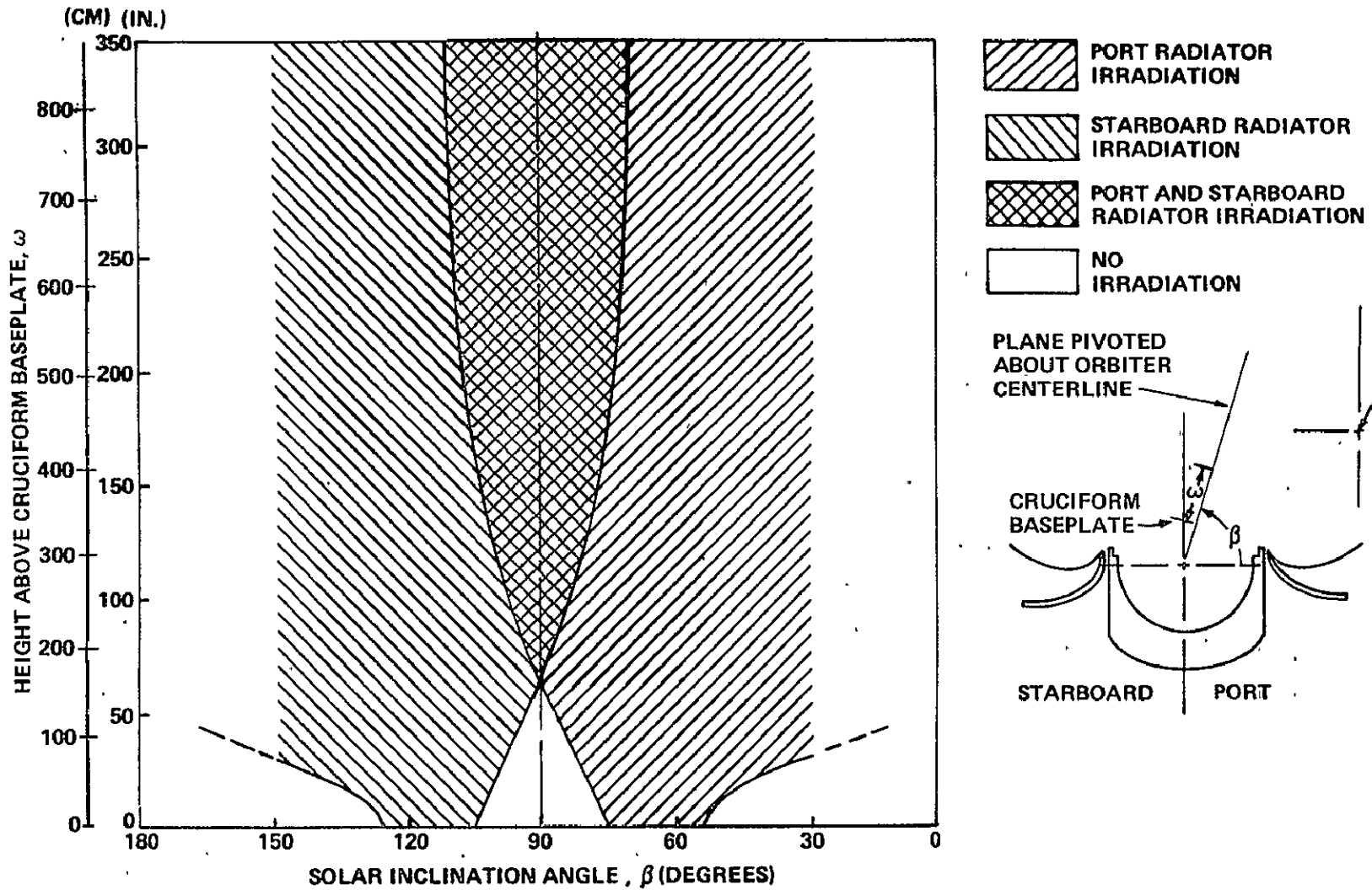


Figure 28. Projection of specular energy reflections from radiators to plane parallel to sun's rays.

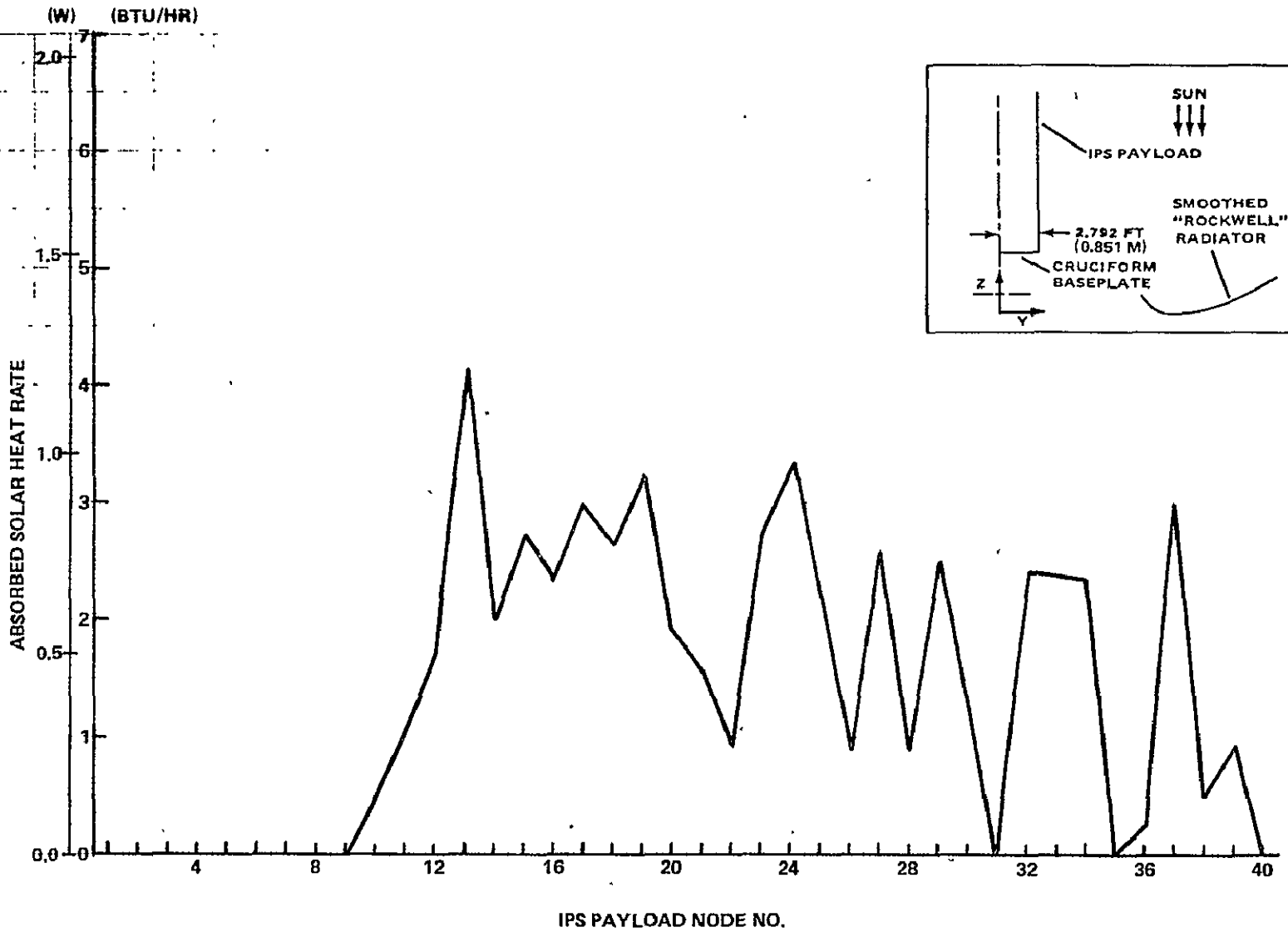


Figure 29. Payload heat rates computed with "two-dimensional" TRASYS II based model for a 0° payload inclination angle.

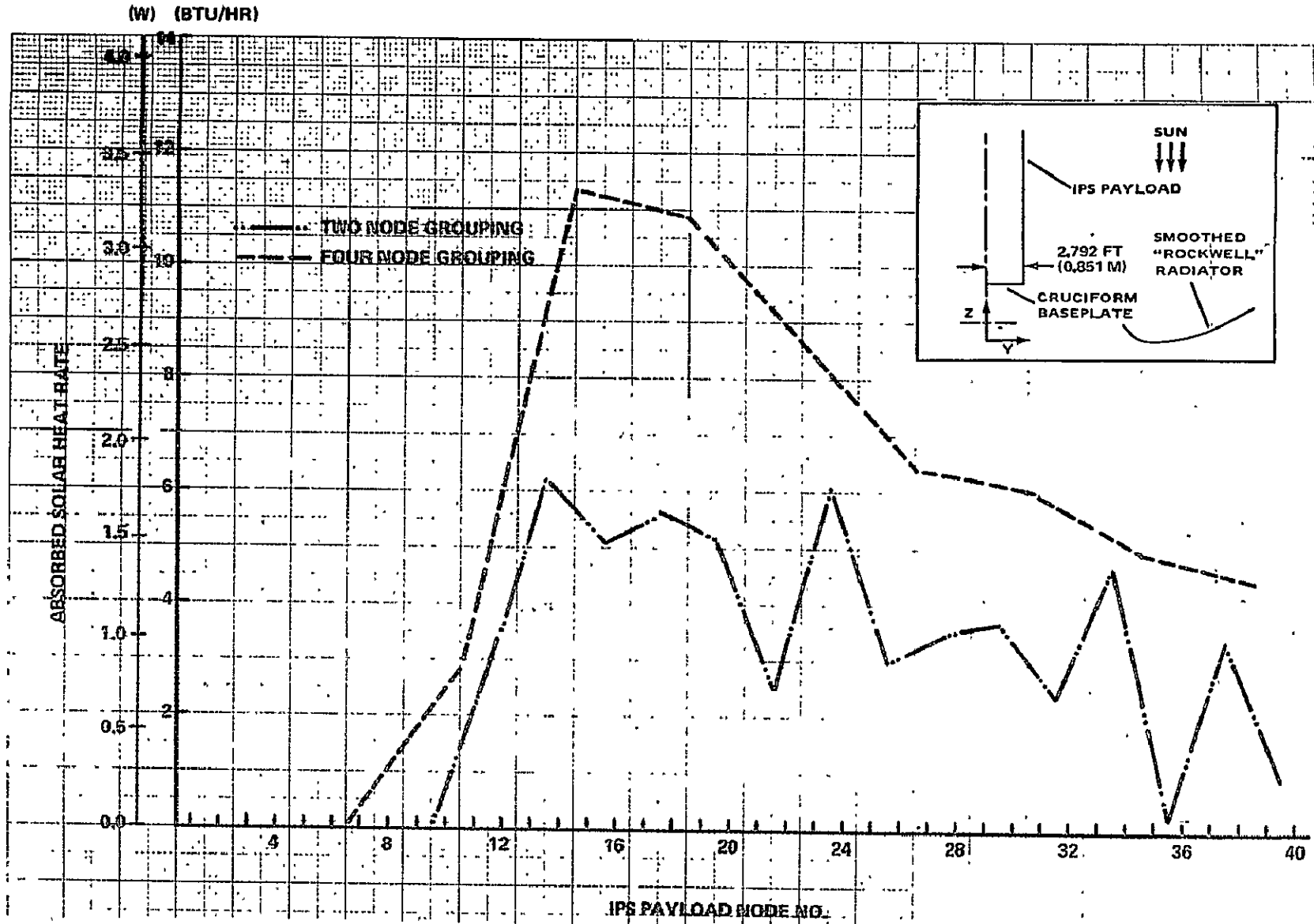


Figure 30. Grouping of nodes to smooth heat rates calculated with "two-dimensional" TRASYS II based model.

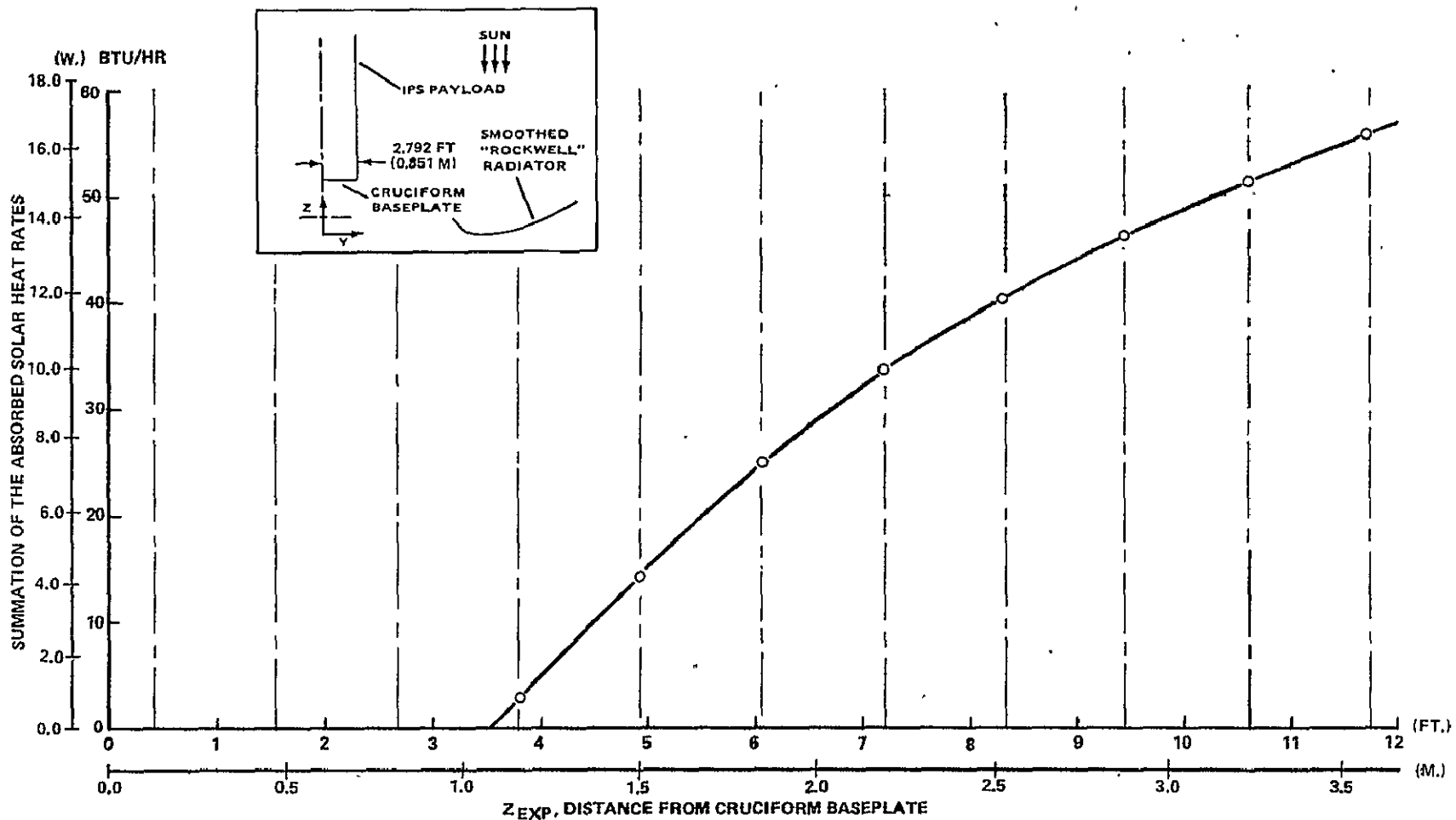


Figure 31. Cumulative solar energy absorbed on IPS payload from "two-dimensional" TRASYS II based model data.

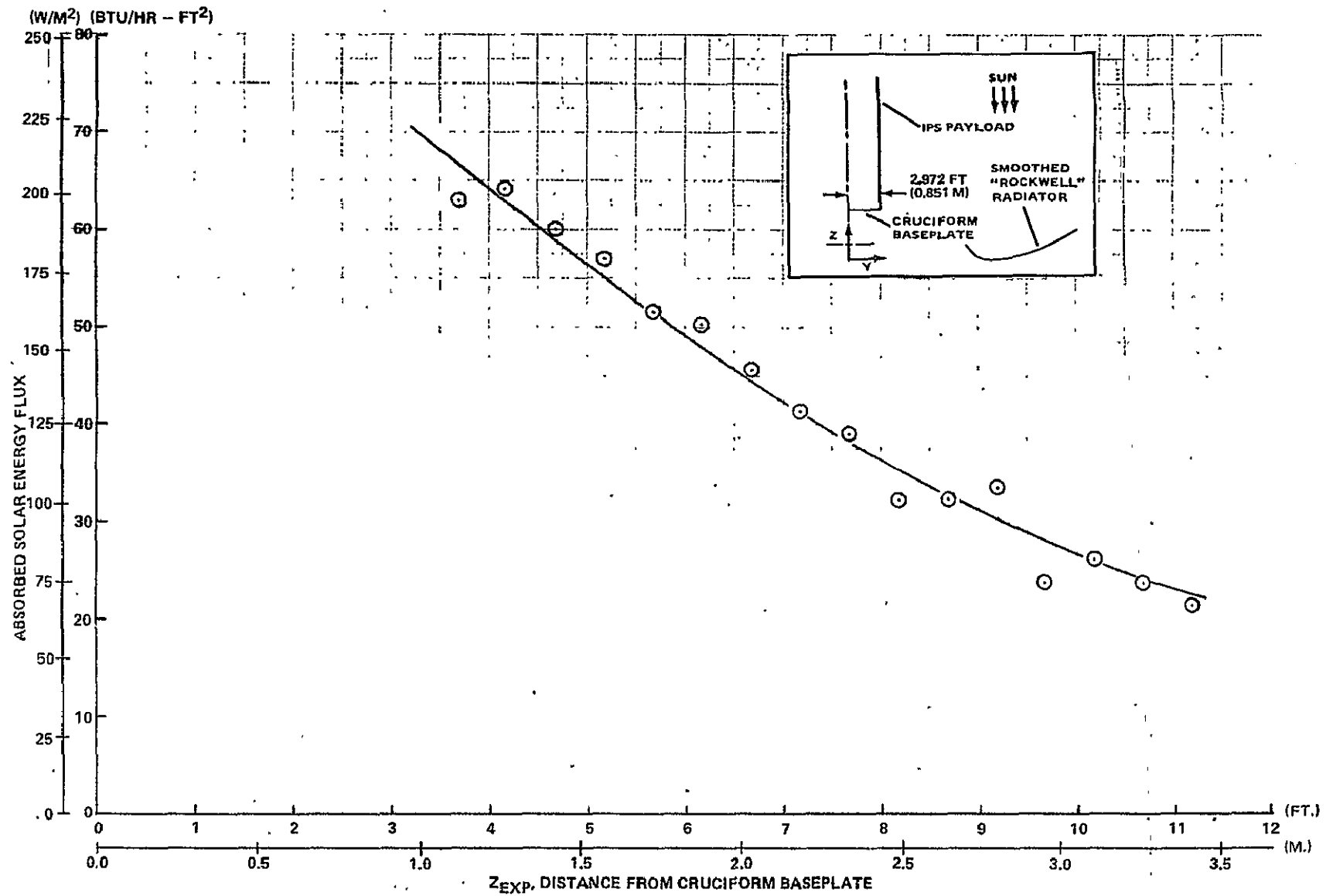


Figure 32. Payload heat flux computed with "two-dimensional" TRASYS II based model for a 0° payload inclination angle.

ORIGINAL PAGE IS
OF POOR QUALITY

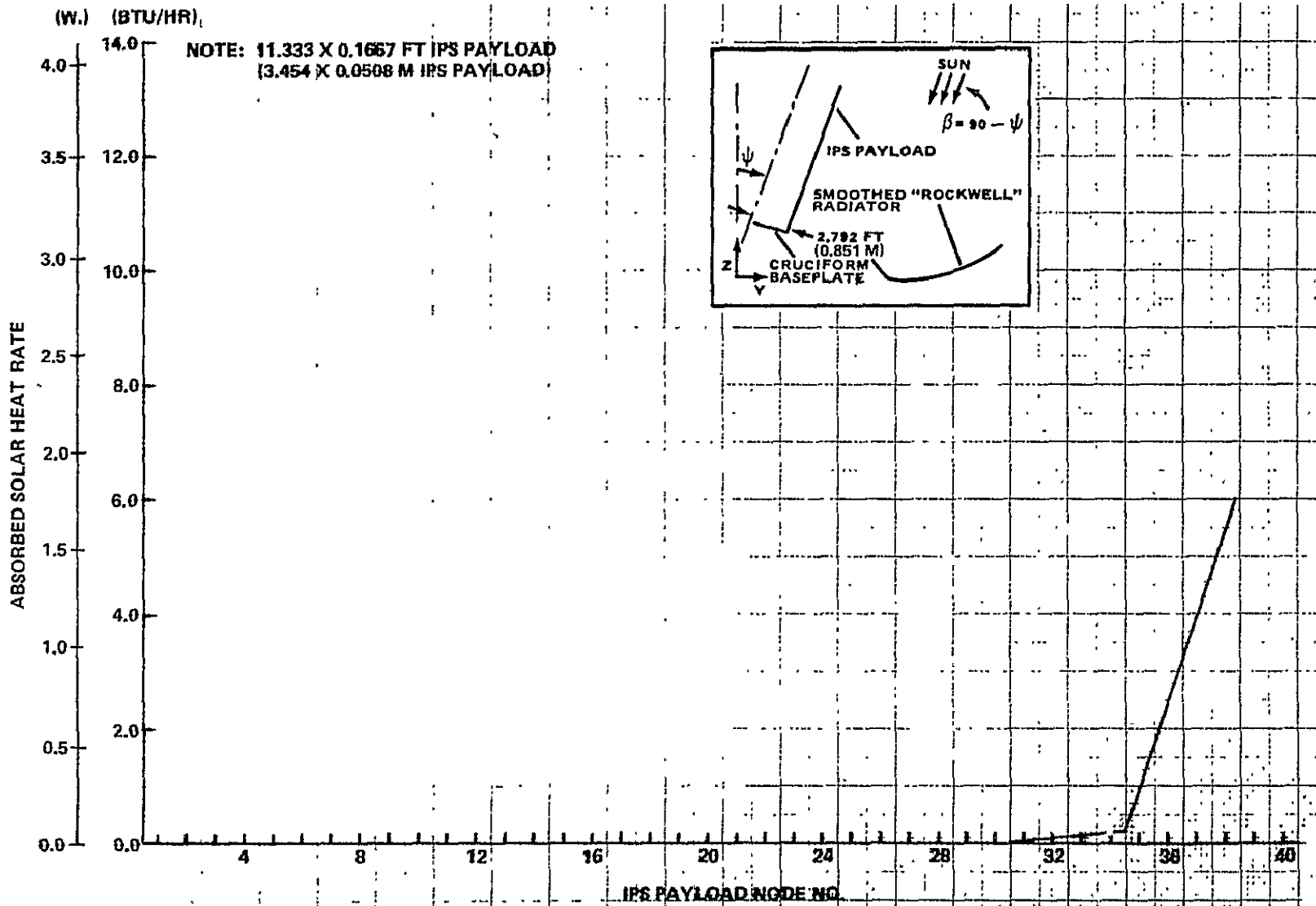


Figure 33. Payload heat rates computed with "two-dimensional" TRASYS II based model for a -15° payload inclination angle.

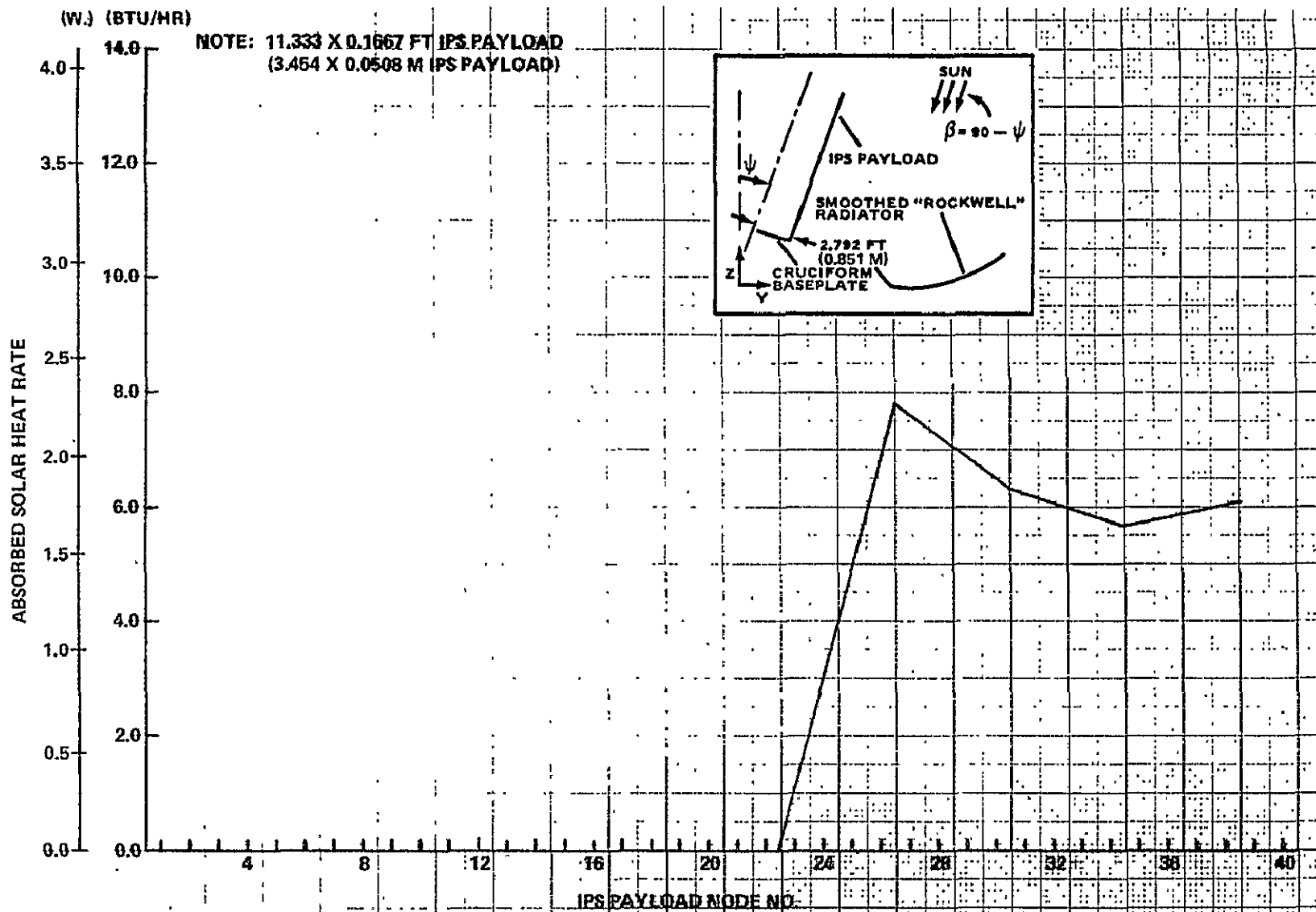


Figure 34. Payload heat rates computed with "two-dimensional" TRASYS II based model for a -10° payload inclination angle.

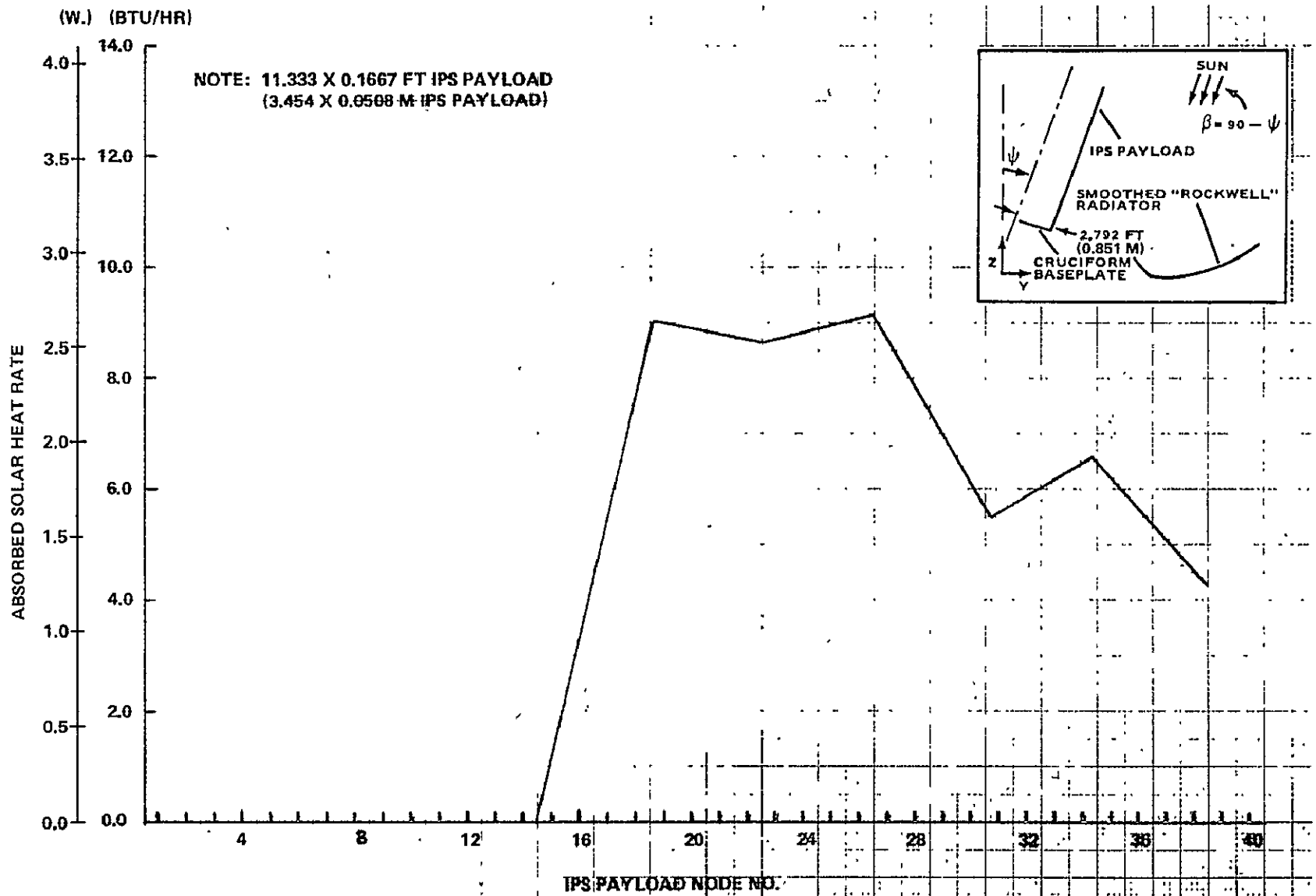


Figure 35. Payload heat rates computed with "two-dimensional" TRASYS II based model for a -5° payload inclination angle.

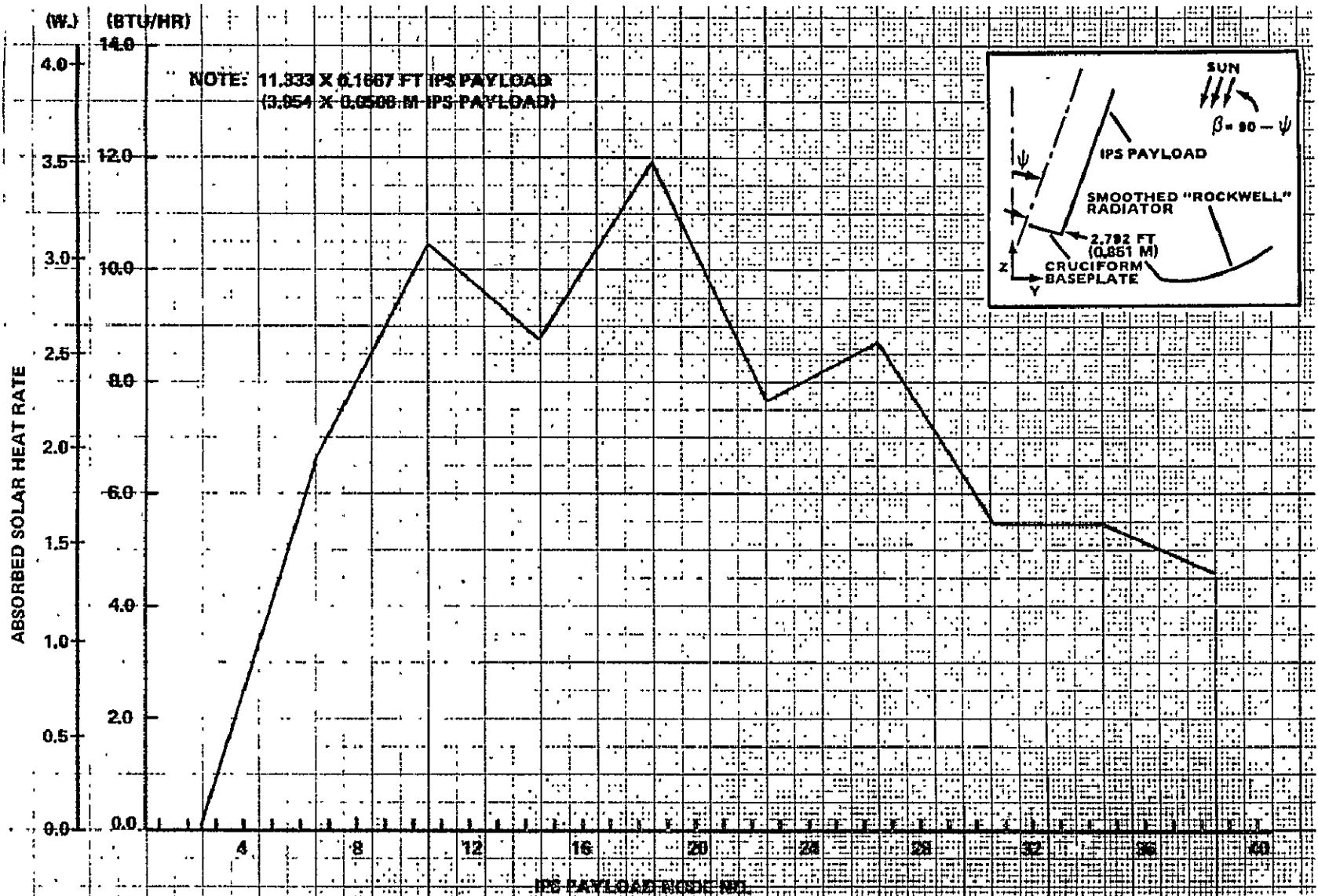
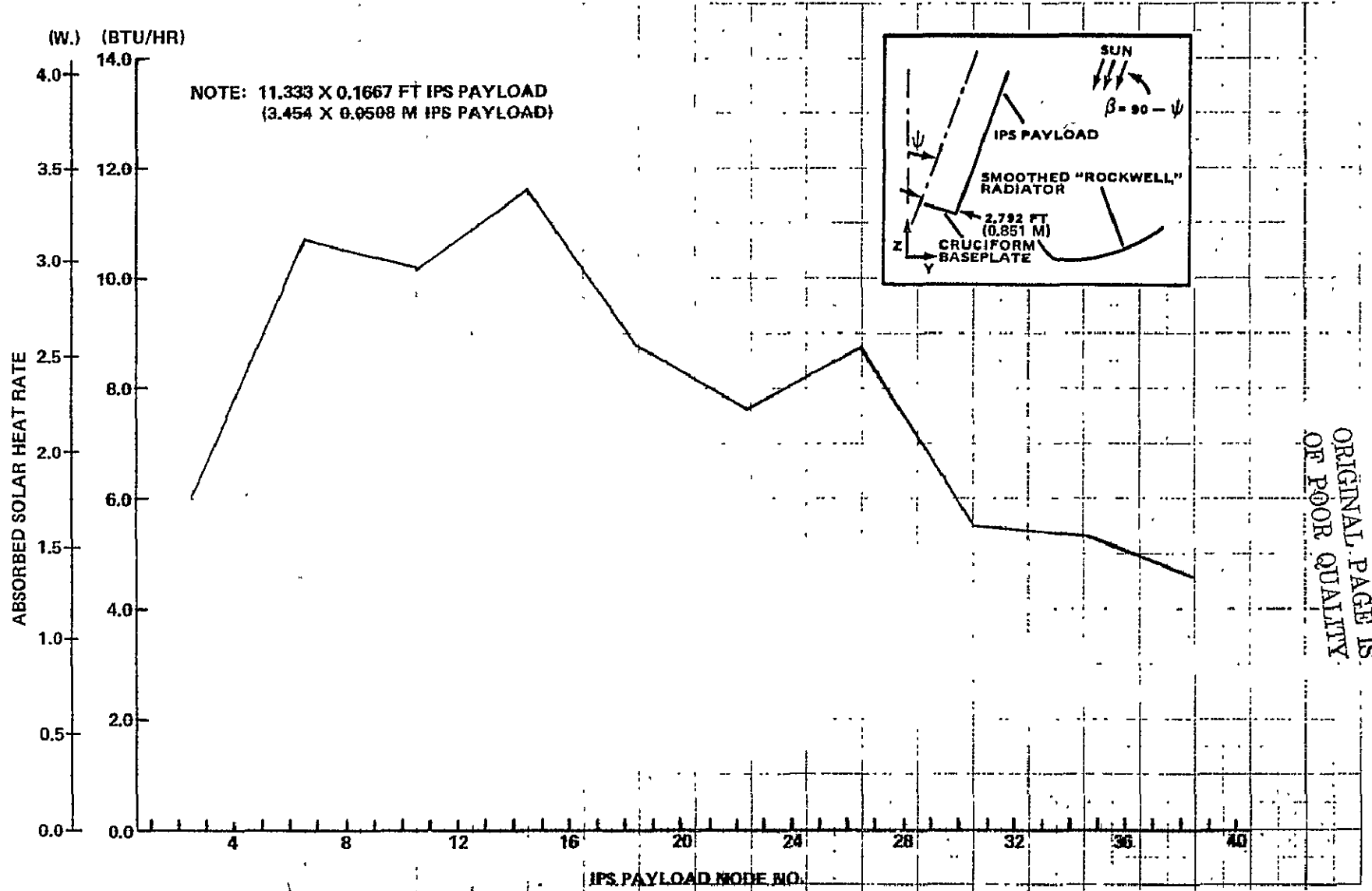


Figure 36. Payload heat rates computed with "two-dimensional" TRASYS II based model for a 5° payload inclination angle.

ORIGINAL PAGE IS
OF POOR QUALITY



ORIGINAL PAGE IS
OF POOR QUALITY

Figure 37. Payload heat rates computed with "two-dimensional" TRASYS II based model for a 10° payload inclination angle.

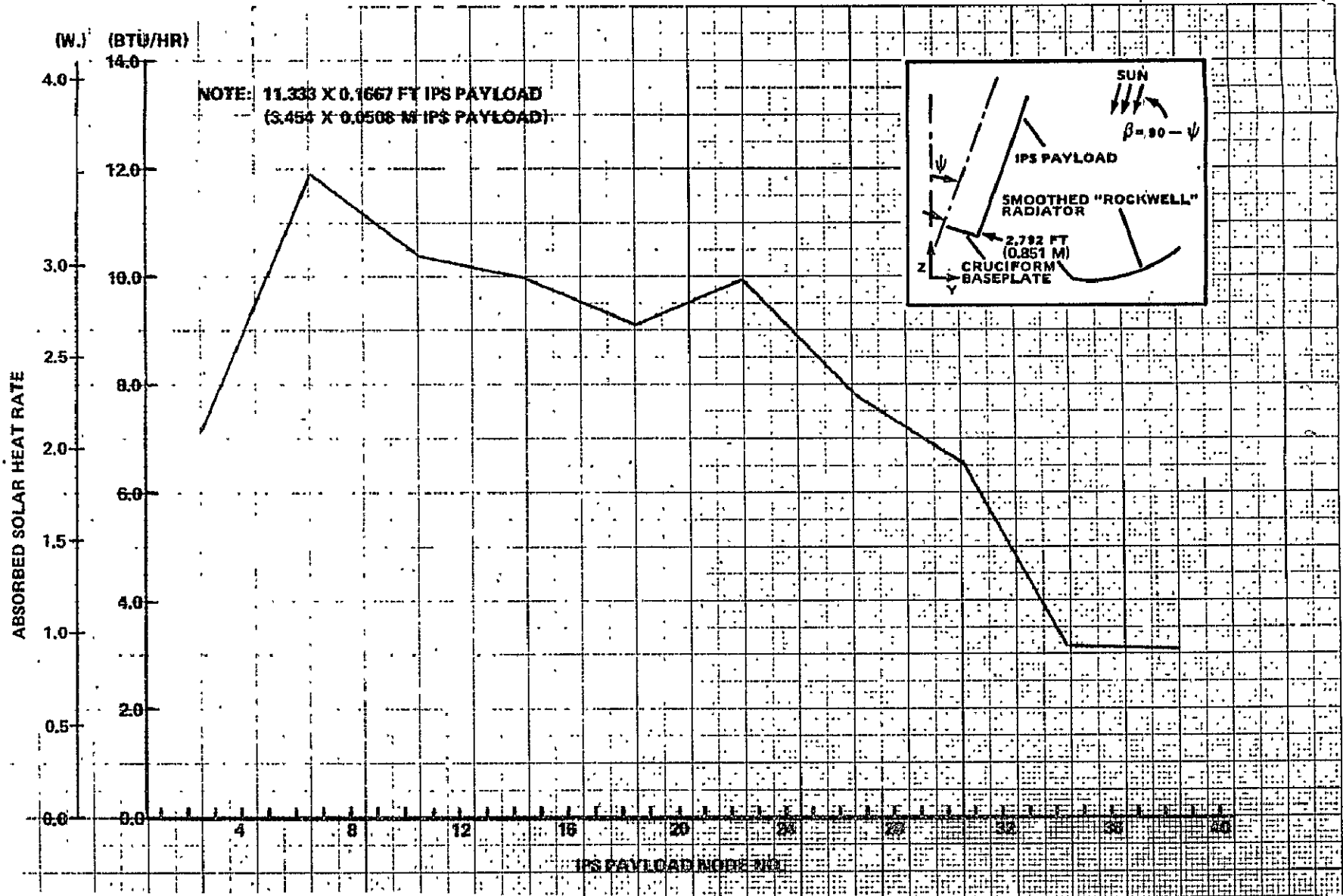
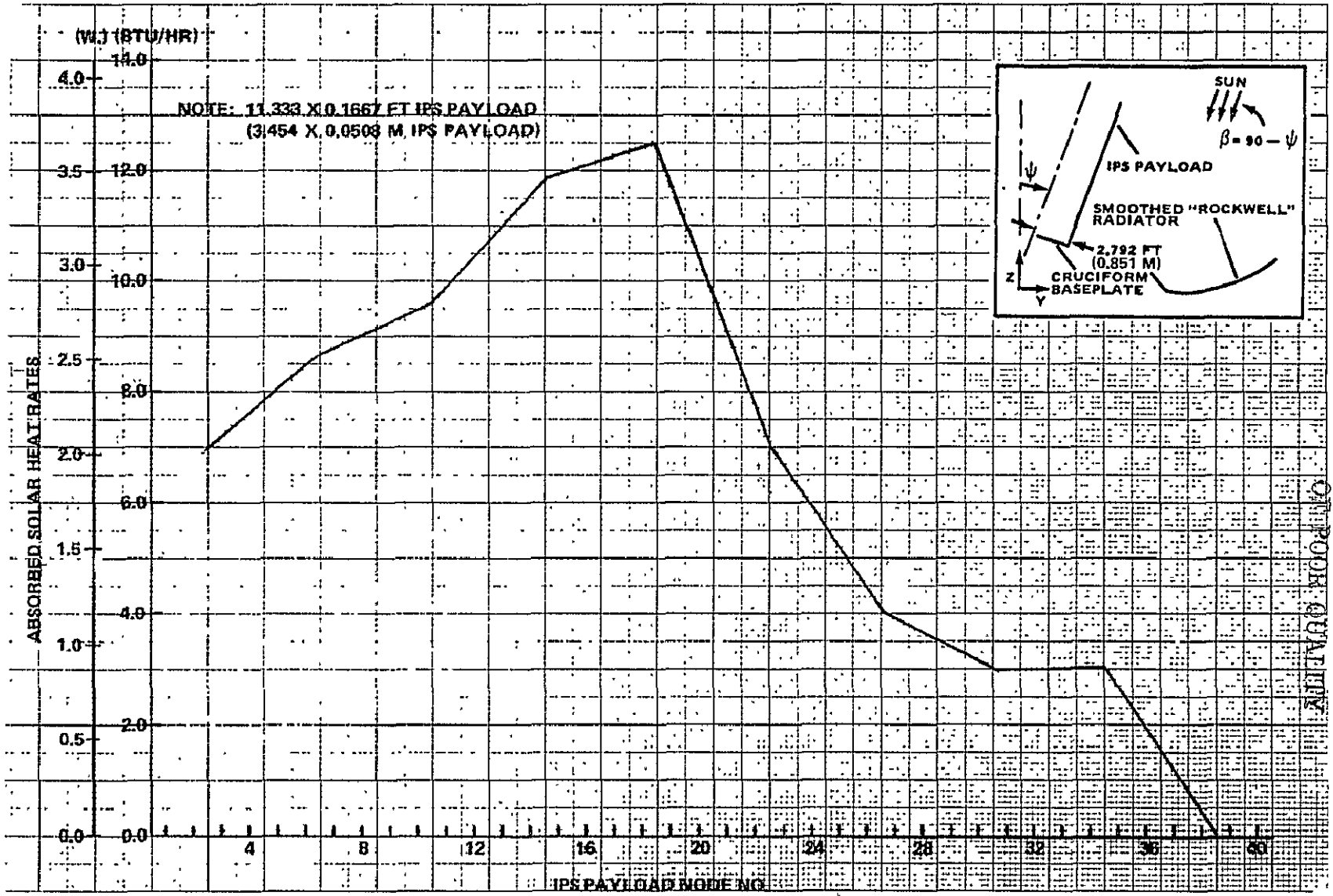


Figure 38. Payload heat rates computed with "two-dimensional" TRASYS II based model for a 20° payload inclination angle.



ORIGINAL PAGE IS OF POOR QUALITY

Figure 39. Payload heat rates computed with "two-dimensional" TRASYS II based model for a 30° payload inclination angle.

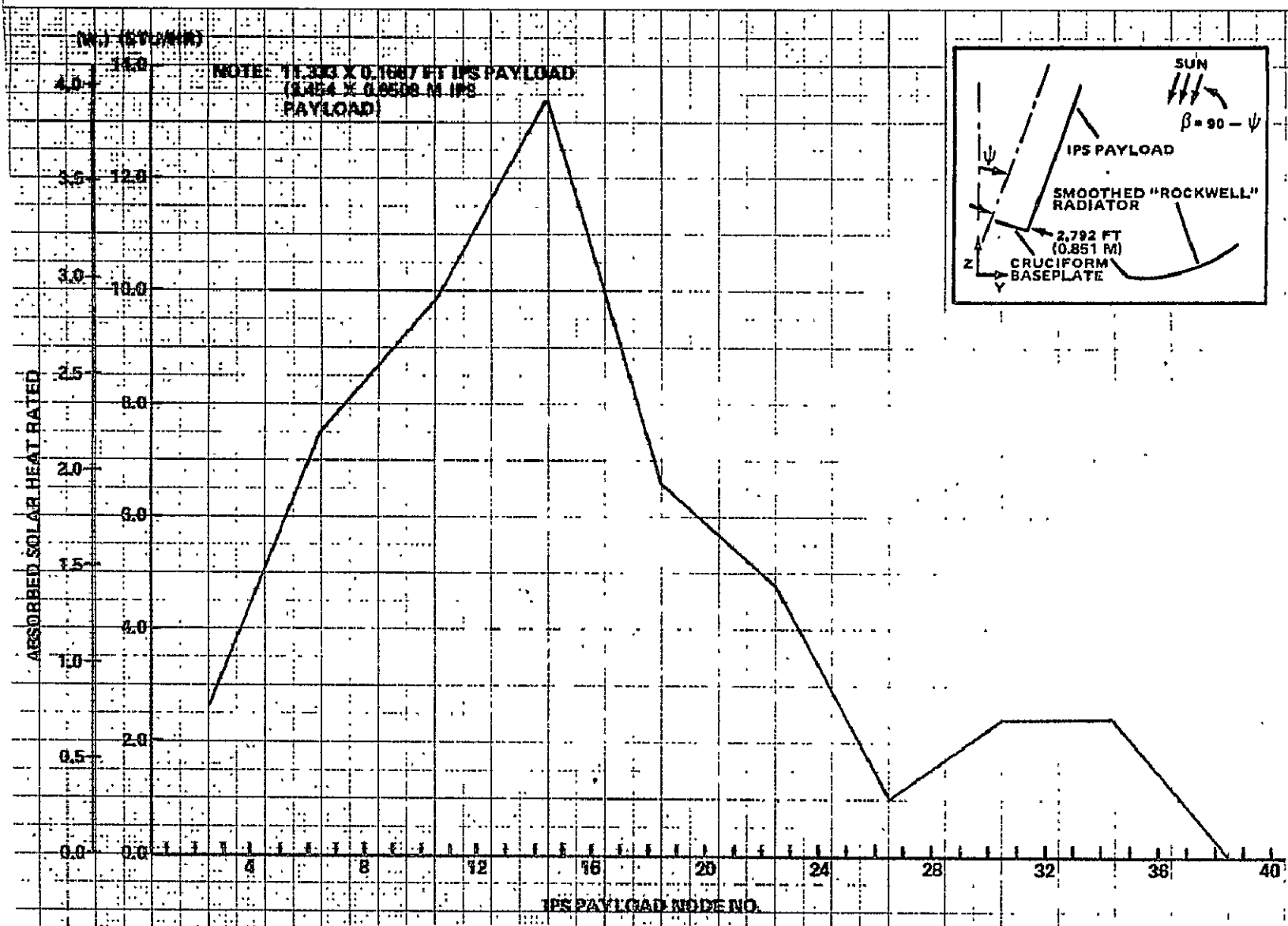


Figure 40. Payload heat rates computed with "two-dimensional" TRASYS II based model for a 40° payload inclination angle.

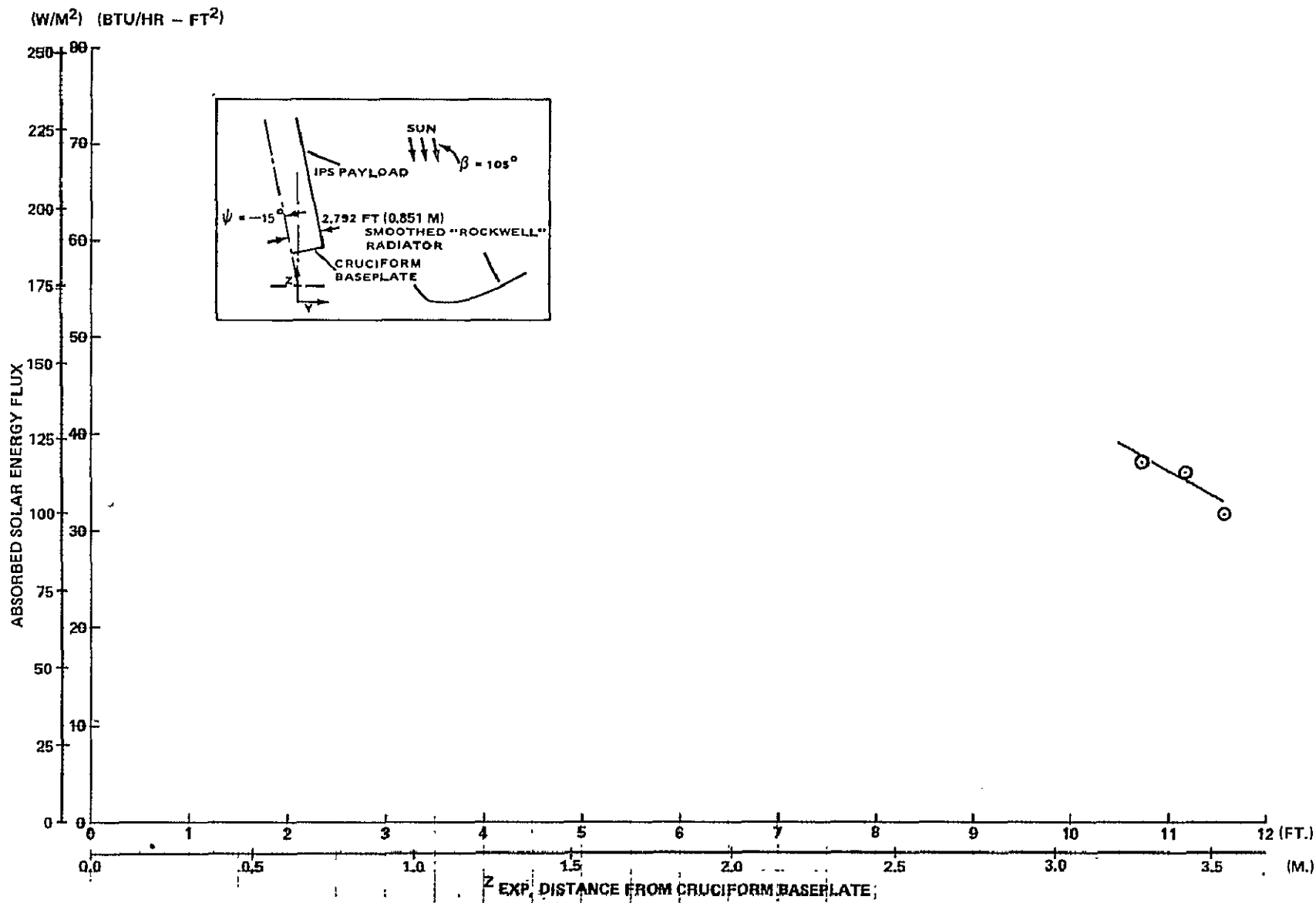


Figure 41. Payload heat flux computed with the "two-dimensional" TRASYS II based model for a -15° payload inclination angle.

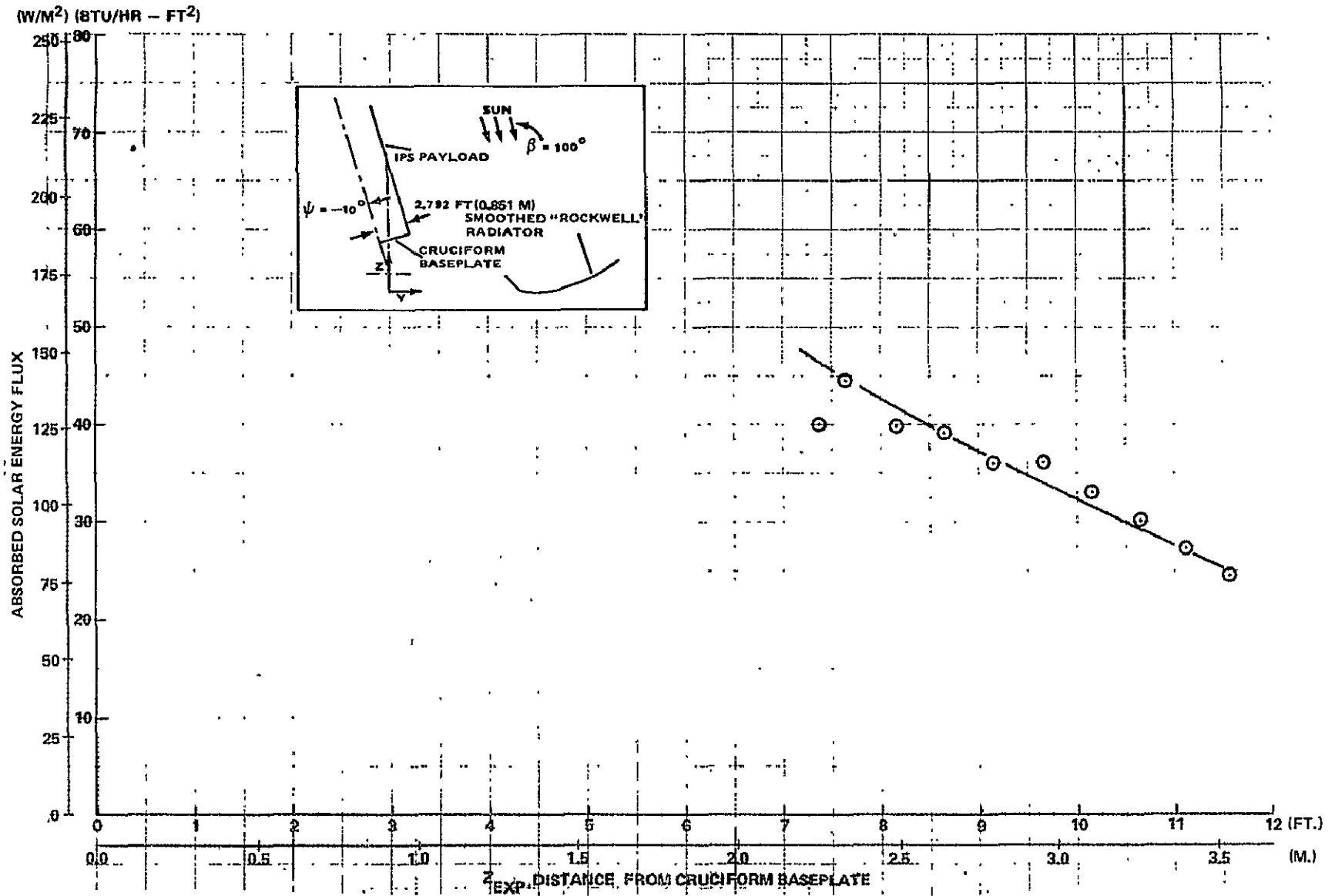


Figure 42. Payload heat flux computed with the "two-dimensional" TRASYS II based model for a -10° payload inclination angle.

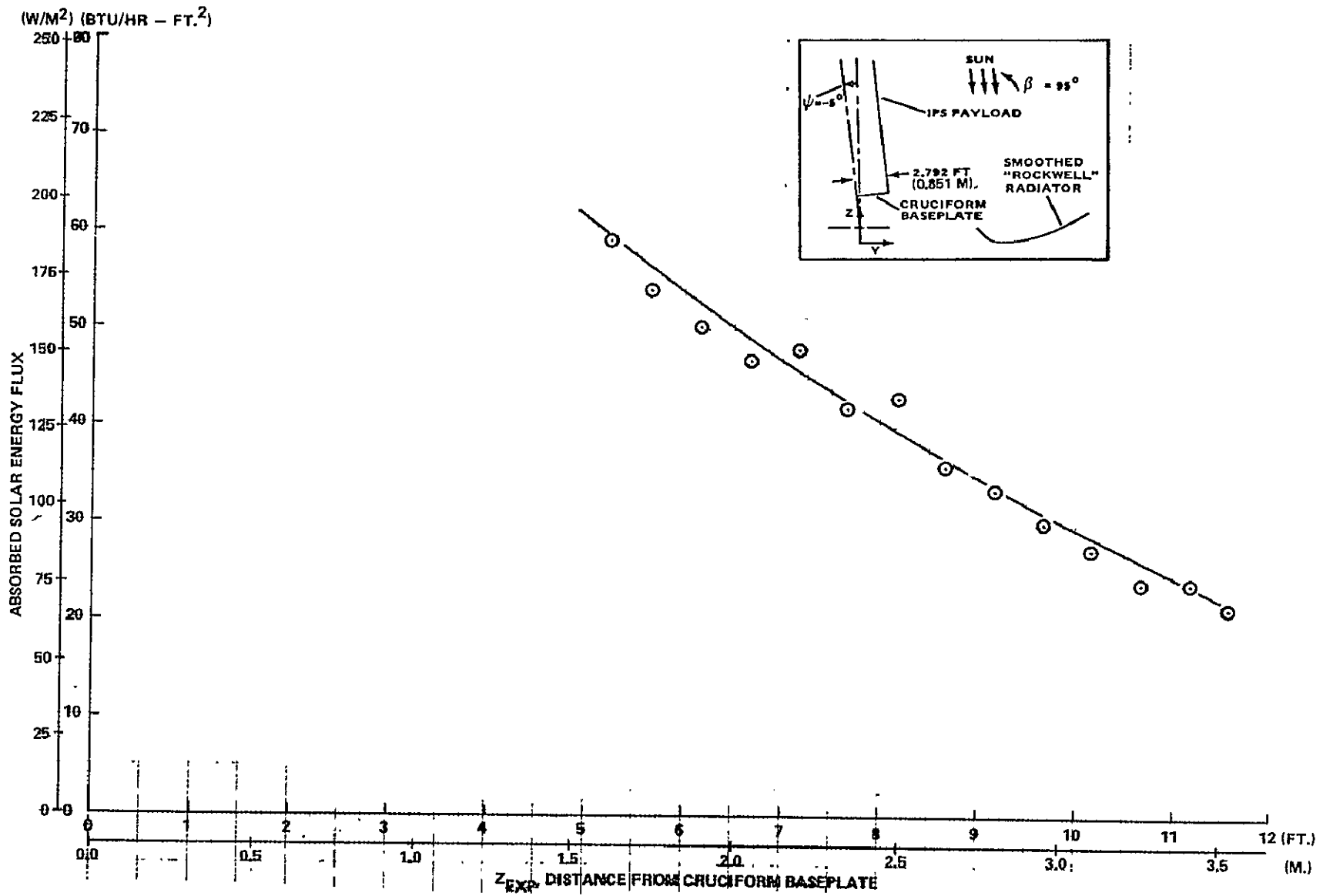


Figure 43. Payload heat flux computed with the "two-dimensional" TRASYS II based model for a -5° payload inclination angle.

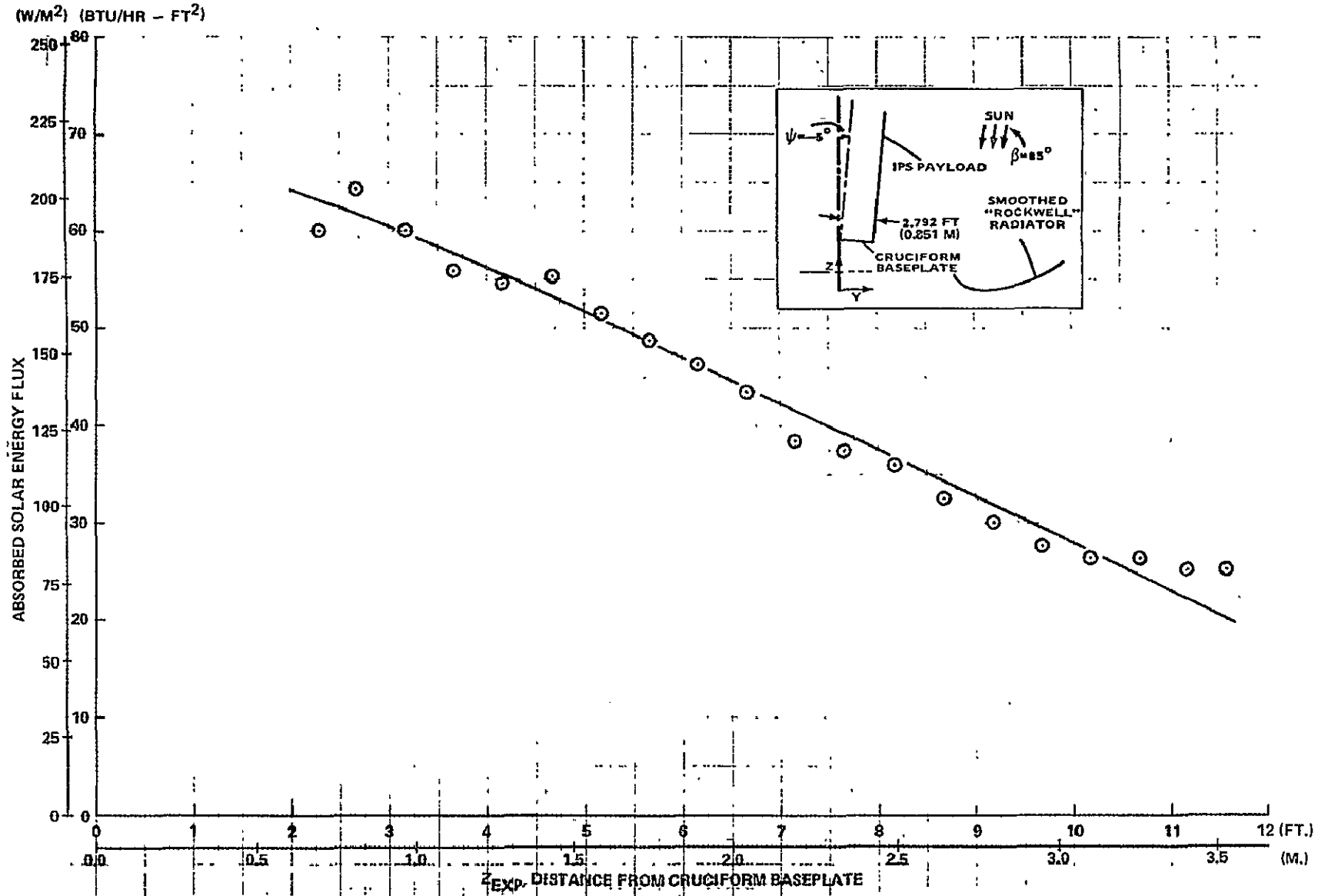


Figure 44. Payload heat flux computed with the "two-dimensional" TRASYS II based model for a 5° payload inclination angle.

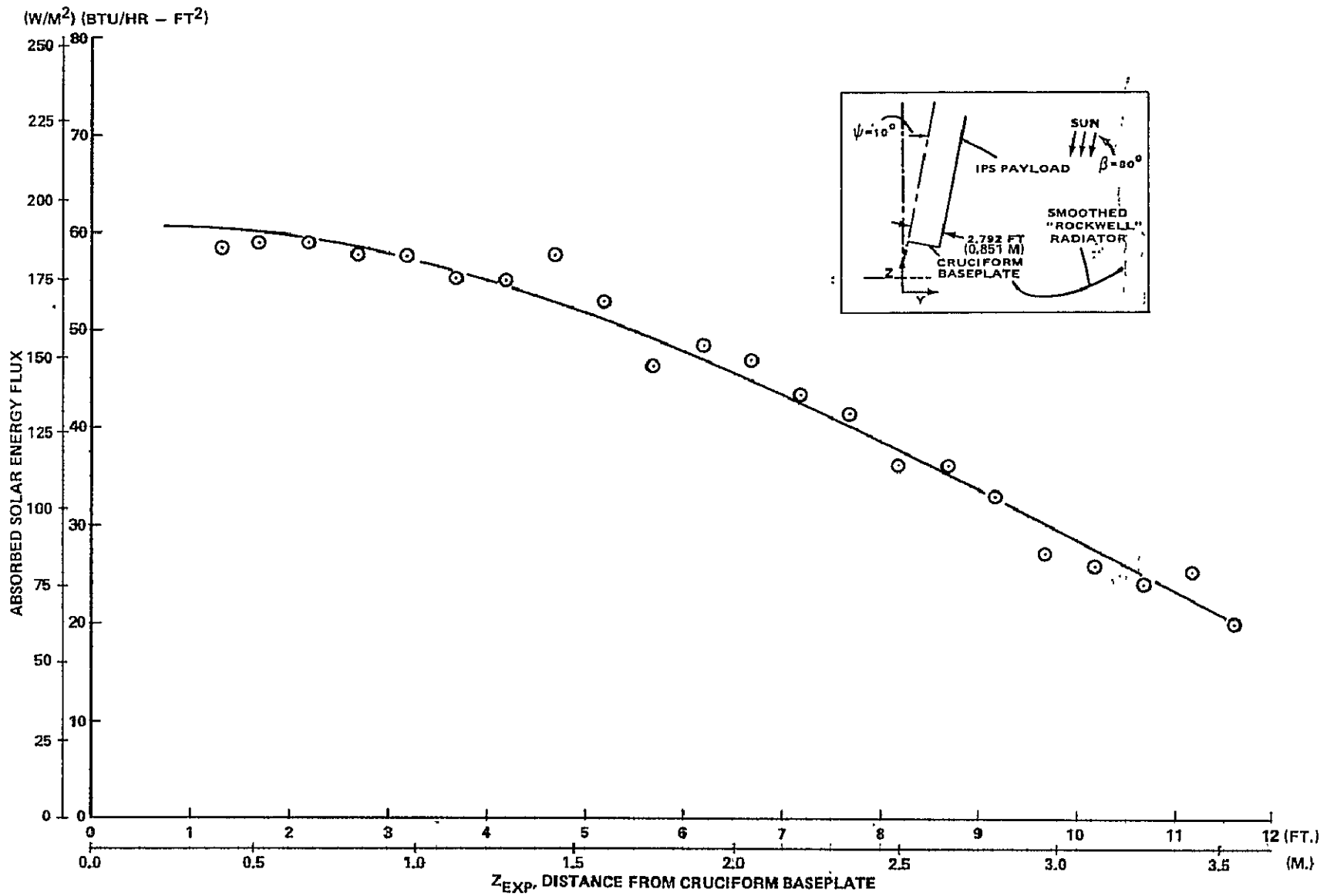


Figure 45. Payload heat flux computed with the "two-dimensional" TRASYS II based model for a 10° payload inclination angle.

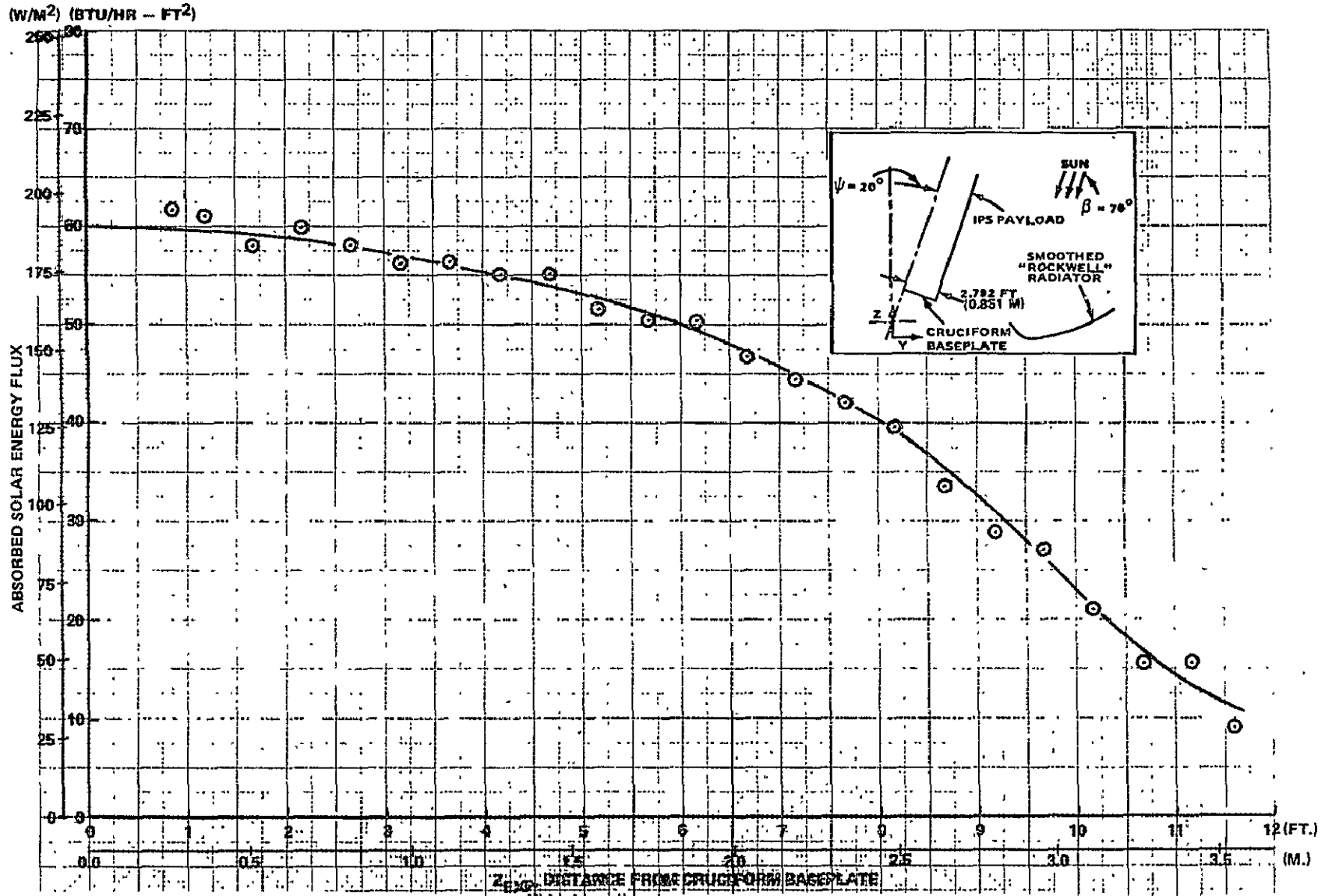


Figure 46. Payload heat flux computed with the "two-dimensional" TRASYS II based model for a 20° payload inclination angle.

ORIGINAL PAGE IS
OF POOR QUALITY

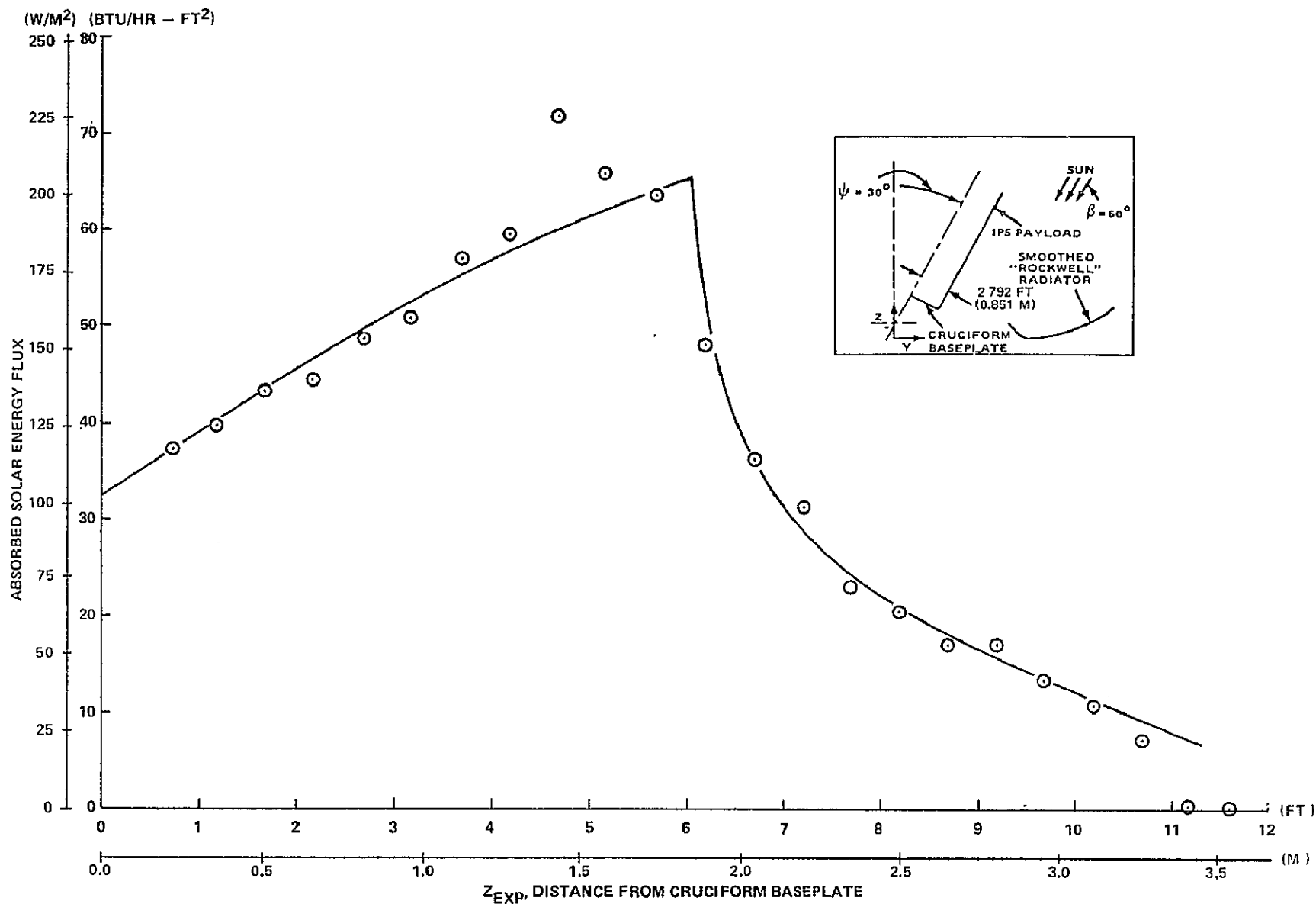


Figure 47. Payload heat flux computed with the "two-dimensional" TRASYS II based model for a 30° payload inclination angle.

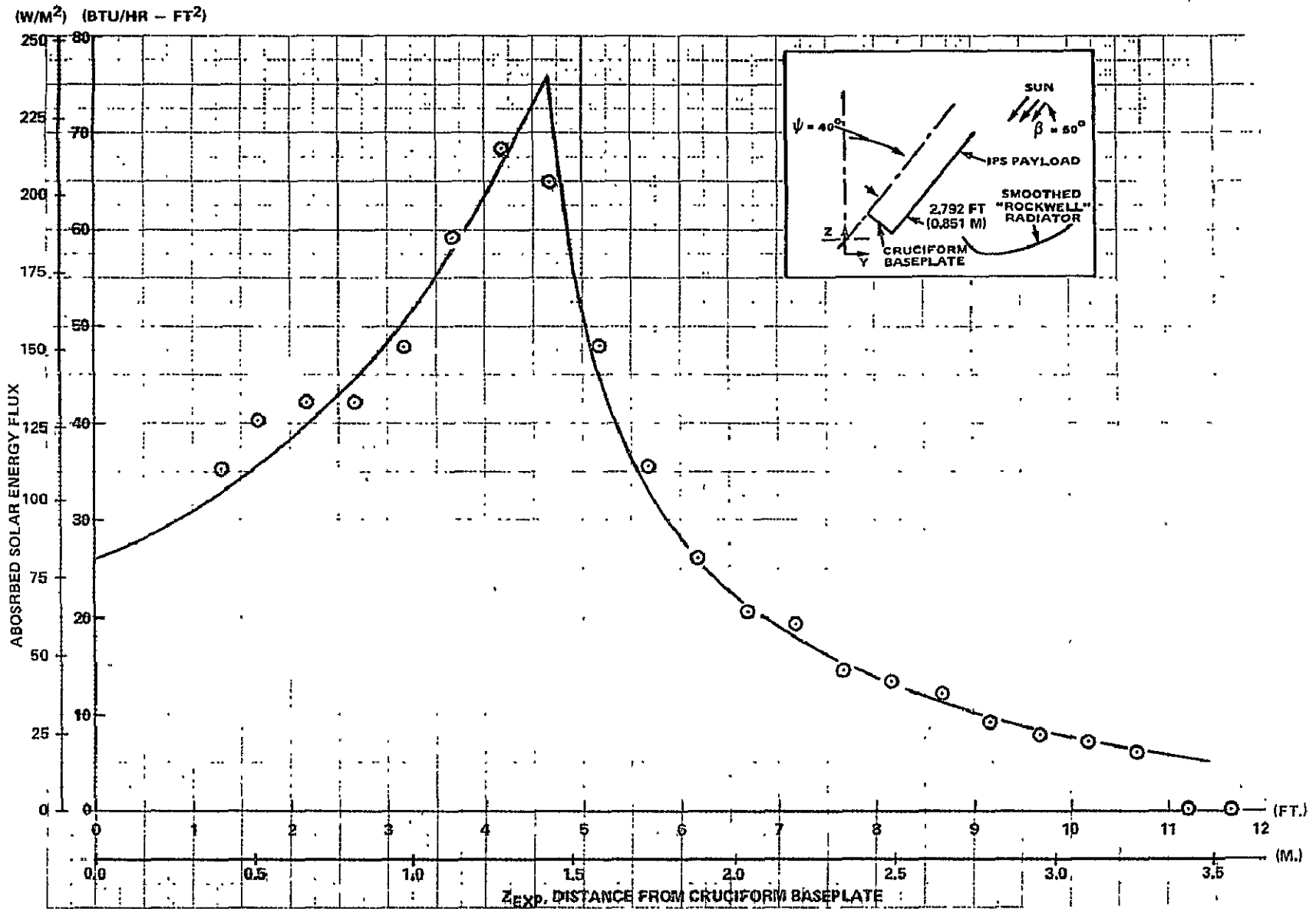


Figure 48. Payload heat flux computed with the "two-dimensional" TRASYS II based model for a 40° payload inclination angle.

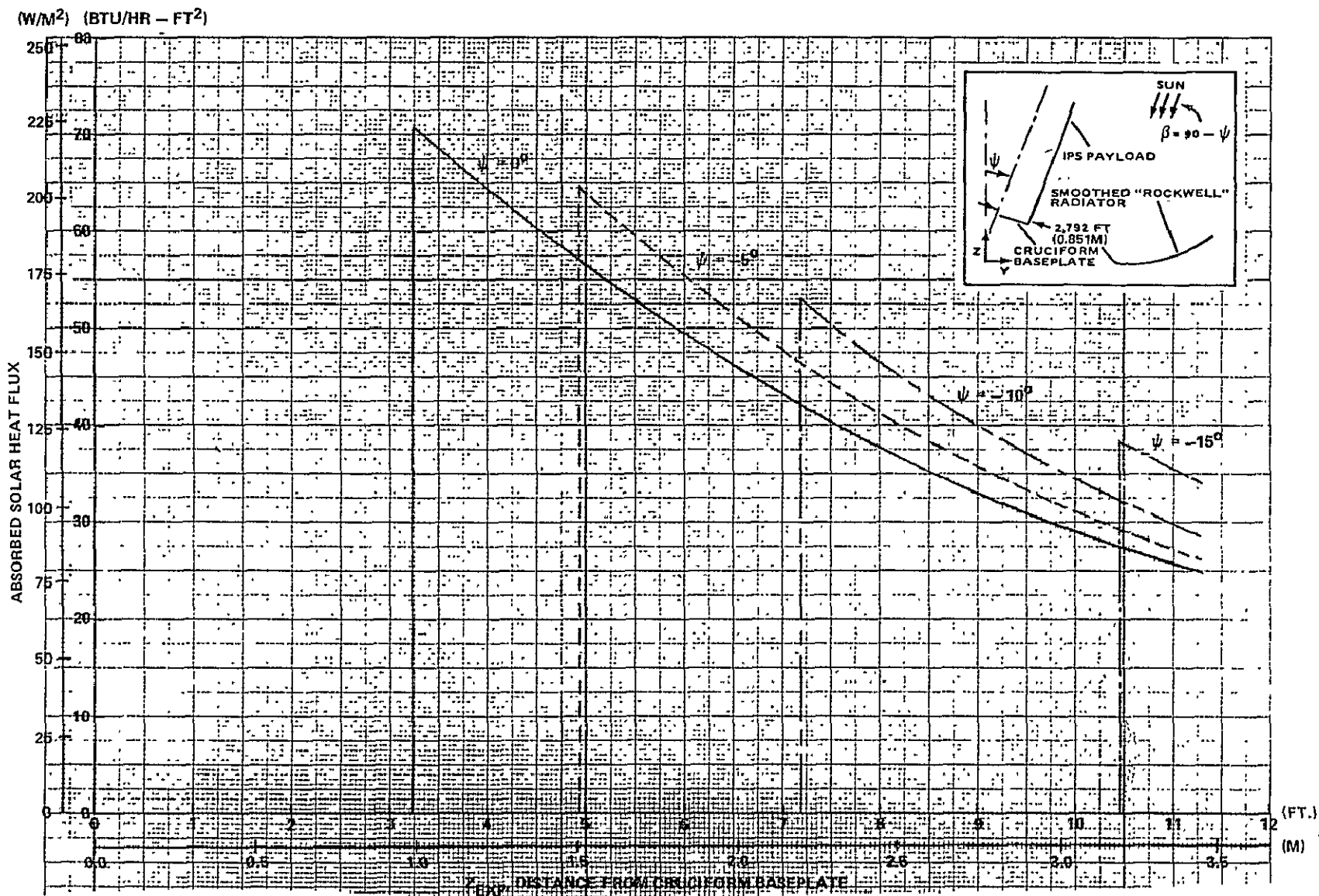


Figure 49. IPS payload heat flux computed with the two-dimensional specular heat flux program for payload inclination angles from -15° to 0°.

0-2

06

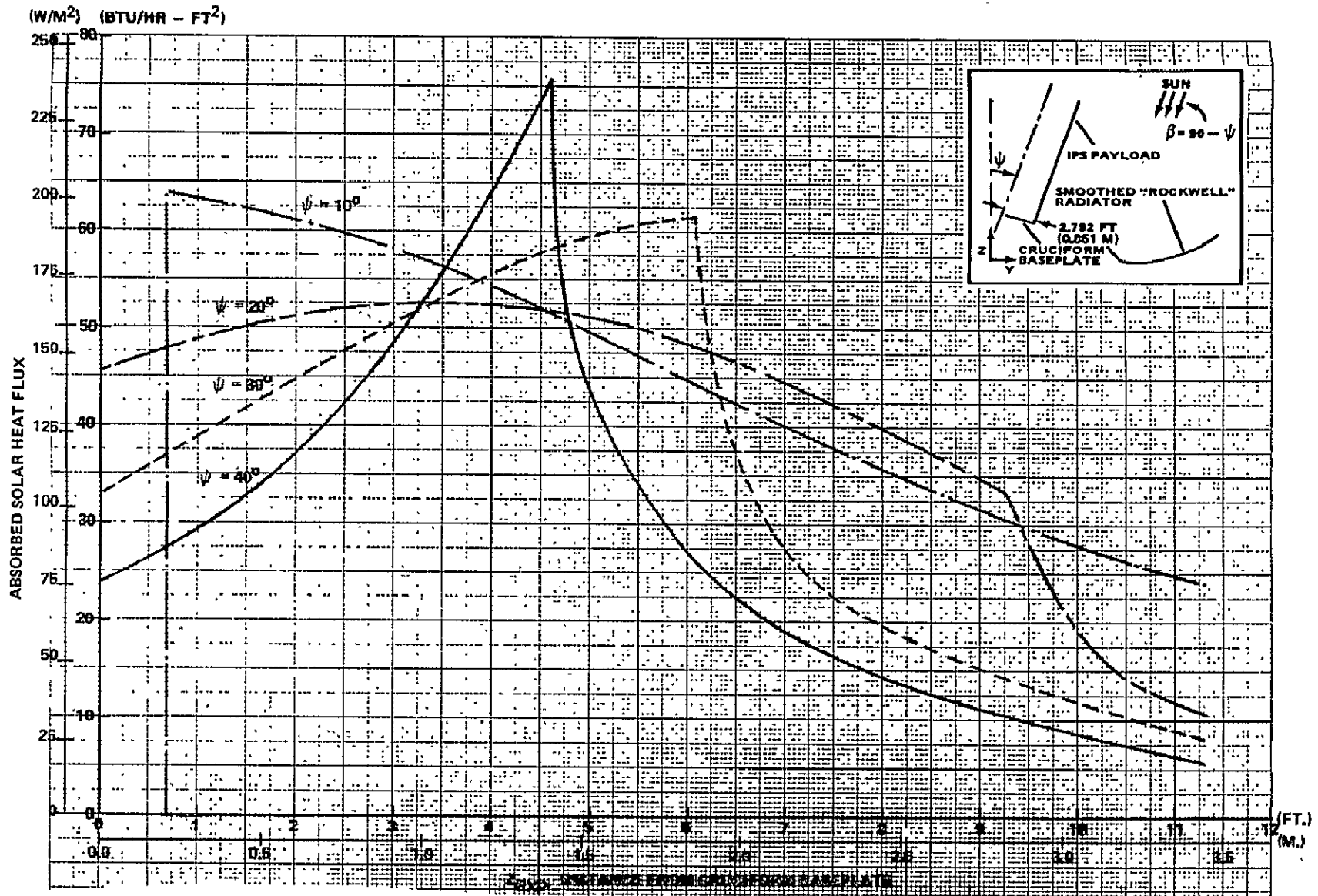


Figure 50. IPS payload heat flux computed with the two-dimensional specular heat flux program for payload inclination angles from 10° to 40° .

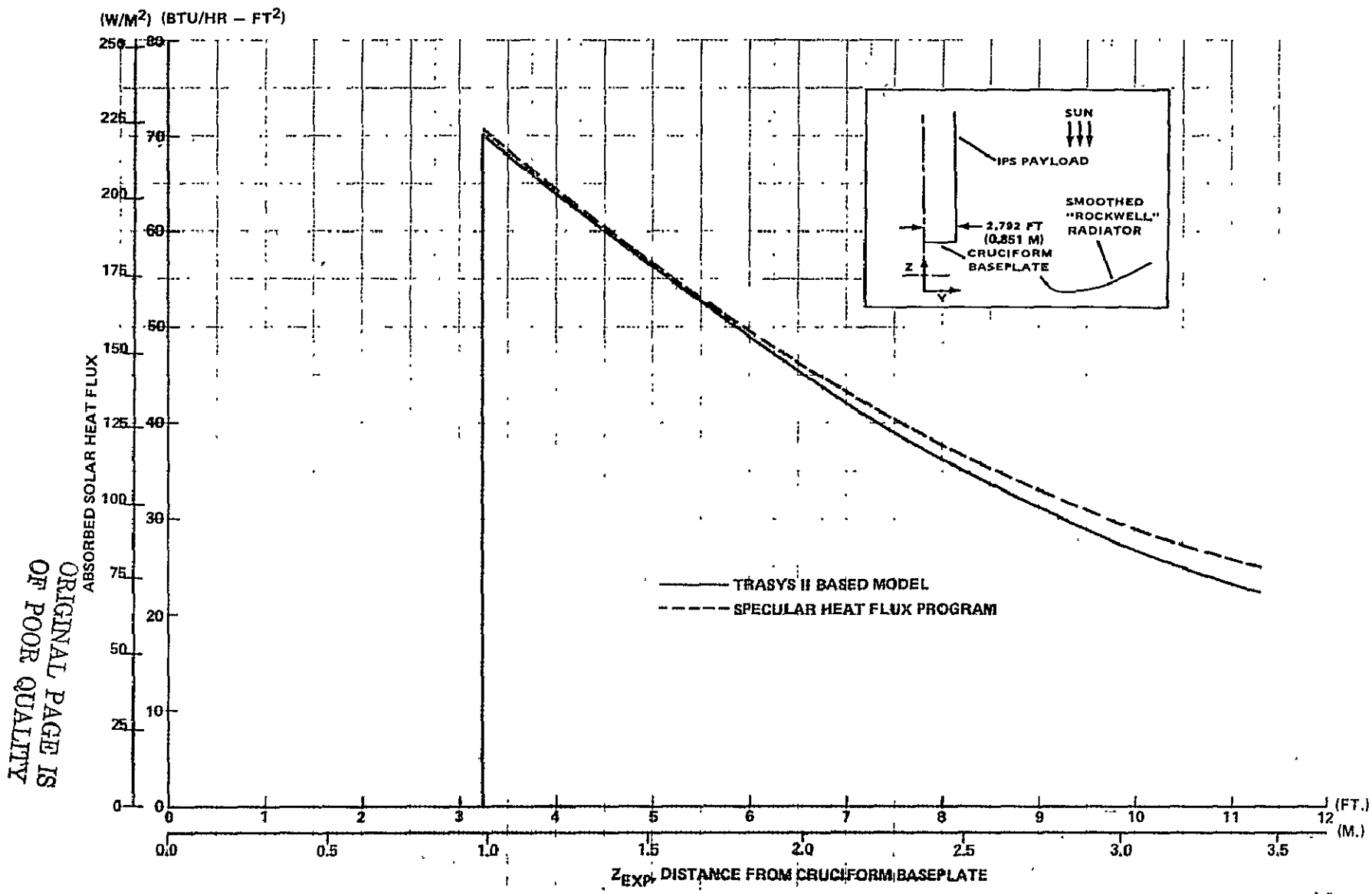


Figure 51. Comparison of "two-dimensional" TRASYS II based model and two-dimensional specular heat flux program for heat flux on the IPS payload at a 0° payload inclination angle.

ORIGINAL PAGE IS OF POOR QUALITY

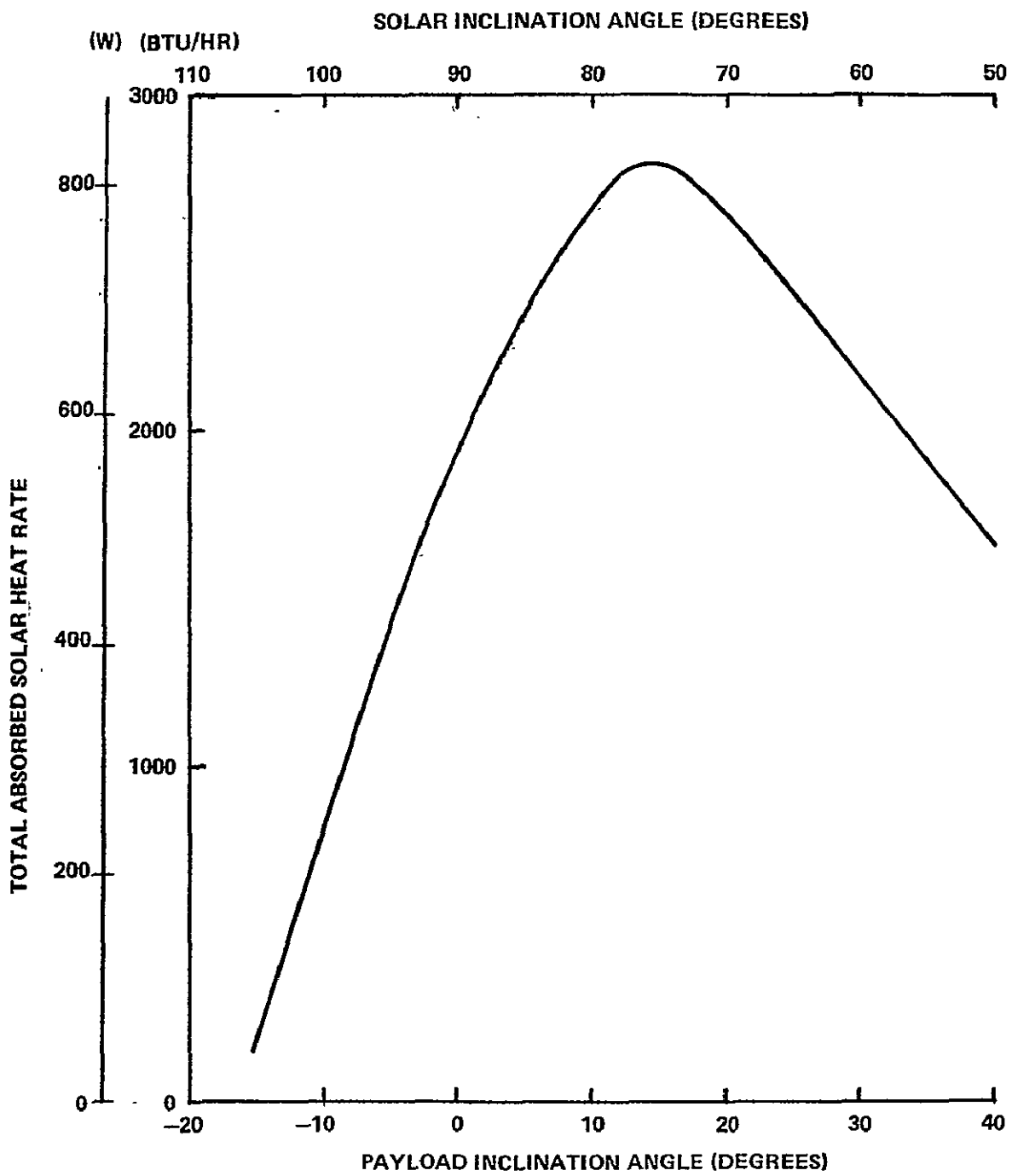


Figure 52. Characteristics of energy absorbed on the IPS payload for various payload inclination angles.

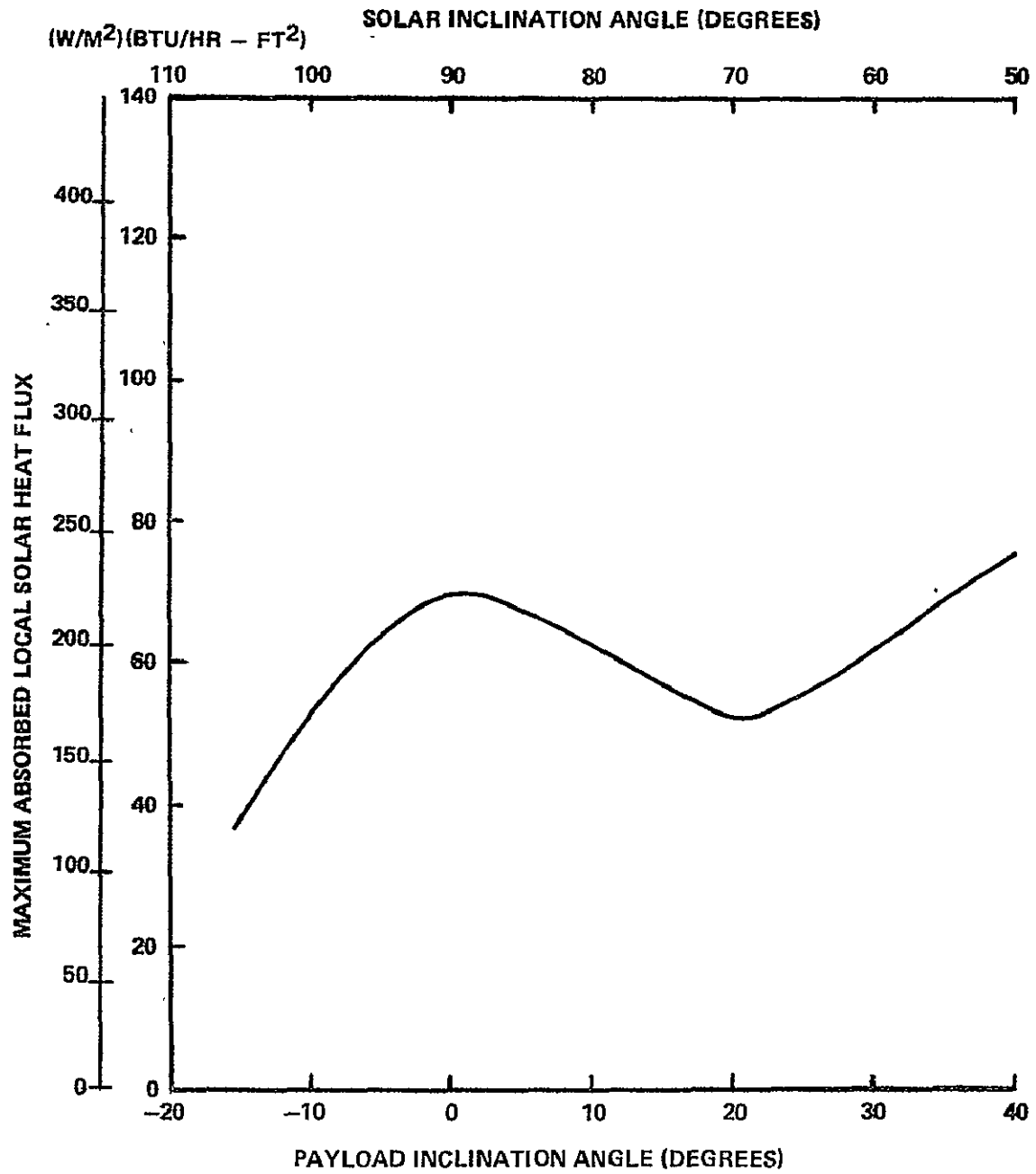


Figure 52. (Concluded).

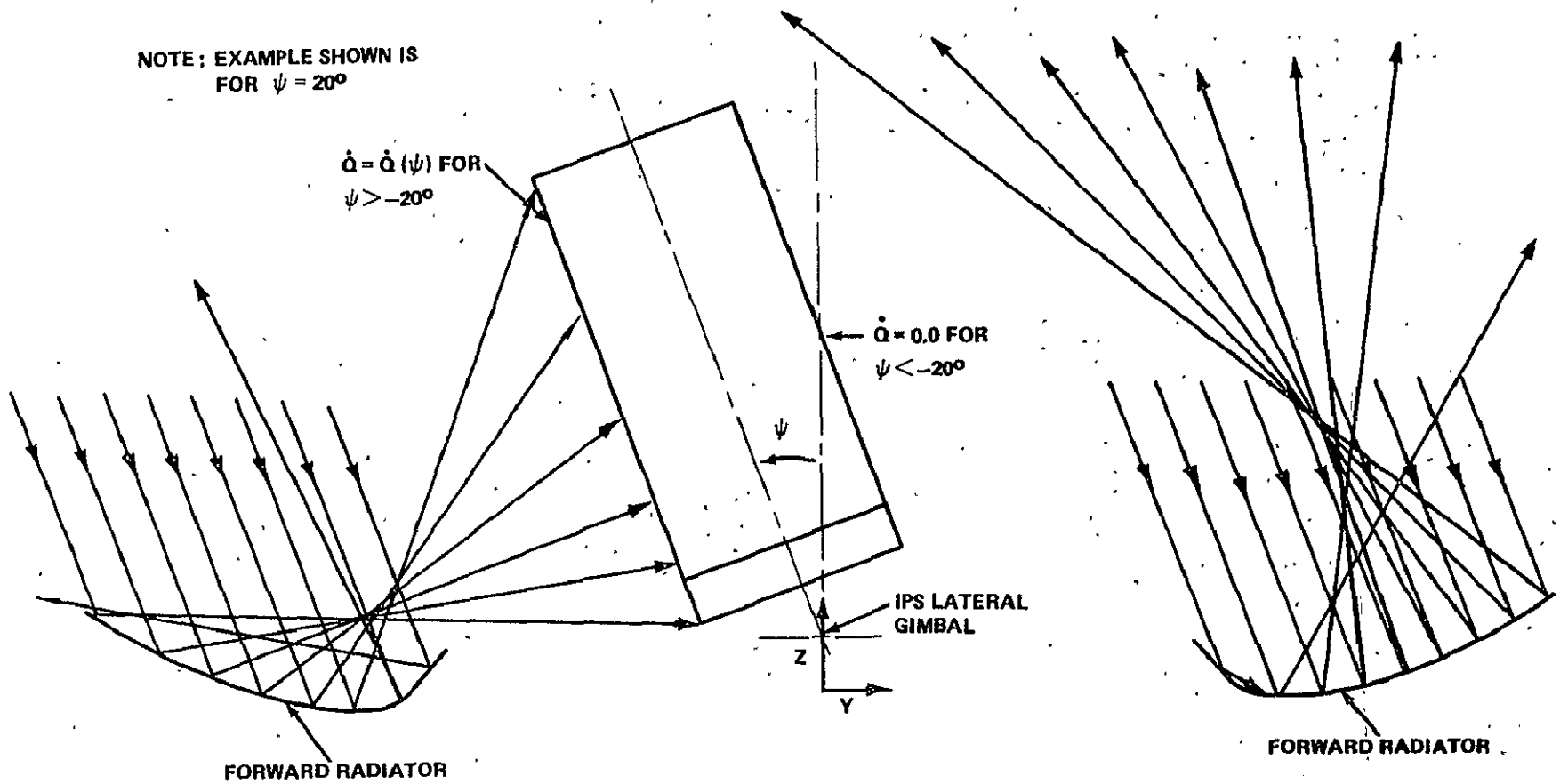


Figure 53. Unsymmetrical irradiation of IPS payload.

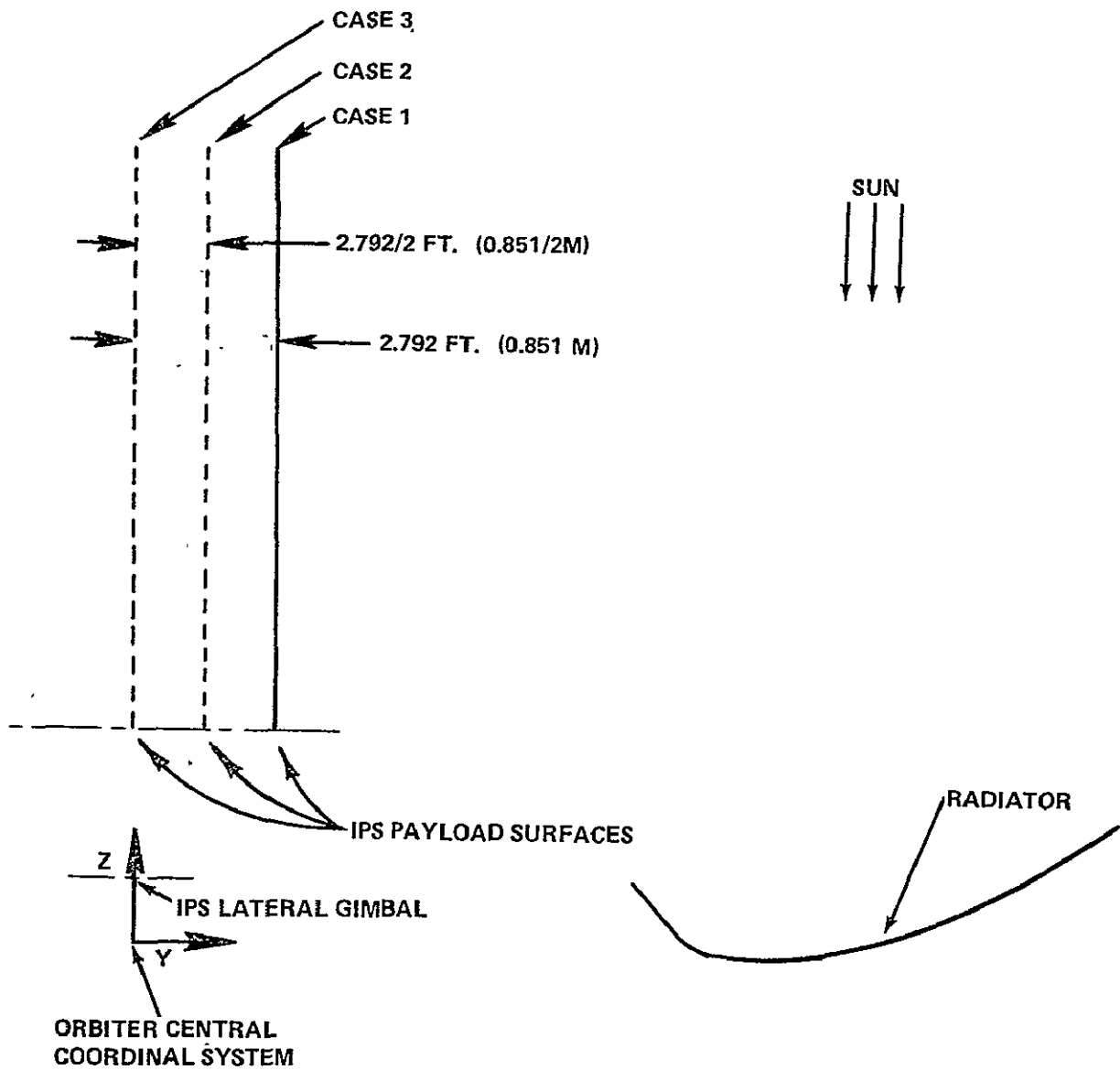


Figure 54. Cases defined to determine the effect of the IPS payload surface lateral location on the absorbed solar flux levels.

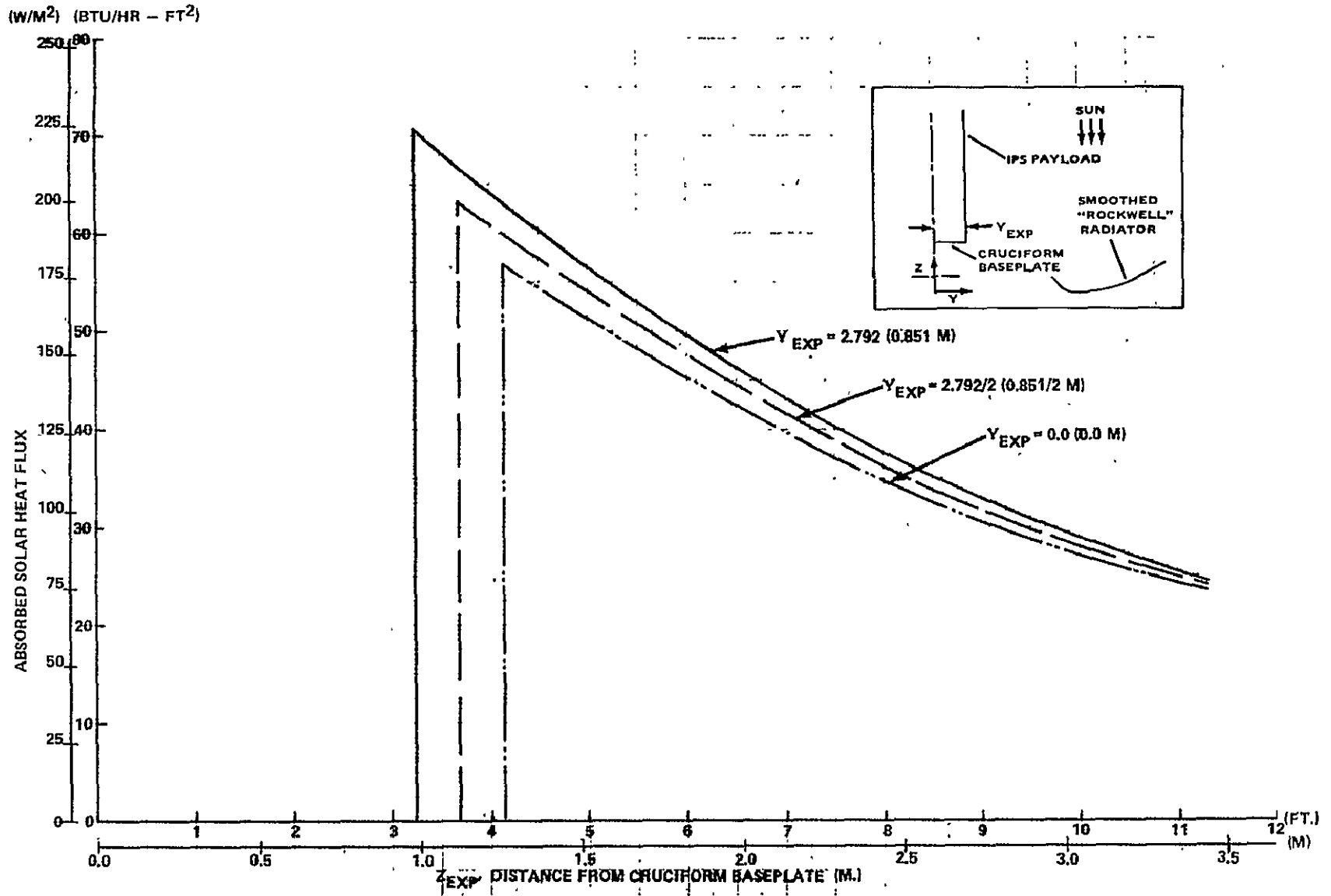


Figure 55. Effect of the IPS payload surface lateral location on the absorbed solar heat flux levels of the IPS payload.

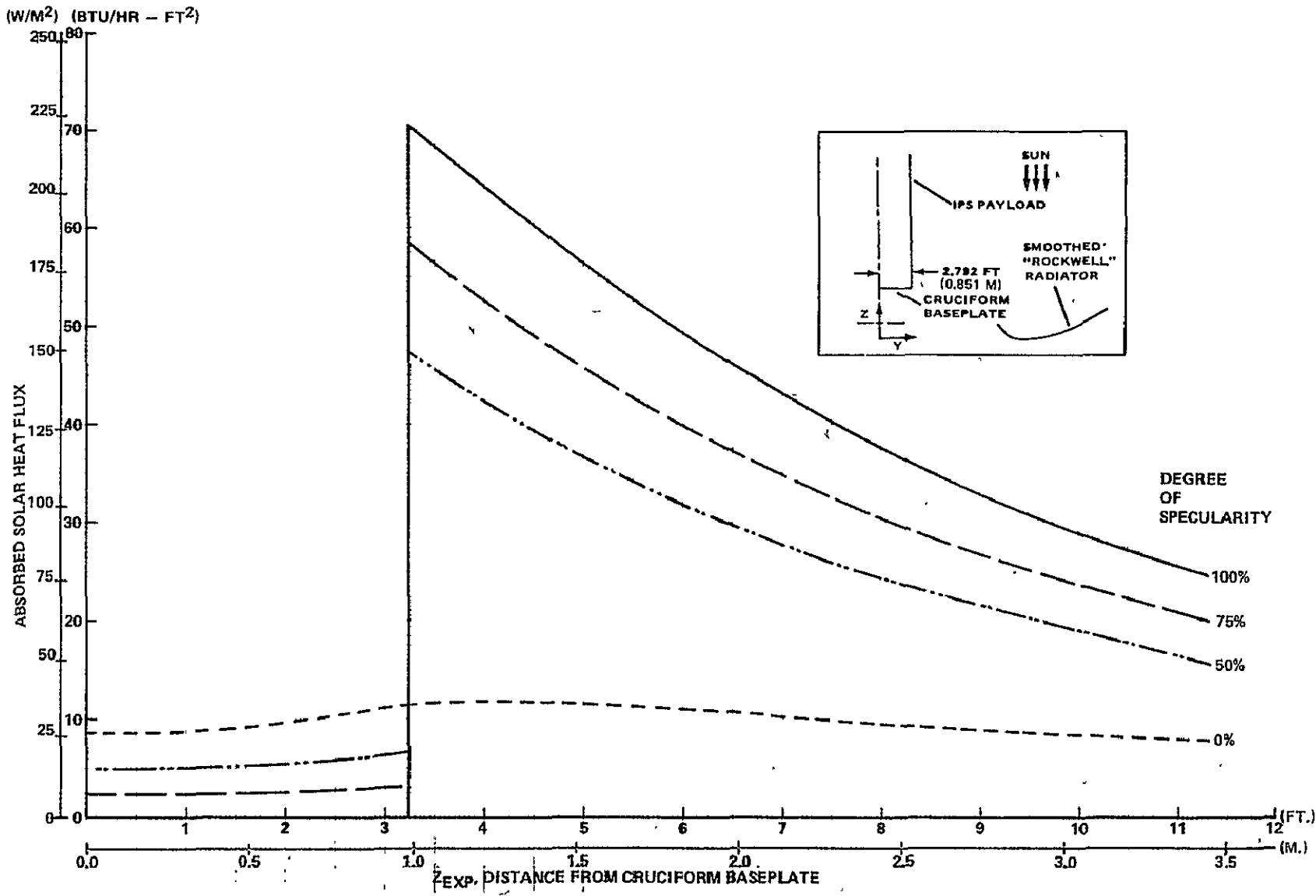


Figure 56. Effect of the degree of the radiator specularity on the absorbed solar flux levels of the IPS payload.

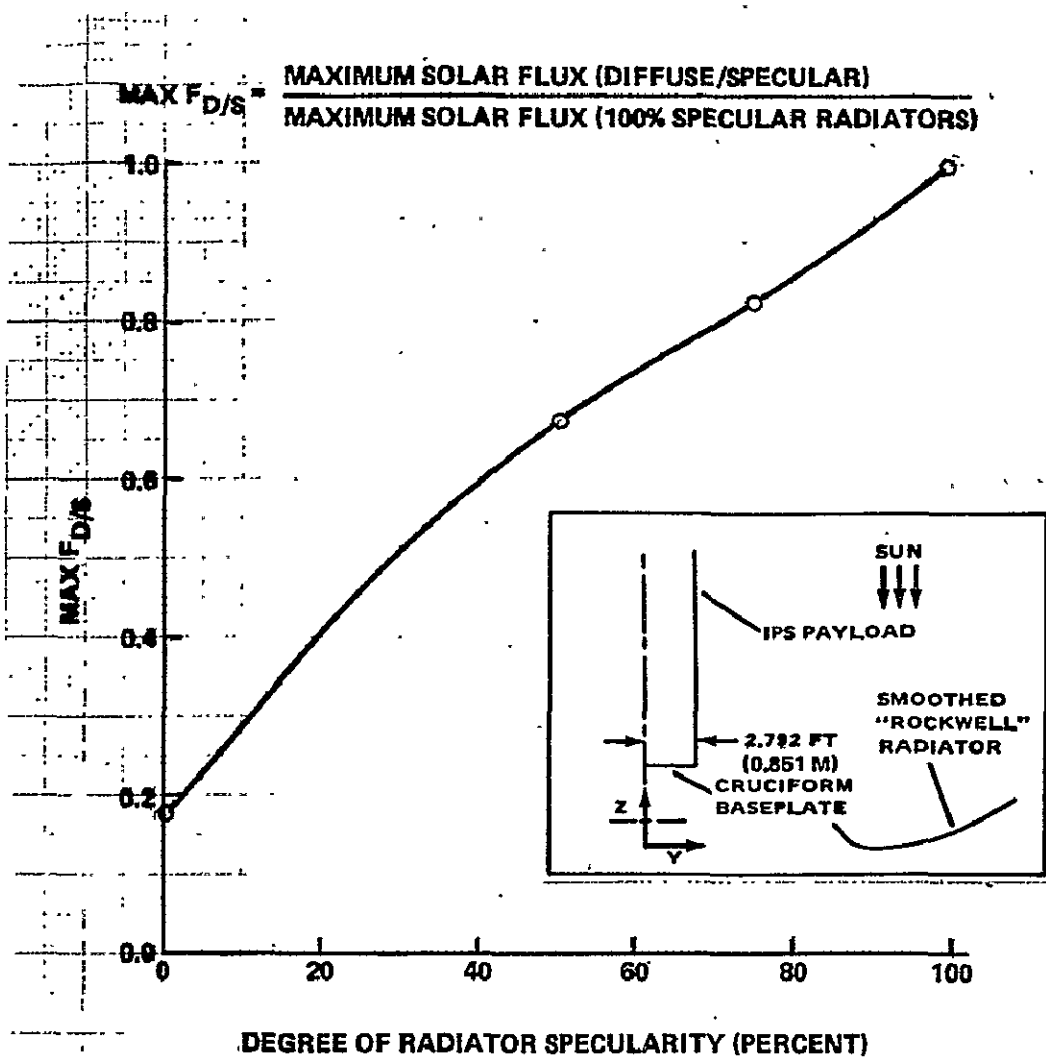


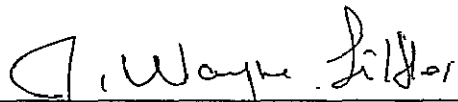
Figure 57. Effect of radiator specularity on the maximum solar heat flux absorbed by the IPS payload.

APPROVAL

A STUDY OF THE EFFECT ON A TYPICAL ORBITER PAYLOAD
THERMAL ENVIRONMENT RESULTING FROM SPECULAR
REFLECTIONS FROM THE FORWARD ORBITER
RADIATORS

By R. Humphries, L. Turner, and J. W. Littles

The information in this report has been reviewed for technical content. Review of any information concerning Department of Defense or nuclear energy activities or programs has been made by the MSFC Security Classification Officer. This report, in its entirety, has been determined to be unclassified.



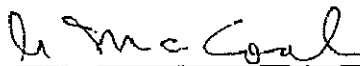
J. WAYNE LITTLES

Chief, Life Support and Environmental Branch



J. B. STERETT

Acting Chief, Engineering Analysis Division



A. A. McCOOL

Director, Structures and Propulsion Laboratory

DISTRIBUTION

EA01
Mr. Kingsbury

EE45
Mr. Emanuel
Mr. McKay

NA01
Mr. Lee

NA31
Mr. Compton

JA11
Mr. Pace

JA13
Mr. Lester

JA31
Mr. Sims
Mr. Lake

JA51
Mr. Ise
Mr. Galey
Mr. Harwell
Mr. Guynes

EP01
Mr. McCool
Mr. Coldwater
Mr. Morea

EP41
Mr. Sterett
Mr. Cody

EP43
Mr. Worlund

EP44
Mr. Vaniman

EP45
Dr. Littles (5)
Dr. Humphries (20)
Mr. Turner (5)
Mr. Patterson
Mr. Moses
Mr. Clark
Mr. Moss
Mr. White
Mr. Ray

ED01
Mr. Hopson

EL32
Mr. Hueter

EL34
Mr. Sells

EL52
Mr. Loose
Mr. Genter

EL54
Mr. Smith

AS61 (2)

AS61L (8)

CC01/Mr. Wofford

AT01/Mr. Smith

NASA-Scientific and Technical Information
Facility (25)

P. O. Box 8757

Baltimore/Washington International Airport
Baltimore, MD 21240